Organozinc Reagents

DOI: 10.1002/anie.200((will be filled in by the editorial staff))

Organozinc Pivalate Reagents: Segregation, Solubility, Stabilisation and Structural Insights**

Alberto Hernán-Gómez, Emma Herd, Eva Hevia, Alan R. Kennedy, Paul Knochel,* Konrad Koszinowski, Sophia M. Manolikakes, Robert E. Mulvey,* and Christoph Schnegelsberg

It has long been known that salt additives can activate or deactivate organometallic compounds.[1] The former has been demonstrated to great effect recently through new classes of organozinc and other organometallic reagents that exhibit enhanced reactivity due to participation of halide salts within their THF solutions as for example in $(TMP)_2Zn.2MgCl_2.2LiCl$ (TMP is 2,2,6,6-tetramethylpiperidide).[2] Combined with activation, a new salt effect was reported for the magnesium-zinc pivalate systems "RZnOPiv.Mg(OPiv)X.nLiCl" (where OPiv = pivalate; R = aryl, heteroaryl or benzyl; X = Cl, Br or I), namely stabilisation since these systems boast a high degree of resistance to attack by air and moisture, especially when isolated as solids.[3] Rapid decomposition is the normal outcome when such organometallic compounds are exposed to these antagonists since metal-C bonds are generally thermodynamically unstable with respect to the metal-O bonds that form as a result. Inert atmosphere protocols are thus mandatory for handling these air sensitive organometallic compounds so any advances that slow down or ideally stop altogether such air degradation processes would have a massive impact in the numerous academic and especially industrial laboratories that utilise these compounds. While the synthetic usefulness of these salt-stabilised pivalates in Negishi cross coupling or carbonyl addition applications has been documented,[3] their multicomponent heterotrimetallic-heterotrianionic compositions make for highly complicated chemistry which challenges our understanding of them. To begin unravelling this complexity we present herein the opening study of these intriguing pivalate cocktails in their own right gathering information from solutions, solids and gas phase. As a consequence, light is thrown on solubility, segregation and stabilisation issues.

Reported methods of synthesising these pivalates, by inserting Mg into an organic halide RX, magnesiating RX via salt-activated (TMP)MgCl.LiCl, or performing Mg-I/Mg-Br exchange on RI or RBr with *i*PrMgCl.LiCl involve a common second step, namely transmetallation with zinc pivalate [(Eqn. 1)].

$$RMgCl + Zn(OPiv)_2 \xrightarrow{LiCl} RZn(OPiv) + MgCl(OPiv) \quad (\mathbf{1})$$

We initially probed this transmetallation studying the mixture of the arylester reagent $EtO_2C(p\text{-}C_6H_4)MgCl.LiCl$ and zinc pivalate in THF solution by NMR spectroscopy.[4] This solution was found previously to be effective in Negishi cross-coupling reactions under mild conditions, while the solid obtained on evaporation of solvent remained 45% active after 1 hr air exposure. Surprisingly ^1H NMR and COSY spectra of this mixture revealed only 1 pivalate signal and 2 distinct sets of aryl signals,[4] in contrast to the 2 pivalate and 1 set of aryl signals expected from the transmetallation in Eqn. 1.

^1H DOSY NMR[5, 6] experiments implied the presence of two major species[7] with distinct diffusion coefficients, the lighter one of which could be assigned to free $C_6H_5CO_2Et$, presumably due to partial hydrolysis from prolonged storage of the sample prior to NMR study. Supporting this hydrolysis presumption, crystals grown from THF solution were revealed by X-ray crystallography to be cocrystals that include a heptanuclear mixed cluster whose core can be formalized as $[\{Mg(OPiv)_2\}_5\{Mg(OH)_2\}(MgO)\cdot 4THF]$ **1** (See Fig. S4 in Supporting Information).[4,8] The most telling features of **1** are OH^- or O^{2-} incorporation and the presence of excess pivalate where a 1:1, Mg:(OPiv) stoichiometry would be expected from the transmetallation reaction in Eqn. 1. These observations prompted two questions. First, could the Mg pivalate products of these reactions be acting as moisture and/or oxygen scavengers? Second, could the transmetallation process be going beyond monopivalate Mg(OPiv)Cl products to bispivalate $Mg(OPiv)_2$ products?[9] Seeking possible answers to these questions we devised different experiments. First we attempted to prepare an authentic sample of $Mg(OPiv)_2$ via an alternative metallation approach, avoiding zinc transmetallation, by magnesiating pivalic acid in heptane/THF solution and crystallising the product from hot toluene [(Eqn. 2)].

$$2\ Me_3CCO_2H + MgBu_2 \longrightarrow [\{Mg_6(OPiv)_{12}\}(MgO)_2] \quad (\mathbf{2})$$

Significantly, X-ray crystallography revealed this product $[\{Mg_6(OPiv)_{12}\}(MgO)_2]\cdot C_7H_8$, **2**, was also contaminated by O^{2-} ions, trapped within the discrete octanuclear cluster (Fig. 1).[4] As this preparation of **2** proved reproducible we initially assumed that the O^{2-} was coming from pivalic acid solution since it was used as received without drying. However on thoroughly drying the pivalic acid by using a desiccator filled with P_2O_5 we still observed O^{2-} contamination. Eventually we traced the contamination to the commercial $Mg(^nBu)_2$ used to prepare the pivalate [(Eqn.2)] as on switching to $Mg(CH_2SiMe_3)_2$ which we prepared ourselves, purified by sublimation and stored as a solid in a dry box, no contamination was observed (confirmed by NMR and elemental analysis data, see S.I.). This result suggests that $Mg(OPiv)_2$ could be functioning as a decontaminating agent mopping up any OH^- or related ions and trapping them in clusters, to thus protect zinc organometallic species present in the same solution from such contaminants.

[*] Dr. A. Hernán-Gómez, E. Herd, Prof. E. Hevia, Dr. A. R. Kennedy, Prof. R. E. Mulvey
WestCHEM, Department of Pure and Applied Chemistry
University of Strathclyde, Glasgow, G1 1XL (UK)
E-mail: r.e.mulvey@strath.ac.uk

Prof. Dr. P. Knochel, S. M. Manolikakes
Department Chemie, Ludwig Maximilians-Universität München
Butenandstrasse 5-13, Haus F, 81377 München (Germany)
E-mail: paul.knochel@cup.uni-muenchen.de

Prof. Dr. K. Koszinowski, C. Schnegelsberg
Institut für Organische und Biomolekulare Chemie
Georg-August Universität Göttingen
Tammannstrasse 2, 37077 Göttingen (Germany)

[**] We thank the UK Engineering and Physical Science Research Council (R.E.M.), the European Research Council (E.H. and P.K.), the Royal Society (E.H. and R.E.M.), and the Deutsche Forschungsgemeinschaft (K.K. and C.S.) for sponsoring this research. K.K. and C.S. also thank Prof. Dietmar Stalke for the access to his glove box.

Supporting information for this article is available on the WWW under http://www.angewandte.org

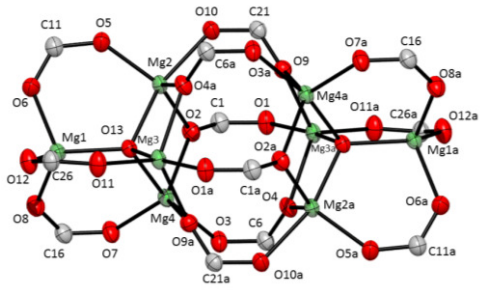

Figure 1. Molecular structure of $[\{Mg_6(OPiv)_{12}\}(MgO)_2]\cdot C_7H_8$ (**2**) with hydrogen atoms, solvent molecule, *t*-Bu group and disorder omitted.

Secondly we revisited the transmetallation monitoring it by ^{1}H (including DOSY) and ^{13}C NMR spectroscopy in d$_8$-THF solution but now using a less sensitive *p*-tolyl probe to follow the fate of the aryl ligand [(Eqn. 3)].

$$Me(p\text{-}C_6H_4)MgCl + Zn(OPiv)_2 \xrightarrow[n\ LiCl]{THF} Me(p\text{-}C_6H_4)ZnCl + Mg(OPiv)_2 \quad (3)$$
$$(n = 1 \text{ or } 2 \text{ eq})$$

For comparison we also recorded the spectra of the individual components of the mixture Me(*p*-C$_6$H$_4$)MgCl.LiCl and Me(*p*-C$_6$H$_4$)ZnCl.LiCl. Most informatively ^{13}C NMR spectra (Fig. 2) revealed well separated C$_{ipso}$ resonances for Me(*p*-C$_6$H$_4$)MgCl.LiCl (165.8 ppm) and Me(*p*-C$_6$H$_4$)ZnCl.LiCl (153.0 ppm).

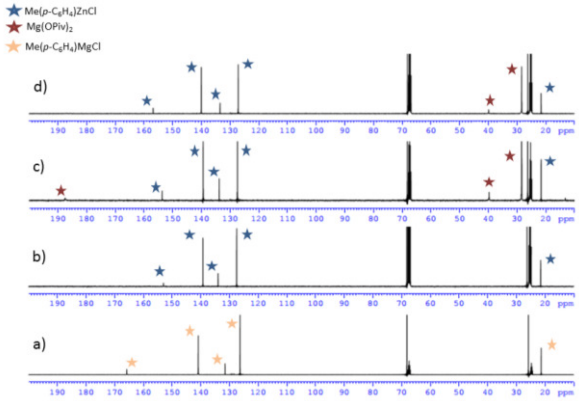

Figure 2. ^{13}C NMR spectrum of a) Me(*p*-C$_6$H$_4$)MgCl·LiCl; b) Me(*p*-C$_6$H$_4$)ZnCl·LiCl; c) Zn(OPiv)$_2$·LiCl and Me(*p*-C$_6$H$_4$)MgCl; d) Zn(OPiv)$_2$·2LiCl and Me(*p*-C$_6$H$_4$)MgCl in [D$_8$]THF at 25°C.

Significantly the reaction mixture of Me(*p*-C$_6$H$_4$)MgCl and Zn(OPiv)$_2$.nLiCl (n = 1 or 2) shows aromatic resonances matching those of Me(*p*-C$_6$H$_4$)ZnCl.LiCl with none corresponding to Me(*p*-C$_6$H$_4$)MgCl.LiCl. Also, the ^{1}H DOSY NMR spectrum of the reaction mixture revealed that the aromatic resonances and pivalate resonance belong to distinct molecules as their diffusion coefficients differ, being 6.87 10^{-10} m^2/s and 5.42 10^{-10} m^2/s respectively.

Complementary insight was obtained from electrospray ionization (ESI) mass spectrometry, which selectively probes the charged components of the sampled solution. Analysis of the reaction mixture of Me(*p*-C$_6$H$_4$)MgCl and Zn(OPiv)$_2$.nLiCl (n = 1 or 2) in the negative-ion mode identified various zincate species $Me(p\text{-}C_6H_4)_yZn_yCl_yX(LiCl)_z^-$ (y = 1-3; z = 0, 1; X = Cl, OPiv), which were largely depleted in pivalate ligands (Figs S19 and S20). These complexes are similar to ordinary zincates made by transmetallation of zinc halides by RLi reagents.[10] In contrast, pivalate-rich species were detected upon positive-ion mode ESI of the reaction mixture of Me(*p*-C$_6$H$_4$)MgCl and Zn(OPiv)$_2$LiCl (Fig. S33). The most abundant cations observed also contained an OH group, thus resembling **1** in this respect.

Collectively these observations are consistent with almost complete transmetallation of Zn(OPiv)$_2$ to Mg(OPiv)$_2$ with Zn receiving the aryl and Cl ligands. This Zn heteroleptic complex was successfully trapped as its TMEDA solvate (TMEDA)ZnMe(*p*-C$_6$H$_4$)Cl, **3**. X-ray crystallography shows **3** is a simple distorted tetrahedral monomer.[4] Unit cell checks of crystals grown by adding TMEDA to the original reaction mixture [Me(*p*-C$_6$H$_4$)ZnCl.LiCl and Mg(OPiv)$_2$ in toluene solution] revealed **3** also, confirming that complete transmetallation to Me(*p*-C$_6$H$_4$)ZnCl had occurred and that the latter was not interacting with Mg(OPiv)$_2$ coproduct but segregated from it.

Light has also been shed on the solubilising effect of LiCl on Zn(OPiv)$_2$. Barely soluble in THF, Zn(OPiv)$_2$ dissolves on addition of LiCl (one equivalent). The resulting solution deposited crystals elucidated by X-ray crystallography as [(THF)$_2$Li$_2$(μ-Cl)$_2$(μ-OPiv)$_2$Zn], **4**. Solubility can therefore be attributed to forming this molecular complex (Fig. 3) through the amphoteric Lewis acidic-Lewis basic resource of the salt which completes the coordination of both the Lewis basic OPiv group and Lewis acidic Zn atom.

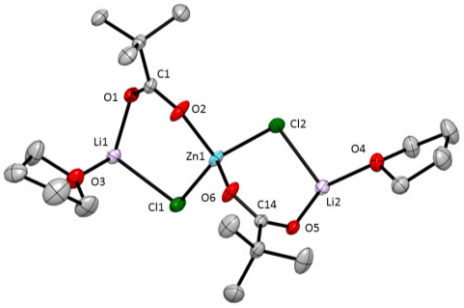

Figure 3. Molecular structure of [(THF)$_2$Li$_2$(μ-Cl)$_2$(μ-OPiv)$_2$Zn] (**4**) with hydrogen atoms omitted for clarity.

Having established that the reaction mixture in Eqn. 3 gave Me(*p*-C$_6$H$_4$)ZnCl and Mg(OPiv)$_2$ products, next we studied the air stability of the former both in the absence and presence of the latter (see Table S5 in S.I.). When a THF solution of the arylzinc reagent was exposed to air for 1 hr, 90% survived with only 10% hydrolysed to toluene (as determined from NMR spectra: note that the error associated with these values are accordingly ± 5% so trends observed are more significant than absolute values).[4] A modest increase in decomposition (to 12%) was observed on exposing solid Me(*p*-C$_6$H$_4$)ZnCl in the same way. These already high stabilities increased to 95% (solution form) and slightly decreased to 83% (solid form) in the presence of in situ generated Mg(OPiv)$_2$. These values decreased to 87% and 69% respectively on using two equivalents of LiCl. The hygroscopic property of LiCl may be a factor in this deterioration as captured H$_2$O could hydrolyse *p*-C$_6$H$_4$Me anions to toluene especially as the salt is incorporated within the molecular structure of Zn complex **4.** Changing the *p*-C$_6$H$_4$Me ligand to Bu also proved insightful. NMR (^{1}H and ^{13}C) studies[4] suggested reaction of Bu$_2$Mg and Zn(OPiv)$_2$ with added LiCl (1 or 2 equivalents) in THF solution followed a similar complete transmetallation course [(Eqn. 4)] to that of its aryl analogue generating Bu$_2$Zn.2LiCl and Mg(OPiv)$_2$.

$$MgBu_2 + Zn(OPiv)_2 \xrightarrow[n\ LiCl]{THF} ZnBu_2 + Mg(OPiv)_2 \quad (4)$$
$$(n = 1 \text{ or } 2 \text{ eq})$$

Repeating air exposure experiments revealed that both Bu$_2$Zn.2LiCl and the mixture Bu$_2$Zn.2LiCl/Mg(OPiv)$_2$ hydrolyse completely in both THF solution and solid form. Remarkably, however, on adding 5 equivalents of Mg(OPiv)$_2$, 39% of Bu$_2$Zn.2LiCl survived. Moreover, 51% survival was seen for a THF solution mixture of Bu$_2$Zn.LiCl and Mg(OPiv)$_2$ as determined by the Bu$^-$: ^{t}BuCO$_2^-$ ratio seen in NMR spectra. Moist air had a slightly more detrimental effect than dry air as the mixture Me(*p*-C$_6$H$_4$)MgCl/Zn(OPiv)$_2$.2LiCl

experienced 13 and 7% decomposition respectively on such exposure, presumably because water reacts faster than O_2 with the aryl species. To study more the effect of moisture we stored an NMR sample of a [D_8-THF] solution of $Mg(OPiv)_2$ outside of the glovebox. After 3 days a small amount of pivalic acid was detectable.[4] Collectively these experiments suggest that $Mg(OPiv)_2$ deprotonates water extremely slowly which supports our earlier view that the OH^- and O^{2-} contamination in **1** and **2** came "preformed" in the starting Mg reagent.

While these experiments show that $Mg(OPiv)_2$ can mop up OH^- and O^{2-} ions in contaminated solutions the question remains "how can $Mg(OPiv)_2$ protect organozinc compounds from air in non-contaminated solutions?" A clue may lie in how Mg salts incorporate water in their coordination spheres. For example, the acetate tetrahydrate $Mg(MeCOO)_2(H_2O)_4$ contains dative Mg-O(H_2O) bonds but also intermolecular hydrogen bonds.[11] To probe this idea with $Mg(OPiv)_2$ we evaporated a THF solution containing it and water in a 1:3 ratio. This produced [{$Mg(OPiv)(THF)_2$}(μ-$OPiv)_2$(μ-H_2O){$Mg(H_2O)(OPiv)(HOPiv)$}].H_2O, **5**. X-ray studies[4] revealed a dinuclear subunit of 2 Mg centres linked via 1 H_2O and 2 pivalate anion bridges. Another pivalate and 2 THF ligands also terminally bind to 1 Mg, while the other Mg carries a terminal pivalate, pivalic acid and H_2O ligand set. Completing the structure (Fig. 4) is a H_2O molecule of crystallization, which engages in hydrogen bonds to 2 pivalates and 1 H_2O molecule from different dinuclear subunits to give a tetrameric unit overall. Since pivalic acid was not observed in the characterization of the $Mg(OPiv)_2$ used for crystallization, a small degree of metallation of H_2O by $Mg(OPiv)_2$ takes place over the 2 week period needed to grow crystals.

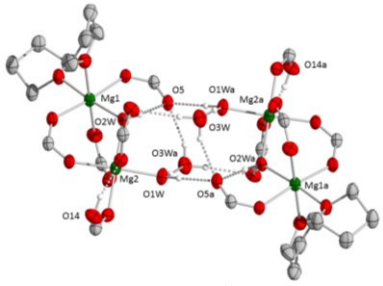

Figure 4. X-ray crystallographic structure of [{$Mg(OPiv)(THF)_2$}(μ-$OPiv)_2$(μ-H_2O){$Mg(H_2O)(OPiv)(HOPiv)$}].H_2O (**5**) with *t*-Bu group and disorder omitted for clarity.

Next we checked whether in addition to its stabilising role $Mg(OPiv)_2$ had any appreciable effect on the Negishi cross-coupling capability of the Me(*p*-C_6H_4)ZnX reagent. The answer appears no, as indicated by the narrow range of high yields obtained for the biaryl product **11** (Table 1) from reactions of ethyl 4-iodobenzoate with different zinc reagents [X = Cl.$MgCl_2$.LiCl; Cl.$Mg(OPiv)_2$.LiCl; Cl.LiCl; or OPiv.LiOPiv] in THF under identical conditions. We then turned to the much slower reaction with 4-bromoanisole to probe the effect of air and the more polar solvent EtOAc. To make sure the reactivity was the same, the cross-coupling with **12** (0.8 equiv.) in the presence of 3 mol% $Pd(OAc)_2$ and 6 mol% of DavePhos in THF under argon have been repeated to give biphenyl **13** in 82 to 86 % yield (Table 2, entries 1, 5, 9 and 13; note that the homocoupled biphenyl **14** was also observed in reactions but always as the minor product in about 10% yield). Cross-couplings were then performed in air in non-dried glassware but in dry THF. For pivalate-free reactions the yield dropped slightly from 85 to 77 % for reagent **6** and from 86 to 81 % for reagent **8** (entries 2 and 10). For pivalate-containing reagents **7** and **9** however, the yield increased from 82 to 88 % for both reagents (entries 6 and 14).

Table 1. Reactivity of zinc reagents 6-9 towards cross-coupling with ethyl 4-iodobenzoate (**10**).

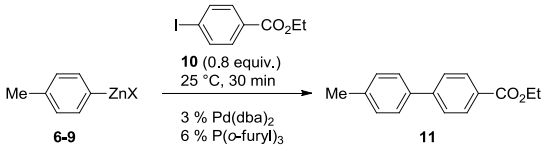

Entry	X	Isolated yield of **11**
1	Cl·$MgCl_2$·LiCl (**6**)	91 %
2	Cl·$Mg(OPiv)_2$·LiCl (**7**)	89 %
3	Cl·LiCl (**8**)	94 %
4	OPiv·LiOPiv (**9**).	93 %

Table 2. Reactivity of zinc reagents **6-9** towards cross-coupling with 4-bromoanisole (**12**).

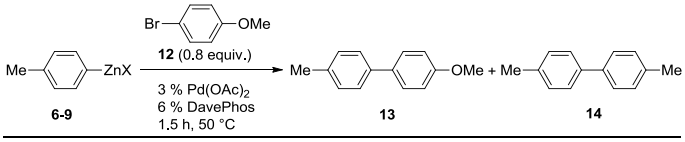

Entry	X	Solvent	Reaction Conditions	Isolated yield of **13** (%)
1	Cl•$MgCl_2$•LiCl (**6**)	THF	under Ar	85
2	Cl·$MgCl_2$·LiCl (**6**)	THF	in air	77
3	Cl·$MgCl_2$·LiCl (**6**)	EtOAc[a]	under Ar	91
4	Cl·$MgCl_2$·LiCl (**6**)	EtOAc[a]	in air	78
5	Cl·$Mg(OPiv)_2$·LiCl (**7**)	THF	under Ar	82
6	Cl·$Mg(OPiv)_2$·LiCl (**7**)	THF	in air	88
7	Cl·$Mg(OPiv)_2$·LiCl (**7**)	EtOAc[a]	under Ar	85
8	Cl·$Mg(OPiv)_2$·LiCl (**7**)	EtOAc[a]	in air	81
9	Cl·LiCl (**8**)	THF	under Ar	86
10	Cl·LiCl (**8**)	THF	in air	81
11	Cl·LiCl (**8**)	EtOAc[a]	under Ar	trace [b,c]
12	Cl·LiCl (**8**)	EtOAc[a]	in air	trace [b,c]
13	OPiv·LiOPiv (**9**)	THF	under Ar	82 %
14	OPiv·LiOPiv (**9**)	THF	in air	88 %
15	OPiv·LiOPiv (**9**)	EtOAc[a]	under Ar	trace [b,c]
16	OPiv·LiOPiv (**9**)	EtOAc[a]	in air	trace [b,c]

[a] Bought from Fluka in analytical grade (99.9 %) EtOAc was stored in air and used without further drying. [b] Only GC-Analysis of hydrolyzed/iodolyzed reaction aliquots was performed, no product was isolated. [c] Reaction was also done with 6 mol% $Pd(OAc)_2$ and 12 mol% DavePhos and the reaction time increased to 24 h.

When the cross-couplings were done in EtOAc and under Ar the yields for Mg salt containing reagents **6** and **7** increased to 91 % and 85 %, respectively (entries 3 and 7). However the yield dropped slightly for both reagents when the reaction was done in air in non-dried glassware (entries 4 and 8). Remarkably when no Mg salt was present, cross-coupling did not work at all no matter if it was performed under Ar or in air (entries 11-12, 15-16). As GC-samples quenched with I_2 showed the metal species **8** and **9** did not decompose when the reaction was performed under Ar and nor did the amount of electrophile decrease significantly. A longer reaction time and a higher catalyst loading did not lead to any improvements.

However, for the reactions carried out in air a slow decomposition of the metal species could be observed.

In summary, combining RMgX (R = aryl, alkyl) with $Zn(OPiv)_2$ in THF solution gives the fully transmetallated products RZnX and $Mg(OPiv)_2$ which, from NMR and ESI-mass spectrometric evidence seem to exist separately. Air exposure tests disclose that while (aryl)ZnCl reagents show inherently better stability towards air than (alkyl)ZnCl reagents,[12] remarkably $Mg(OPiv)_2$ can enhance this stability by mopping up OH^- or O^{2-} antagonists and capturing and holding on to H_2O molecules making them less accessible for hydrolysing C-Zn bonds.[13] LiCl appears to show an opposite effect in reducing the stability of organozinc pivalate reagents presumably because LiCl is incorporated within the Zn structure [unlike $Mg(OPiv)_2$ which is separated from it] and thus brings H_2O molecules into close proximity to Zn-C bonds.

Experimental Section

Full experimental details are included in Supporting Information. CCDC-953398 (**1**), 953399 (**2**), 953400 (**3**), 953401 (**4**) and 971345 (**5**) contain the supplementary crystallographic data for this paper. These data can be obtained free of charge from The Cambridge Crystallographic Data Centre via www.ccdc.cam.ac.uk/data_request/cif.

Received: ((will be filled in by the editorial staff))
Published online on ((will be filled in by the editorial staff))

Keywords: cross-coupling • ESI mass spectrometry • NMR spectroscopy • organomagnesium reagents • organozinc reagents • salt effects • X-ray crystallography

[1] a) D. Seebach, A. K. Beck, A. Studer in Modern Synthetic Methods (Eds.: B. Ernst, C. Leumann), Wiley-VCH, **1995**, pp. 1-178; b) E. Juaristi, A. K. Beck, J. Hansen, T. Matt, T. Mukhopadhyay, M. Simson, D. Seebach, *Synthesis*, **1993**, 12, 1271-1290; c) M. Hatano, K. Ishihara in *Acid Catalysis in Modern Organic Synthesis* Vol. 1, (Eds.: H. Yamamoto, K. Ishihara), Wiley-VCH, Weinheim, **2008**, pp. 175–182; d) M. Hatano, S. Suzuki, K. Ishihara, *J. Am. Chem. Soc*. **2006**, 128, 9998; e) M. Hatano, O. Ito, S. Suzuki, K. Ishihara, *Chem. Commun.* **2010**, 46, 2674; f) M. Hatano, S. Suzuki, K. Ishihara, *Synlett*, **2010**, 321; g) M. Hatano, K. Ishihara, *Synthesis,* **2008**, 1647; h) L. Jin, C. Liu, J. Liu, F. Hu, Y. Lan, A. S. Batsanov, J. A. K. Howard, T. D. Marder, A. Lei, *J. Am. Chem. Soc*. **2009**, 131, 16656; i) A. Metzger, S. Bernhardt, G. Manolikakes, P. Knochel, *Angew. Chem.* **2010**, 122, 4769; *Angew. Chem. Int. Ed.* **2010**, 49, 4665; j) E. Hevia, R. E. Mulvey, *Angew. Chem. Int. Ed.* **2011**, 50, 6448

[2] a) B. Haag, M. Mosrin, H. Ila, V. Malakhov, P. Knochel, *Angew. Chem., Int. Ed.* **2011**, 50, 9794; b) R. R. Kadiyala, D. Tilly, E. Nagaradja, T. Roisnel, V. E. Matulis, O. A. Ivashkevich, Y. S. Halauko, F. Chevallier, P. C. Gros, F. Mongin, *Chem. Eur. J.*, **2013**, 19, 7944; c) K. Snégaroff, S. Komagawa, F. Chevallier, P. C. Gros, S. Golhen, T. Roisnel, M. Uchiyama, F. Mongin, *Chem. Eur. J.*, **2010**, 16, 8191.

[3] a) S. Bernhardt, G. Manolikakes, T. Kunz, P. Knochel, *Angew. Chem., Int. Ed.* **2011**, 50, 9205; b) C. I. Stathakis, S. Bernhardt, V. Quint, P. Knochel, *Angew. Chem., Int. Ed.*, **2012**, 51, 9428; c) C. I. Stathakis, S. M. Manolikakes, P. Knochel, *Org. lett.*, **2013**, 15, 1302.

[4] See supporting information for full experimental details.

[5] a) D. Li, C. Sun, P. G. Williard, *J. Am. Chem. Soc*. **2008**, 130, 11726; b) D. Li, R. Hopson, W. Li, J. Liu, P. G. Williard, *Org. Lett.*, **2008**, 10, 909; c) G. Kagan, W. Li, R. Hopson, P. G. Williard, *Org. Lett*, **2009**, 11, 4818; d) D. Li, G. Kagan, R. Hopson, P. G. Williard, *J. Am.Chem. Soc.*, **2009**, 131, 5627.; e) D. R. Armstrong, P. G. Alvarez, A. R. Kennedy, R. E. Mulvey, J. A. Parkinson, *Angew. Chem., Int. Ed.* **2010**, 49, 3185; f) D. R. Armstrong, A. R. Kennedy, R. E. Mulvey, J. A. Parkinson, S. D. Robertson, *Chem. Sci.*, **2012**, 3, 2700.

[6] For DOSY reviews see: a) D. Li, I. Keresztes, R. Hopson, P. Williard, *Acc. Chem. Res.,* **2009**, 42, 270; b) A. Macchioni, G. Ciancaleoni, C. Zuccaccia, D. Zuccaccia, *Chem. Soc. Rev.*, **2008**, 37, 479; c) B. Antalek, *Concepts Magn. Reson. Part A*, **2007**, 30, 219.

[7] Additional small signals were observed in the aromatic region, which can possibly be assigned to the minor presence of a biaryl side product; see supporting information for ^{1}H DOSY NMR spectroscopy.

[8] Substitutional disorder for Mg2 was observed with an occupancy of 87% for Mg2 and 13% for Zn2, possibly due to the presence of an excess of $Zn(OPiv)_2$ in the reaction media.

[9] A. Cote, A.B. Charette, *J Am. Chem. Soc.*, **2008**, 130, 2771.

[10] J. E. Fleckenstein, K. Koszinowski, *Organometallics* **2011**, *30*, 5018.

[11] D. E. Irish, J. Semmler, N. J. Taylor, G. E. Toogood, *Acta Cryst.,* **1991**, *C47*, 2322.

[12] The diminished sensitivity of Zn-C(aryl) bonds has been commented on: A.R. Katritzky, Z. Luo, *Heterocycle*, **2011**, *55*, 1467.

[13] R.E. Mulvey, *Dalton Trans.*, **2013**, *42*, 6676.

Entry for the Table of Contents (Please choose one layout)

Layout 1:

Organozinc Reagents

Alberto Hernán-Gómez, Emma Herd, Eva Hevia, Alan R. Kennedy, Paul Knochel,* Konrad Koszinowski, Sophia M. Manolikakes, Robert E. Mulvey,* and Christoph Schnegelsberg

_____ Page – Page

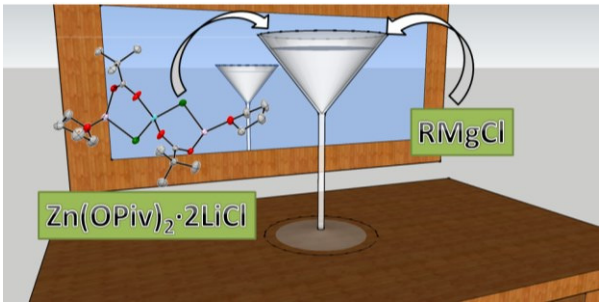

(un)Mixing Cocktails: The secret ingredient in complicated multicomponent organozinc solution mixtures is magnesium pivalate, which enhances the air stability of Zn-C bonds by cleaning up OH^- or O^{2-} antagonists and capturing H_2O molecules making them less accessible for hydrolysis.

Supporting Information

Organozinc Pivalate Reagents: Segregation, Solubility, Stabilisation and Structural Insights

Alberto Hernán-Gómez,[a] Emma Herd,[a] Eva Hevia,[a] Alan R. Kennedy,[a] Paul Knochel,[b] Konrad Koszinowski,[c] Sophia M. Manolikakes,[b] Robert E. Mulvey,[a] and Christoph Schnegelsberg.[c]

[a]*WestCHEM, Department of Pure and Applied Chemistry, University of Strathclyde, Glasgow, UK, G1 1XL. E-mail: eva.hevia@strath.ac.uk.*

[b] *Department Chemie, Ludwig Maximilians-Universität München, Butenandstrasse 5-13, Haus F, 81377 München (Germany), E-mail: paul.knochel@cup.uni-muenchen.de*

[c] *Institut für Organische und Biomolekulare Chemie, Georg-August Universität Göttingen, Tammannstrasse 2, 37077 Göttingen (Germany)*

General Methods

All reactions were performed under a protective argon atmosphere using standard Schlenk techniques. *n*-Hexane, THF and toluene were dried by heating to reflux over sodium benzophenone ketyl and distilled under nitrogen prior to use. $Zn(OPiv)_2$, $Zn(OPiv)_2{\cdot}2LiCl$[1], and $Me(p\text{-}C_6H_4)Li$ [2] were synthesized as described in the literature. Pivalic acid was purchased from Sigma Aldrich Chemicals, and dried prior to use by storing it for one week in a dessicator at reduced pressure containing fresh P_2O_5 as a drying agent. Methyllithium (1.6M in diethyl ether), zinc chloride, diethylzinc (1M in heptane) and di-*n*-butylmagnesium (1M in heptane) were purchased from Sigma Aldrich Chemicals, *p*-tolylmagnesium chloride (2M in THF) was purchased from Acros organics and all of them were used as received. $Mg(CH_2SiMe_3)_2$ was prepared from the Grignard reagent $(Me_3SiCH_2)MgCl$ by manipulation of the Schlenk equilibrium via the dioxane precipitation method. The resultant off white solid was purified via sublimation at 175°C (10-2 torr) to furnish pure $Mg(CH_2SiMe_3)_2$. NMR spectra were recorded on a Bruker DPX 400 MHz spectrometer, operating at 400.13 MHz for ^1H, 155.50 MHz for ^7Li, and 100.62 MHz for $^{13}C\{^1H\}$, and on a Bruker AV 500 MHz spectrometer operating at 500 MHz for ^1H and 125 MHz for $^{13}C\{^1H\}$. Elemental analyses were obtained using a Perkin-Elmer 2400 elemental analyzer.

---

[1] C. I. Stathakis, S. Bernhardt, V. Quint and P. Knochel, *Angew. Chem. Int. Ed.* **2012**, 51, 9428-9432
[2] M. P. R. Spee, J. Boersma, M. D. Meijer, M. Q. Slagt, G. van Koten and J. W. Geus, *J. Org. Chem.* **2001**, 66, 1647-1656.

Transmetallation study of the mixture of the arylester reagent $EtO_2C(p\text{-}C_6H_4)MgCl.LiCl$ and zinc pivalate

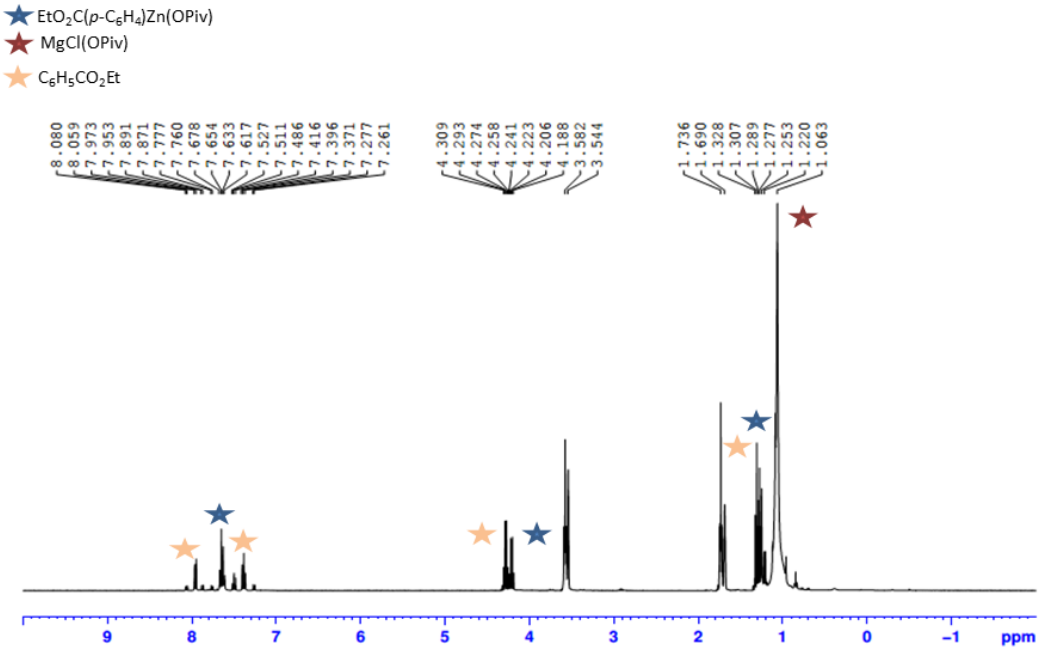

Figure S1. ^1H NMR spectrum of $Zn(OPiv)_2$ and $EtO_2C(p\text{-}C_6H_4)MgCl{\cdot}LiCl$ in [D8]THF at 25°C

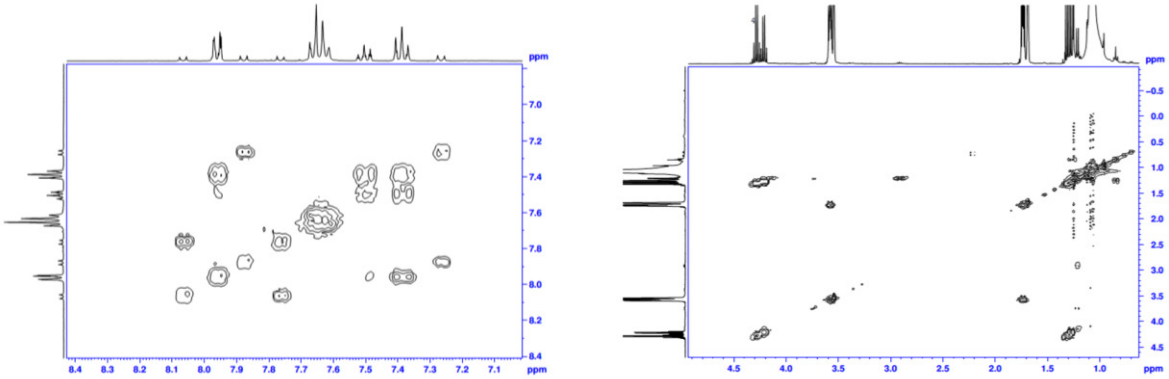

Figure S2. COSY NMR spectrum of $Zn(OPiv)_2$ and $EtO_2C(p\text{-}C_6H_4)MgCl{\cdot}LiCl$ in [D8]THF at 25°C

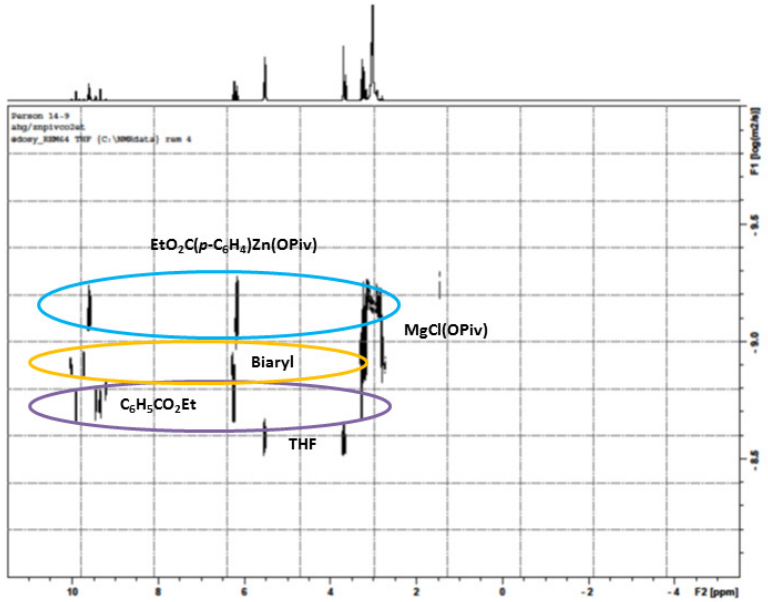

Figure S3. ^1H DOSY NMR spectrum of $Zn(OPiv)_2$ and $EtO_2C(p\text{-}C_6H_4)MgCl{\cdot}LiCl$ in [D8]THF at 25°C

X-ray crystallographic studies: Single-crystal X-ray diffraction data were measured with Oxford Diffraction (now Agilent Technologies) Xcalibur or Gemini diffractometers using MoKα (λ = 0.71073) or Cu-Kα (λ = 1.54180) radiation (see Table S1 of selected crystallographic data). The structures were solved by direct methods and refined against all unique F^2 values using programs from the SHELX suit.[3] In **1** the metal site Mg2 is partially occupied by Zn. This refined to a 0.874(4):0.126(4) Mg:Zn ratio. The THF groups were modeled as disordered over two sites. In **2** disorder was modeled for both the toluene solvate and the butyl groups. Refinement of CCDC-953398 (**1**), 953399 (**2**), 953400 (**3**) and 953401 (**4**) contain the supplementary crystallographic data for this paper. These data can be obtained free of charge from The Cambridge Crystallographic Data Centre via www.ccdc.cam.ac.uk/data_request/cif.

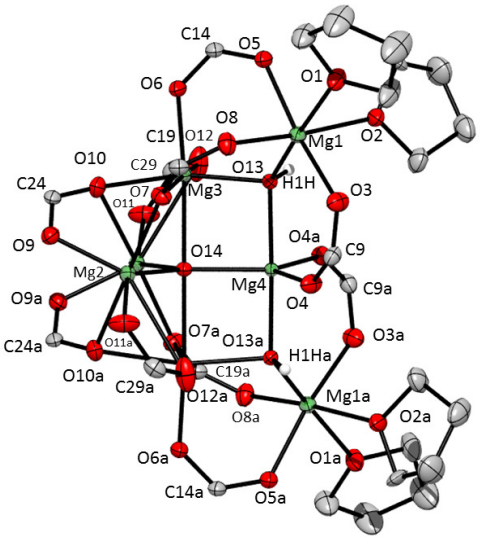

Figure S4. Crystallographically derived structure of the [{Mg(OPiv)$_2$}$_5${Mg(OH)$_2$}(MgO)·4THF] (**1**) core with hydrogen atoms, solvent molecule, tert-butyl substituent and disorder omitted for clarity. This Mg_7 species cocrystallizes with the isostructural Mg_6Zn species in a 4:1 ratio.

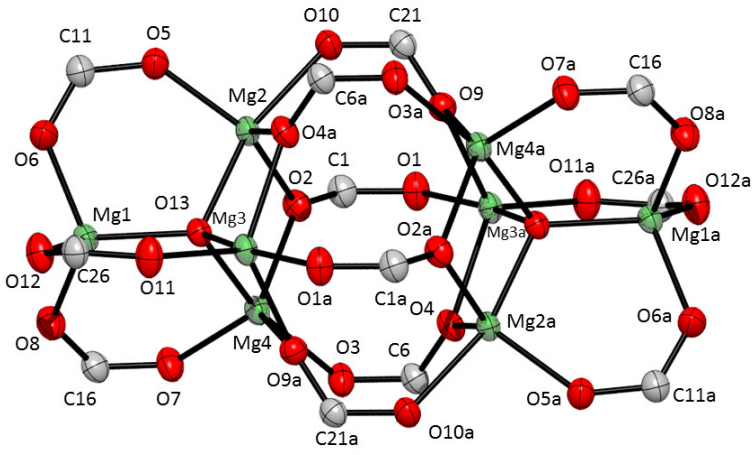

Figure S5. X-ray crystallographic structure of [{Mg_6(OPiv)$_{12}$}(MgO)$_2$]·C_7H_8 (**2**) with hydrogen atoms, solvent molecule, *tert*-butyl substituent and disorder omitted for clarity.

[3] G. M. Sheldrick, *Acta Crystallogr.* A64, **2008**, 112

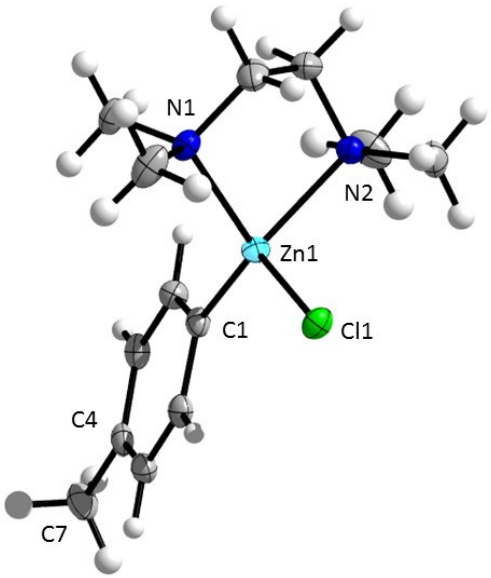

Figure S6. Molecular structure of (TMEDA)ZnMe(*p*-C_6H_4)Cl, (**3**)

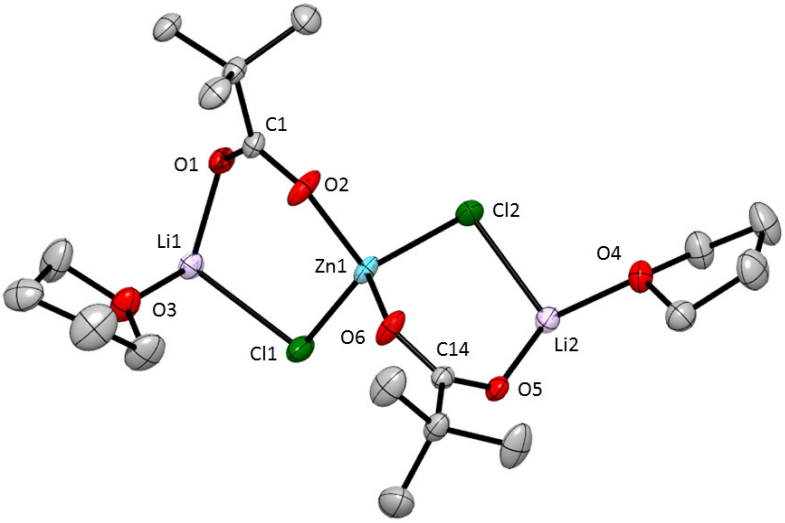

Figure S7. Molecular structure of [$(THF)_2Li_2(\mu\text{-}Cl)_2(\mu\text{-}OPiv)_2Zn$] (**4**) with H atoms omitted for clarity.

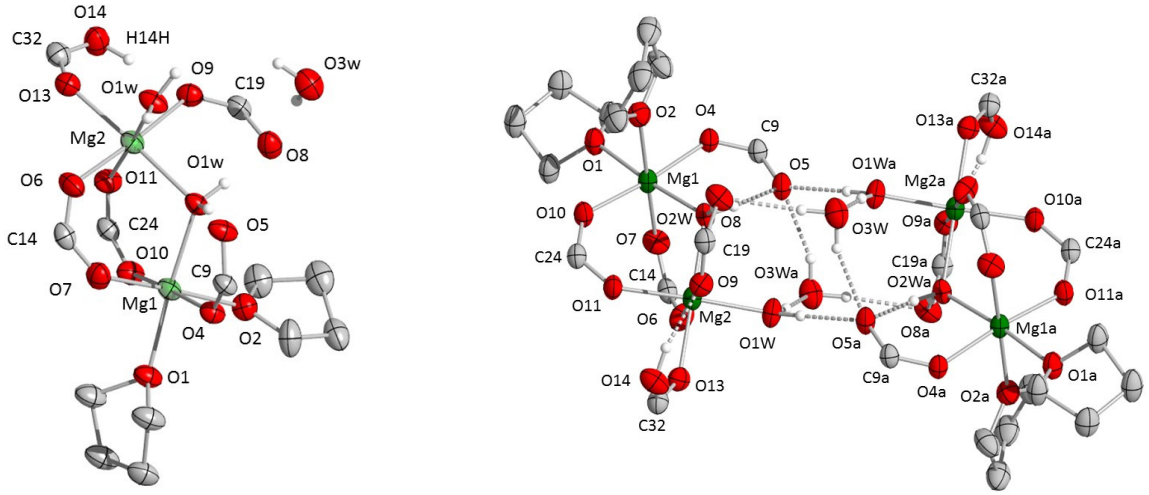

Figure S8. X-ray crystallographic structure of [{Mg(OPiv)(THF)$_2$}(μ-OPiv)$_2$(μ-H$_2$O){Mg(H$_2$O)(OPiv)(HOPiv)}].H$_2$O (**5**) with *tert*-butyl substituent and disorder omitted for clarity.

Table S1: Selected crystallographic data for new compounds **1** - **5**

	1	**2**	**3**	**4**	**5**
Empirical formula	$C_{68.64}H_{129.28}Mg_{6.75}O_{27.66}Zn_{0.25}$	$C_{74}H_{124}Mg_8O_{26}$	$C_{13}H_{23}Cl_1N_2Zn_1$	$C_{18}H_{34}Cl_2Li_2O_6Zn_1$	$C_{33}H_{68}Mg_2O_{15}$
Molecular Weight	1577.76	1624.21	308.17	496.6	753.49
Temperature (K)	123(2)	123(2)	123(2)	123(2)	123(2)
Wavelenght (Å)	0.71073	1.54180	0.71073	0.71073	0.71073
Crystal system,	Orthorhombic	Monoclinic	Monoclinic	Orthorhombic	Triclinic
Space group	C2cb	$P2_1/c$	$P2_1/c$	Pbca	P-1
a (Å)	19.2990(6)	13.1072(2)	9.9500(3)	14.9325(3)	10.753(1)
b (Å)	24.0340(7)	15.5468(3)	11.8823(3)	17.9451(5)	14.575(2)
c (Å)	18.7974(6)	23.2630(4)	12.6338(4)	18.2119(4)	15.652(1)
α (°)	90	90	90	90	67.564(10)
β (°)	90	105.827(2)	95.329(3)	90	73.940(9)
γ (°)	90	105.827(2)	90	90	76.094(9)
Cell volume (Å^3)	8718.8(5)	90	1487.22(8)	4880.2(2)	2153.7(4)
Z	4	2	4	8	2
ρ_{calc} (g.cm^{-3})	1.204	1.183	1.376	1.352	1.162
μ (mm^{-1})	0.200	1.207	1.813	1.253	1.002
2θ max(°)	58.00	147.02	60.50	58.00	140.0
Index ranges	-16≤*h*≤26 -32≤*k*≤32 -25≤*l*≤18	-16≤*h*≤15 -19≤*k*≤19 -26≤*l*≤28	-14≤*h*≤14 -16≤*k*≤16 -16≤*l*≤17	-19≤*h*≤18 -23≤*k*≤20 -24≤*l*≤14	-13≤*h*≤13 -17≤*k*≤17 -18≤*l*≤19
Reflections collected	21834	36435	14826	29165	25470
Reflections unique	8210	9049	4064	6343	8150
Reflections obs.	6661	6967	3349	4693	5546
R_{int}	0.0378	0.0597	0.0400	0.0401	0.0299
No. Parameters	533	508	159	268	591
Goodnes-of-fit-on F^2 (*GOF*)	1.063	1.053	1.032	1.098	1.035
Final *R* indices [$I>2\sigma(I)$]	0.0582	0.0636	0.0329	0.0399	0.0594
R indices (all data)	0.1557	0.193	0.081	0.0911	0.1819
Largest diff. peak and hole (e Å^{-3})	0.796 and -0.276	1.021 and -0.620	0.629 and -0.456	0.628 and -0.353	0.335 and -0.277

Synthesis of [{$Mg_6(OPiv)_{12}$}(MgO_2)]·C_7H_8 (2)

$MgBu_2$ (4 mL of a 1 M solution in heptane, 4 mmol) was added to a solution cooled at -30°C of pivalic acid (0.817 g, 8 mmol) in THF (10 mL) and the resulting yellow pale solution was stirred at room temperature for 1 h. The solvent was then removed in vacuo and toluene (10 mL) was added affording a suspension. Gentle heating gave a clear solution which was left to slow cooling, resulted in the formation of colourless crystals (0.23 g, yield 32% based on $MgBu_2$). ^{1}H NMR (400.13 MHz, [D_8]THF, 300 K): δ(ppm) = 7.20-7.08 (m, 5 H, C_6H_5, Toluene), 2.30 (s, 3 H, *Me*, Toluene), 1.14 (s, 36 H, C*Me*$_3$,.Pivalate), 1.13 (s, 18 H, C*Me*$_3$,.Pivalate), 1.11(s, 54 H, C*Me*$_3$,.Pivalate). ^{13}C{^{1}H} NMR (100.62 MHz, [D_8]THF, 300 K): δ(ppm) = 193.3, 187.8, 186.9 (O_2*C*CMe$_3$, Pivalate), 138.6, 129.7, 128.9, 126.0 (C_6H_4, Toluene), 40.0 (O_2C*C*Me$_3$, Pivalate), 28.5, 28.4, 28.1 (O_2CC*Me*$_3$, Pivalate), 21.5 (*Me*, Toluene).

Synthesis of [$Mg(OPiv)_2$]·1/2 THF

MgR_2 (0.40 g, 2 mmol) was added to a solution cooled at -30°C of pivalic acid (0.41 g, 4 mmol) in THF (10 mL) and the resulting colorless solution was stirred at room temperature for 1 h. The solvent was then removed in vacuo affording a microcrystalline white solid (0.38 g, 73%). ^{1}H NMR (400.13 MHz, [D_8]THF, 300 K): δ(ppm) = 3.62 (m, 2H, OC*H*$_2$, THF), 1.10 (s, 18 H, C*Me*$_3$,.Pivalate), 1.77 (m, 2H, C*H*$_2$, THF). ^{13}C{^{1}H} NMR (100.62 MHz, [D_8]THF, 300 K): δ(ppm) = 187.8 (O_2*C*CMe$_3$, Pivalate), 68.2 (O*C*H$_2$, THF), 39.6 (O_2C*C*Me$_3$, Pivalate), 28.4 (O_2CC*Me*$_3$, Pivalate) 26.4 (*C*H$_2$, THF). Anal. Calcd for $C_{12}H_{22}MgO_{4.5}$: C, 54.88; H, 8.44; Found: C, 54.89; H, 8.64.

Crystallization of [{Mg(OPiv)(THF)$_2$}(μ-OPiv)$_2$(μ-H_2O){Mg(H_2O)(OPiv)(HOPiv)].H_2O, (5)

Slow evaporation of a THF solution containing $Mg(OPiv)_2$ and water in a 1:3 ratio produced [{Mg(OPiv)(THF)$_2$}(μ-OPiv)$_2$(μ-H_2O){Mg(H_2O)(OPiv)(HOPiv)}].H_2O, **5** as colourless crystals suitable for X-ray crystallographic study.

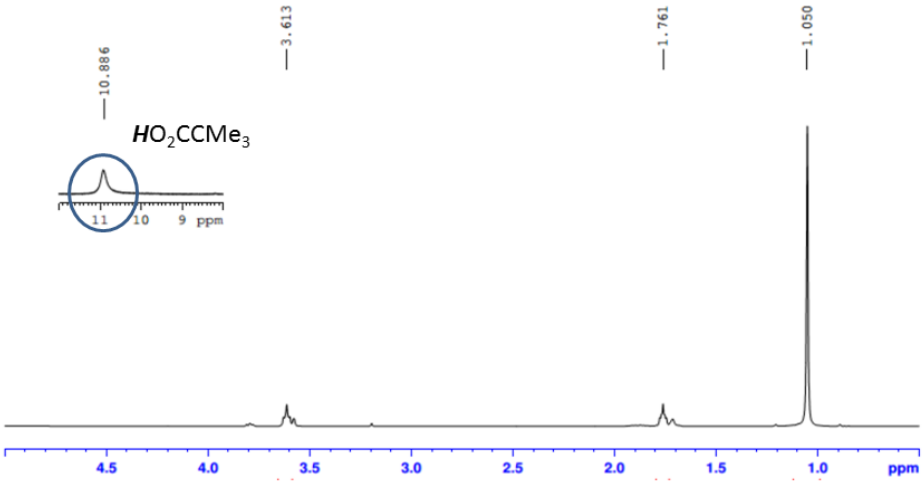

Figure S9. ^{1}H NMR spectrum of [{Mg(OPiv)(THF)$_2$}(μ-OPiv)$_2$(μ-H_2O){Mg(H_2O)(OPiv)(HOPiv)}].H_2O, **5** in [D_8]THF at 25°C.

Table S2: Hydrogen bonds parameters observed for compound [{Mg(OPiv)(THF)$_2$}(μ-OPiv)$_2$(μ-H$_2$O){Mg(H$_2$O)(OPiv)(HOPiv)}].H$_2$O, (**5**).

D-H	d(D-H) (Å)	d(H..A) (Å)	DHA (°)	d(D..A) (Å)	A
O1W-H1W	0.87	1.88	174	2.753	O3W [-x+1, -y+1, -z+2]
O1W-H2W	0.88	1.86	174	2.732	O5 [-x+1, -y+1, -z+2]
O2W-H3W	0.88	1.76	169	2.625	O5
O2W-H4W	0.87	1.73	166	2.587	O8
O3W-H5W	0.89	2.07	175	2.955	O8
O3W-H6W	0.89	2.04	158	2.887	O5 [-x+1, -y+1, -z+2]
O14-H14H_a	0.88	1.83	166	2.699	O9
O14A-H15H_b	0.93	1.87	179	2.796	O6

Stability study of [Mg(OPiv)$_2$]

Stability of [Mg(OPiv)$_2$] (0.02 g, 0.08 mmol) was tested through ^{1}H-NMR spectroscopy study at different times. Initially, ^{1}H-NMR spectrum of a [D$_8$]THF solution containing [Mg(OPiv)$_2$]·1/2 THF (0.02 g, 0.08 mmol) was recorded (Fig S10) and after storing the sample outside of the glovebox for 3 days rerecording its NMR spectrum showed formation of a small amount of pivalic acid (Fig S11), suggesting that Mg(OPiv)$_2$ deprotonates water but extremely slowly.

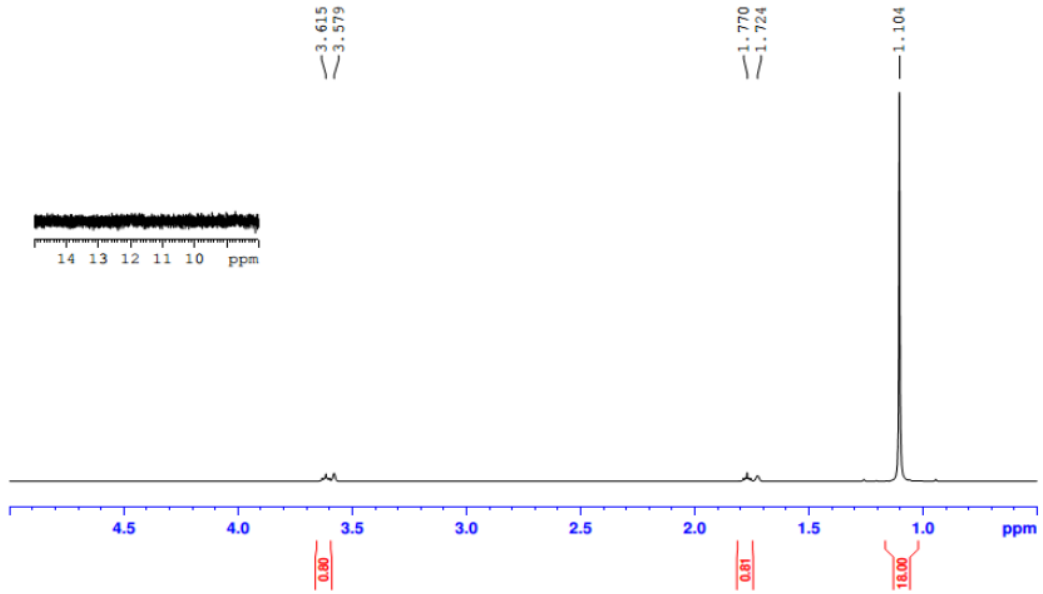

Figure S10. ^{1}H NMR spectrum of [Mg(OPiv)$_2$]·1/2 THF in [D$_8$]THF at 25°C.

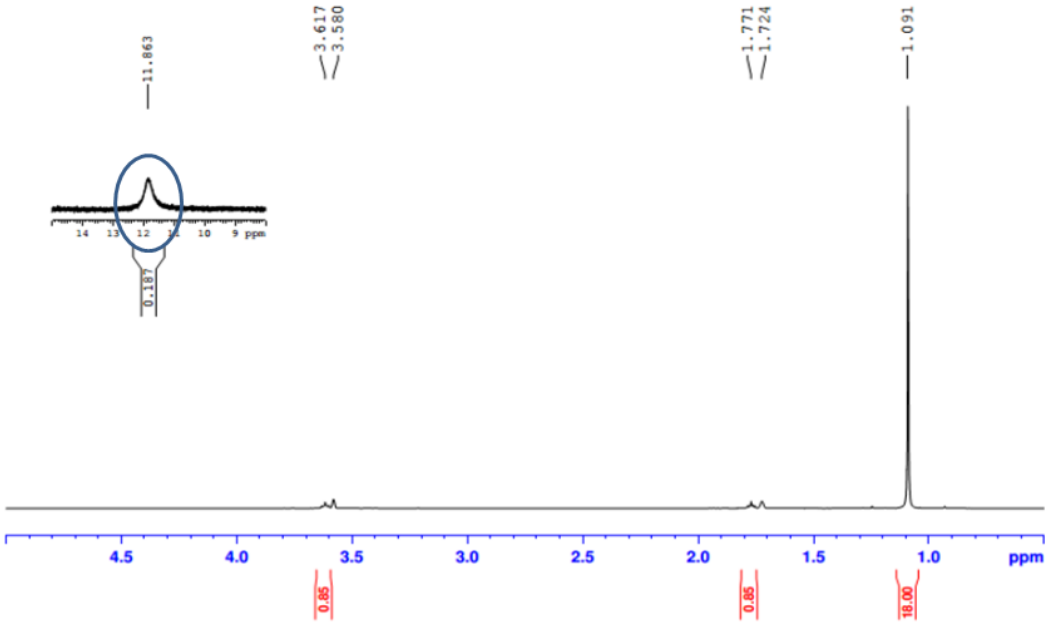

Figure S11. ^{1}H NMR spectrum of [Mg(OPiv)$_2$]·1/2 THF [D$_8$]THF at 25°C after storing the NMR sample outside of the glovebox for 3 days.

Reaction of Zn(OPiv)$_2$·nLiCl with RMgX (n=1, 2; R = p-C$_6$H$_4$Me, Bu; X = Cl, Bu)

To a solution of Zn(Opiv)$_2$·nLiCl (2 mmol) in 10 mL of THF was added Me(*p*-C$_6$H$_4$)MgCl or MgBu$_2$ (2 mmol) offering a colourless solution. After stirring the mixture at 25°C for one hour, determination of the contents for the mixture by NMR spectroscopy was carried out.

Table S3. NMR data in [D$_8$]THF at 25°C

	^{1}H/δ(ppm)	^{13}C/δ(ppm)
Me(*p*-C$_6$H$_4$)MgCl·LiCl	7.46 (d, J = 7.4 Hz, 2 H, Me(*p*-C$_6$*H$_4$*)), 6.68 (d, J = 7.4 Hz, 2 H Me(*p*-C$_6$*H$_4$*)) 2.06 (s, 3 H, *Me*(*p*-C$_6$H$_4$))	165.1, 140.1, 130.8, 125.5 Me(*p*-C$_6$*H$_4$*), 20.6 *Me*(*p*-C$_6$H$_4$)
Me(*p*-C$_6$H$_4$)ZnCl·LiCl	7.37 (d, J = 7.4 Hz, 2 H, Me(*p*-C$_6$*H$_4$*)), 6.82 (d, J = 7.4 Hz, 2 H, Me(*p*-C$_6$*H$_4$*)) 2.14 (s, 3 H, *Me*(*p*-C$_6$H$_4$))	153.0, 139.3, 134.0, 127.5 Me(*p*-C$_6$*H$_4$*), 21.6 *Me*(*p*-C$_6$H$_4$)
Me(*p*-C$_6$H$_4$)MgCl + Zn(OPiv)$_2$·LiCl	7.39 (d, J = 7.6 Hz, 2 H, Me(*p*-C$_6$*H$_4$*)), 6.81 (d, J = 7.6 Hz, 2 H Me(*p*-C$_6$*H$_4$*)) 2.14 (s, 3 H, *Me*(*p*-C$_6$H$_4$)), 1.08 (s, 18 H, CO$_2$CC*H$_3$*)	187.5 (*C*O$_2$CCH$_3$), 153.7, 139.4, 133.8, 127.4 Me(*p*-C$_6$*H$_4$*), 39.7 (CO$_2$*C*CH$_3$), 28.4 (CO$_2$C*C*H$_3$), 21.6 *Me*(*p*-C$_6$H$_4$)
Me(*p*-C$_6$H$_4$)MgCl + Zn(OPiv)$_2$·2LiCl	7.57 (d, J = 7.6 Hz, 2 H, Me(*p*-C$_6$*H$_4$*)), 6.81 (d, J = 7.6 Hz, 2 H, Me(*p*-C$_6$*H$_4$*)) 2.15 (s, 3 H, *Me*(*p*-C$_6$H$_4$)), 1.06 (s, 18 H, CO$_2$CC*H$_3$*)	Not detected (*C*O$_2$CCH$_3$), 156.8, 140.1, 133.5, 127.2 Me(*p*-C$_6$*H$_4$*), 39.9 (CO$_2$*C*CH$_3$), 28.4 (CO$_2$C*C*H$_3$), 21.6 *Me*(*p*-C$_6$H$_4$)

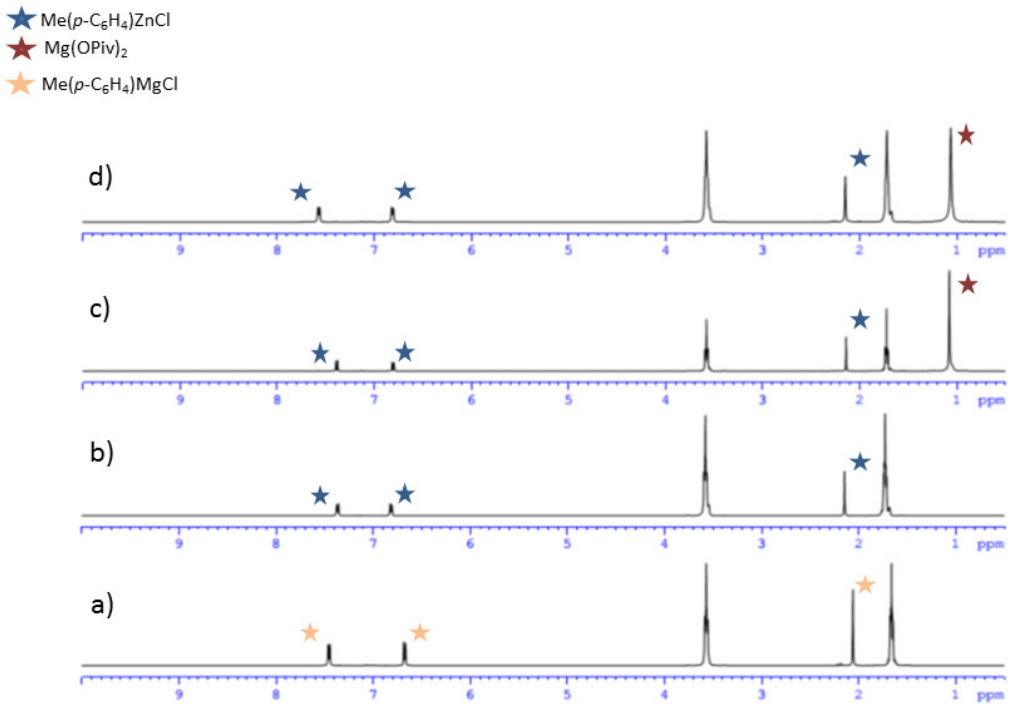

Figure S11. ^{1}H NMR spectrum of a) Me(p-C_6H_4)MgCl·LiCl; b) Me(p-C_6H_4)ZnCl·LiCl; c) Zn(OPiv)$_2$·LiCl and Me(p-C_6H_4)MgCl; d) Zn(OPiv)$_2$·2LiCl and Me(p-C_6H_4)MgCl in [D_8]THF at 25°C.

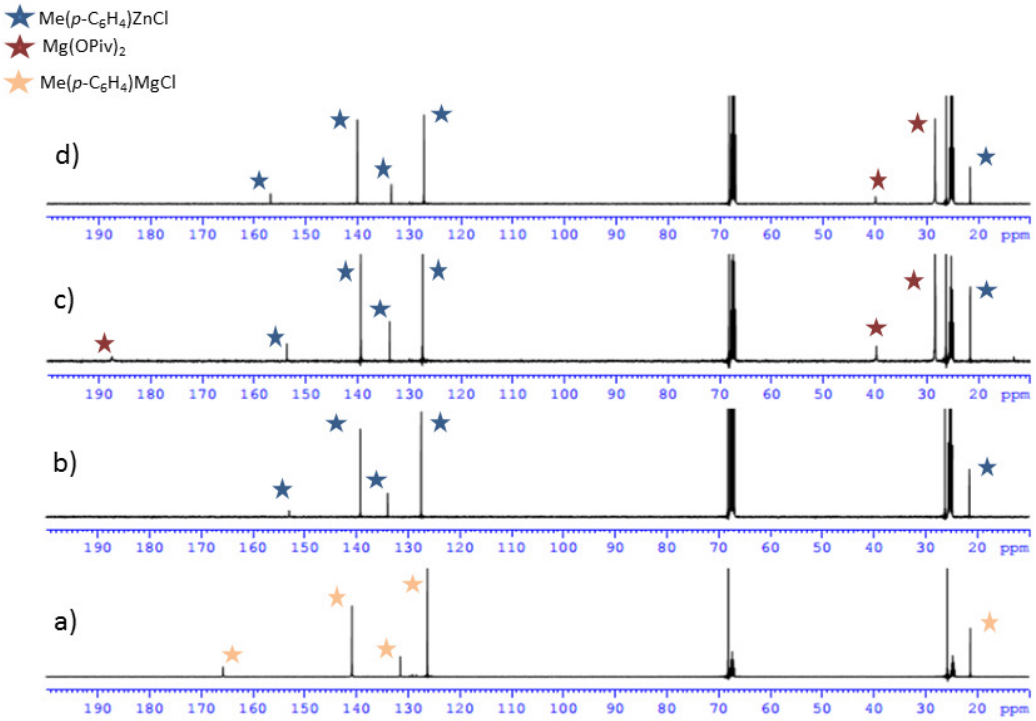

Figure S12. ^{13}C NMR spectrum of a) Me(p-C_6H_4)MgCl·LiCl; b) Me(p-C_6H_4)ZnCl·LiCl; c) Zn(OPiv)$_2$·LiCl and Me(p-C_6H_4)MgCl; d) Zn(OPiv)$_2$·2LiCl and Me(p-C_6H_4)MgCl in [D_8]THF at 25°C

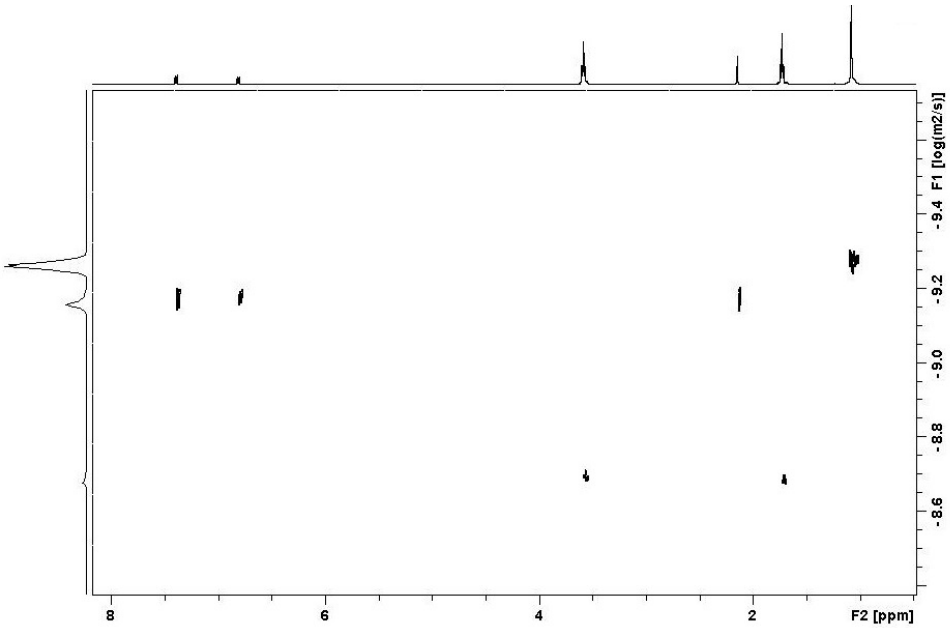

Figure S13. ^{1}H DOSY NMR spectrum of Zn(OPiv)$_2$·LiCl and Me(*p*-C$_6$H$_4$)MgCl in [D$_8$]THF at 25°C

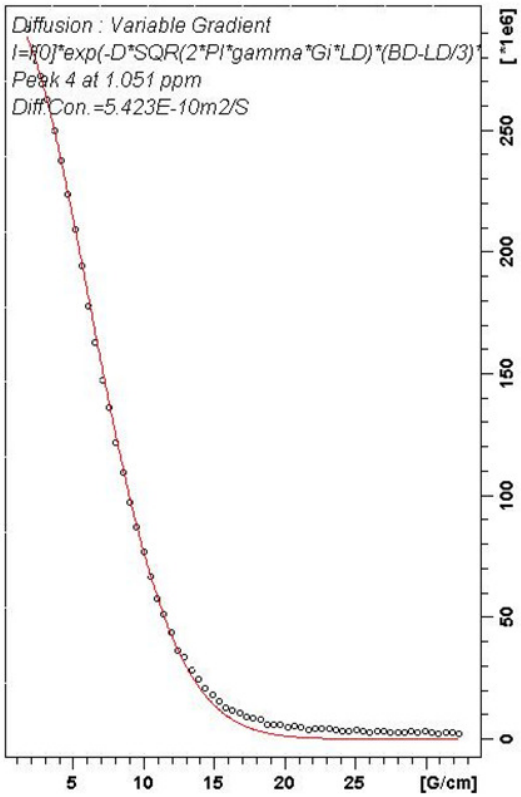

Figure S13.1. Stejskal-Tanner plot for the ^{1}H resonance at 1.051 ppm

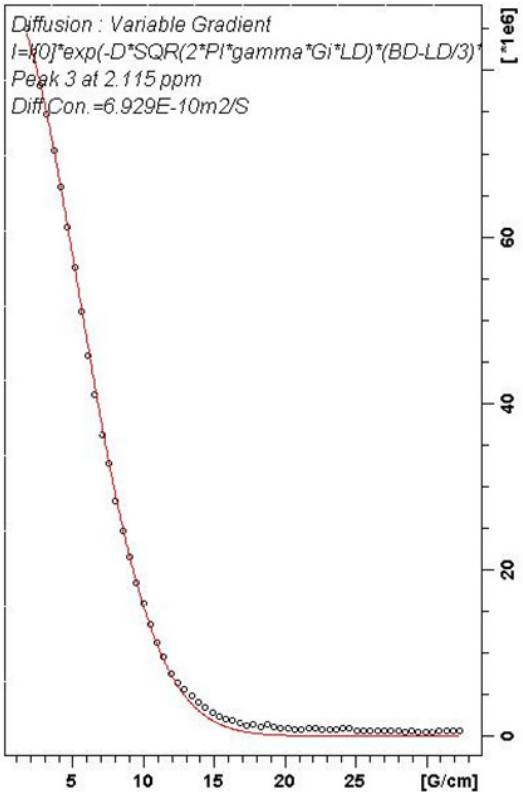

Figure S13.2. Stejskal-Tanner plot for the ^{1}H resonance at 2.115 ppm

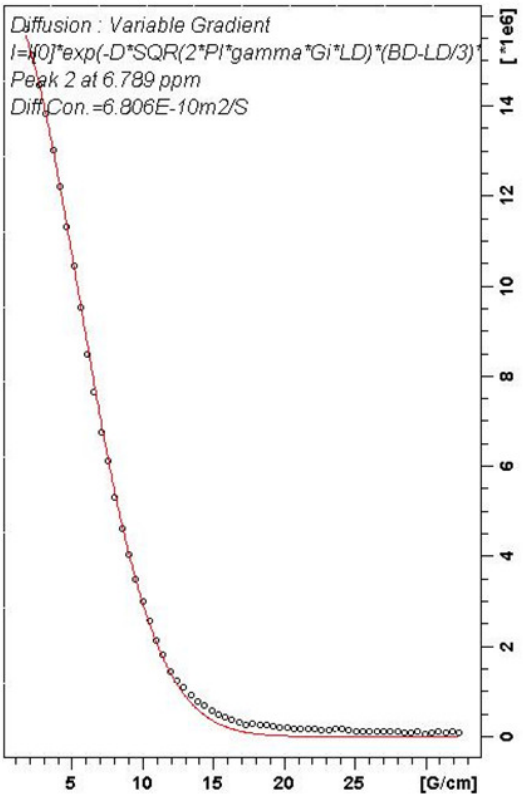

Figure S13.3. Stejskal-Tanner plot for the ^{1}H resonance at 6.789 ppm

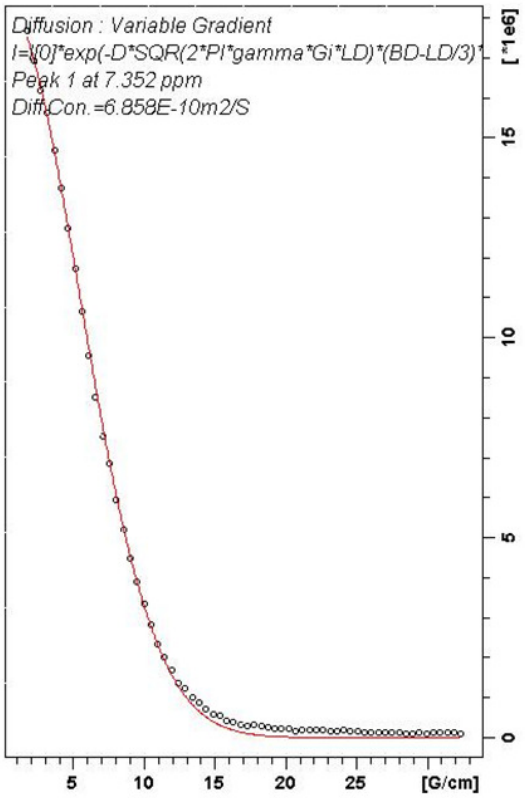

Figure S13.4. Stejskal-Tanner plot for the ^{1}H resonance at 7.352 ppm

Simfit Results

INTENSITY fit : Diffusion : Variable Gradient :

I=I[0]*exp(-D*SQR(2*PI*gamma*Gi*LD)*(BD-LD/3)*1e4)

64 points for Peak 1, Peak Point = 7.352 ppm

Converged after 62 iterations!

Results Comp. 1

I[0] = 6.320e-002
Diff Con. = 6.858e-010 m2/s
Gamma = 4.258e+003 Hz/G
Little Delta = 6.000m
Big Delta = 99.900m

RSS = 1.694e-005
SD = 5.145e-004

Point	Gradient	Expt	Calc	Difference
1	1.703e+000	6.072e-002	6.011e-002	-6.111e-004
2	2.189e+000	5.810e-002	5.818e-002	7.359e-005
3	2.676e+000	5.558e-002	5.584e-002	2.600e-004
4	3.162e+000	5.363e-002	5.317e-002	-4.642e-004
5	3.649e+000	5.044e-002	5.020e-002	-2.325e-004
6	4.135e+000	4.720e-002	4.702e-002	-1.796e-004
7	4.622e+000	4.369e-002	4.368e-002	-6.079e-006
8	5.108e+000	4.031e-002	4.025e-002	-6.331e-005

9	5.595e+000	3.659e-002	3.678e-002	1.928e-004
10	6.081e+000	3.281e-002	3.334e-002	5.302e-004
11	6.568e+000	2.925e-002	2.997e-002	7.202e-004
12	7.055e+000	2.590e-002	2.672e-002	8.185e-004
13	7.541e+000	2.350e-002	2.364e-002	1.403e-004
14	8.028e+000	2.036e-002	2.073e-002	3.678e-004
15	8.514e+000	1.781e-002	1.804e-002	2.291e-004
16	9.001e+000	1.540e-002	1.557e-002	1.635e-004
17	9.487e+000	1.341e-002	1.333e-002	-8.243e-005
18	9.974e+000	1.145e-002	1.131e-002	-1.402e-004
19	1.046e+001	9.654e-003	9.525e-003	-1.282e-004
20	1.095e+001	7.982e-003	7.954e-003	-2.834e-005
21	1.143e+001	6.946e-003	6.590e-003	-3.563e-004
22	1.192e+001	5.755e-003	5.413e-003	-3.418e-004
23	1.241e+001	4.688e-003	4.412e-003	-2.764e-004
24	1.289e+001	4.203e-003	3.565e-003	-6.375e-004
25	1.338e+001	3.440e-003	2.859e-003	-5.810e-004
26	1.387e+001	2.985e-003	2.273e-003	-7.123e-004
27	1.435e+001	2.456e-003	1.793e-003	-6.634e-004
28	1.484e+001	2.026e-003	1.402e-003	-6.237e-004
29	1.532e+001	1.841e-003	1.088e-003	-7.531e-004
30	1.581e+001	1.505e-003	8.369e-004	-6.682e-004
31	1.630e+001	1.361e-003	6.389e-004	-7.222e-004
32	1.678e+001	1.162e-003	4.835e-004	-6.782e-004
33	1.727e+001	1.043e-003	3.632e-004	-6.795e-004
34	1.776e+001	1.084e-003	2.704e-004	-8.138e-004
35	1.824e+001	9.649e-004	1.998e-004	-7.651e-004
36	1.873e+001	8.709e-004	1.463e-004	-7.246e-004
37	1.922e+001	7.996e-004	1.063e-004	-6.933e-004
38	1.970e+001	7.483e-004	7.662e-005	-6.717e-004
39	2.019e+001	7.406e-004	5.475e-005	-6.859e-004
40	2.068e+001	6.125e-004	3.883e-005	-5.737e-004
41	2.116e+001	6.169e-004	2.730e-005	-5.896e-004
42	2.165e+001	6.724e-004	1.905e-005	-6.533e-004
43	2.214e+001	6.710e-004	1.317e-005	-6.579e-004
44	2.262e+001	6.214e-004	9.042e-006	-6.123e-004
45	2.311e+001	5.909e-004	6.151e-006	-5.847e-004
46	2.360e+001	5.682e-004	4.154e-006	-5.641e-004
47	2.408e+001	6.251e-004	2.780e-006	-6.223e-004
48	2.457e+001	5.795e-004	1.847e-006	-5.776e-004
49	2.506e+001	5.417e-004	1.216e-006	-5.404e-004
50	2.554e+001	4.883e-004	7.946e-007	-4.875e-004
51	2.603e+001	4.928e-004	5.146e-007	-4.923e-004
52	2.651e+001	3.956e-004	3.309e-007	-3.953e-004
53	2.700e+001	4.330e-004	2.108e-007	-4.328e-004
54	2.749e+001	4.731e-004	1.333e-007	-4.730e-004
55	2.798e+001	4.255e-004	8.358e-008	-4.254e-004
56	2.846e+001	3.774e-004	5.201e-008	-3.773e-004
57	2.895e+001	3.719e-004	3.207e-008	-3.719e-004
58	2.943e+001	4.785e-004	1.963e-008	-4.785e-004
59	2.992e+001	3.113e-004	1.191e-008	-3.112e-004
60	3.041e+001	4.276e-004	7.170e-009	-4.276e-004
61	3.089e+001	4.726e-004	4.278e-009	-4.726e-004
62	3.138e+001	4.673e-004	2.535e-009	-4.673e-004
63	3.187e+001	4.557e-004	1.488e-009	-4.557e-004
64	3.235e+001	3.443e-004	8.663e-010	-3.443e-004

==========

64 points for Peak 2, Peak Point = 6.789 ppm

Converged after 57 iterations!

Results Comp. 1

I[0] = 5.612e-002
Diff Con. = 6.806e-010 m2/s
Gamma = 4.258e+003 Hz/G
Little Delta = 6.000m
Big Delta = 99.900m

RSS = 1.400e-005
SD = 4.677e-004

Point	Gradient	Expt	Calc	Difference
1	1.703e+000	5.391e-002	5.340e-002	-5.151e-004
2	2.189e+000	5.191e-002	5.169e-002	-2.180e-004
3	2.676e+000	4.968e-002	4.963e-002	-4.948e-005
4	3.162e+000	4.743e-002	4.727e-002	-1.576e-004
5	3.649e+000	4.470e-002	4.466e-002	-4.121e-005
6	4.135e+000	4.191e-002	4.185e-002	-5.625e-005
7	4.622e+000	3.881e-002	3.889e-002	8.728e-005
8	5.108e+000	3.592e-002	3.586e-002	-6.232e-005
9	5.595e+000	3.267e-002	3.279e-002	1.265e-004
10	6.081e+000	2.912e-002	2.975e-002	6.314e-004
11	6.568e+000	2.623e-002	2.676e-002	5.315e-004
12	7.055e+000	2.318e-002	2.388e-002	7.052e-004
13	7.541e+000	2.103e-002	2.114e-002	1.136e-004
14	8.028e+000	1.822e-002	1.856e-002	3.420e-004
15	8.514e+000	1.589e-002	1.617e-002	2.777e-004
16	9.001e+000	1.387e-002	1.397e-002	1.033e-004
17	9.487e+000	1.195e-002	1.197e-002	1.741e-005
18	9.974e+000	1.032e-002	1.017e-002	-1.427e-004
19	1.046e+001	8.787e-003	8.580e-003	-2.076e-004
20	1.095e+001	7.357e-003	7.174e-003	-1.832e-004
21	1.143e+001	6.279e-003	5.952e-003	-3.266e-004
22	1.192e+001	4.951e-003	4.896e-003	-5.420e-005
23	1.241e+001	4.301e-003	3.997e-003	-3.037e-004
24	1.289e+001	3.793e-003	3.235e-003	-5.580e-004
25	1.338e+001	3.206e-003	2.598e-003	-6.081e-004
26	1.387e+001	2.724e-003	2.069e-003	-6.549e-004
27	1.435e+001	2.333e-003	1.635e-003	-6.977e-004
28	1.484e+001	1.936e-003	1.281e-003	-6.550e-004
29	1.532e+001	1.679e-003	9.960e-004	-6.825e-004
30	1.581e+001	1.473e-003	7.677e-004	-7.057e-004
31	1.630e+001	1.293e-003	5.873e-004	-7.056e-004
32	1.678e+001	1.089e-003	4.454e-004	-6.441e-004
33	1.727e+001	9.043e-004	3.352e-004	-5.690e-004
34	1.776e+001	9.991e-004	2.501e-004	-7.490e-004
35	1.824e+001	8.793e-004	1.852e-004	-6.941e-004
36	1.873e+001	8.570e-004	1.360e-004	-7.210e-004
37	1.922e+001	8.344e-004	9.908e-005	-7.353e-004
38	1.970e+001	7.058e-004	7.156e-005	-6.342e-004
39	2.019e+001	7.195e-004	5.127e-005	-6.682e-004
40	2.068e+001	5.615e-004	3.646e-005	-5.250e-004
41	2.116e+001	5.550e-004	2.570e-005	-5.293e-004
42	2.165e+001	6.152e-004	1.798e-005	-5.972e-004
43	2.214e+001	6.039e-004	1.247e-005	-5.914e-004

44	2.262e+001	5.105e-004	8.582e-006	-5.019e-004
45	2.311e+001	4.618e-004	5.855e-006	-4.559e-004
46	2.360e+001	5.453e-004	3.966e-006	-5.413e-004
47	2.408e+001	5.896e-004	2.662e-006	-5.869e-004
48	2.457e+001	5.083e-004	1.774e-006	-5.065e-004
49	2.506e+001	4.132e-004	1.172e-006	-4.120e-004
50	2.554e+001	4.343e-004	7.681e-007	-4.335e-004
51	2.603e+001	4.272e-004	4.991e-007	-4.267e-004
52	2.651e+001	4.071e-004	3.220e-007	-4.068e-004
53	2.700e+001	3.921e-004	2.058e-007	-3.919e-004
54	2.749e+001	3.936e-004	1.306e-007	-3.934e-004
55	2.798e+001	4.023e-004	8.217e-008	-4.022e-004
56	2.846e+001	2.766e-004	5.131e-008	-2.766e-004
57	2.895e+001	2.746e-004	3.175e-008	-2.745e-004
58	2.943e+001	3.717e-004	1.951e-008	-3.716e-004
59	2.992e+001	2.457e-004	1.188e-008	-2.457e-004
60	3.041e+001	3.112e-004	7.181e-009	-3.112e-004
61	3.089e+001	3.727e-004	4.302e-009	-3.727e-004
62	3.138e+001	3.426e-004	2.559e-009	-3.426e-004
63	3.187e+001	3.701e-004	1.508e-009	-3.701e-004
64	3.235e+001	3.453e-004	8.814e-010	-3.453e-004

==========

64 points for Peak 3, Peak Point = 2.115 ppm

Converged after 49 iterations!

Results Comp. 1

I[0] = 3.049e-001
Diff Con. = 6.929e-010 m2/s
Gamma = 4.258e+003 Hz/G
Little Delta = 6.000m
Big Delta = 99.900m

RSS = 3.492e-004
SD = 2.336e-003

Point	Gradient	Expt	Calc	Difference
1	1.703e+000	2.920e-001	2.898e-001	-2.217e-003
2	2.189e+000	2.823e-001	2.804e-001	-1.940e-003
3	2.676e+000	2.687e-001	2.690e-001	3.117e-004
4	3.162e+000	2.565e-001	2.560e-001	-5.541e-004
5	3.649e+000	2.417e-001	2.416e-001	-1.475e-004
6	4.135e+000	2.265e-001	2.261e-001	-3.482e-004
7	4.622e+000	2.098e-001	2.099e-001	3.834e-005
8	5.108e+000	1.934e-001	1.932e-001	-2.098e-004
9	5.595e+000	1.752e-001	1.764e-001	1.175e-003
10	6.081e+000	1.568e-001	1.597e-001	2.958e-003
11	6.568e+000	1.407e-001	1.434e-001	2.758e-003
12	7.055e+000	1.242e-001	1.277e-001	3.559e-003
13	7.541e+000	1.123e-001	1.128e-001	5.269e-004
14	8.028e+000	9.721e-002	9.884e-002	1.626e-003
15	8.514e+000	8.476e-002	8.588e-002	1.124e-003
16	9.001e+000	7.391e-002	7.399e-002	8.089e-005
17	9.487e+000	6.327e-002	6.324e-002	-2.969e-005
18	9.974e+000	5.454e-002	5.359e-002	-9.577e-004

19	1.046e+001	4.602e-002	4.505e-002	-9.734e-004
20	1.095e+001	3.853e-002	3.754e-002	-9.855e-004
21	1.143e+001	3.284e-002	3.104e-002	-1.796e-003
22	1.192e+001	2.569e-002	2.545e-002	-2.456e-004
23	1.241e+001	2.216e-002	2.070e-002	-1.466e-003
24	1.289e+001	1.935e-002	1.669e-002	-2.660e-003
25	1.338e+001	1.641e-002	1.335e-002	-3.054e-003
26	1.387e+001	1.372e-002	1.059e-002	-3.133e-003
27	1.435e+001	1.178e-002	8.332e-003	-3.448e-003
28	1.484e+001	9.836e-003	6.499e-003	-3.337e-003
29	1.532e+001	8.248e-003	5.030e-003	-3.218e-003
30	1.581e+001	6.978e-003	3.859e-003	-3.119e-003
31	1.630e+001	6.344e-003	2.938e-003	-3.406e-003
32	1.678e+001	5.226e-003	2.217e-003	-3.010e-003
33	1.727e+001	4.493e-003	1.660e-003	-2.833e-003
34	1.776e+001	4.570e-003	1.232e-003	-3.338e-003
35	1.824e+001	3.828e-003	9.075e-004	-2.921e-003
36	1.873e+001	4.598e-003	6.625e-004	-3.935e-003
37	1.922e+001	3.575e-003	4.799e-004	-3.095e-003
38	1.970e+001	3.282e-003	3.446e-004	-2.937e-003
39	2.019e+001	3.031e-003	2.454e-004	-2.786e-003
40	2.068e+001	2.614e-003	1.734e-004	-2.441e-003
41	2.116e+001	2.433e-003	1.215e-004	-2.311e-003
42	2.165e+001	3.366e-003	8.444e-005	-3.282e-003
43	2.214e+001	3.237e-003	5.817e-005	-3.178e-003
44	2.262e+001	2.439e-003	3.977e-005	-2.399e-003
45	2.311e+001	2.445e-003	2.695e-005	-2.418e-003
46	2.360e+001	2.858e-003	1.812e-005	-2.840e-003
47	2.408e+001	3.102e-003	1.208e-005	-3.090e-003
48	2.457e+001	3.029e-003	7.990e-006	-3.021e-003
49	2.506e+001	2.191e-003	5.237e-006	-2.186e-003
50	2.554e+001	2.175e-003	3.408e-006	-2.171e-003
51	2.603e+001	2.239e-003	2.197e-006	-2.236e-003
52	2.651e+001	2.008e-003	1.406e-006	-2.006e-003
53	2.700e+001	2.251e-003	8.917e-007	-2.250e-003
54	2.749e+001	1.989e-003	5.613e-007	-1.988e-003
55	2.798e+001	2.230e-003	3.501e-007	-2.230e-003
56	2.846e+001	1.821e-003	2.168e-007	-1.820e-003
57	2.895e+001	2.140e-003	1.330e-007	-2.140e-003
58	2.943e+001	1.865e-003	8.100e-008	-1.865e-003
59	2.992e+001	1.843e-003	4.888e-008	-1.843e-003
60	3.041e+001	1.853e-003	2.928e-008	-1.853e-003
61	3.089e+001	1.949e-003	1.738e-008	-1.949e-003
62	3.138e+001	1.930e-003	1.024e-008	-1.930e-003
63	3.187e+001	2.197e-003	5.977e-009	-2.197e-003
64	3.235e+001	2.087e-003	3.460e-009	-2.087e-003

==========

64 points for Peak 4, Peak Point = 1.051 ppm

Converged after 35 iterations!

Results Comp. 1

I[0] = 1.029e+000
Diff Con. = 5.423e-010 m2/s
Gamma = 4.258e+003 Hz/G
Little Delta = 6.000m

Big Delta = 99.900m

RSS = 6.368e-003
SD = 9.975e-003

Point	Gradient	Expt	Calc	Difference
1	1.703e+000	1.000e+000	9.889e-001	-1.111e-002
2	2.189e+000	9.729e-001	9.636e-001	-9.310e-003
3	2.676e+000	9.353e-001	9.329e-001	-2.424e-003
4	3.162e+000	9.018e-001	8.974e-001	-4.403e-003
5	3.649e+000	8.577e-001	8.576e-001	-1.593e-004
6	4.135e+000	8.158e-001	8.143e-001	-1.458e-003
7	4.622e+000	7.678e-001	7.682e-001	3.701e-004
8	5.108e+000	7.187e-001	7.201e-001	1.386e-003
9	5.595e+000	6.663e-001	6.705e-001	4.181e-003
10	6.081e+000	6.107e-001	6.204e-001	9.701e-003
11	6.568e+000	5.593e-001	5.703e-001	1.103e-002
12	7.055e+000	5.064e-001	5.208e-001	1.447e-002
13	7.541e+000	4.681e-001	4.727e-001	4.543e-003
14	8.028e+000	4.172e-001	4.261e-001	8.904e-003
15	8.514e+000	3.763e-001	3.817e-001	5.394e-003
16	9.001e+000	3.340e-001	3.397e-001	5.718e-003
17	9.487e+000	2.985e-001	3.004e-001	1.957e-003
18	9.974e+000	2.639e-001	2.639e-001	7.287e-006
19	1.046e+001	2.285e-001	2.304e-001	1.820e-003
20	1.095e+001	1.988e-001	1.997e-001	9.250e-004
21	1.143e+001	1.762e-001	1.721e-001	-4.107e-003
22	1.192e+001	1.497e-001	1.473e-001	-2.344e-003
23	1.241e+001	1.254e-001	1.253e-001	-6.830e-005
24	1.289e+001	1.161e-001	1.059e-001	-1.017e-002
25	1.338e+001	9.744e-002	8.893e-002	-8.515e-003
26	1.387e+001	8.452e-002	7.417e-002	-1.035e-002
27	1.435e+001	7.099e-002	6.148e-002	-9.507e-003
28	1.484e+001	6.253e-002	5.062e-002	-1.191e-002
29	1.532e+001	5.255e-002	4.142e-002	-1.113e-002
30	1.581e+001	4.454e-002	3.366e-002	-1.087e-002
31	1.630e+001	3.993e-002	2.719e-002	-1.274e-002
32	1.678e+001	3.621e-002	2.181e-002	-1.439e-002
33	1.727e+001	3.166e-002	1.739e-002	-1.427e-002
34	1.776e+001	2.849e-002	1.377e-002	-1.472e-002
35	1.824e+001	2.668e-002	1.084e-002	-1.583e-002
36	1.873e+001	2.080e-002	8.475e-003	-1.232e-002
37	1.922e+001	1.953e-002	6.586e-003	-1.295e-002
38	1.970e+001	1.987e-002	5.081e-003	-1.479e-002
39	2.019e+001	1.700e-002	3.896e-003	-1.310e-002
40	2.068e+001	1.772e-002	2.969e-003	-1.475e-002
41	2.116e+001	1.694e-002	2.247e-003	-1.469e-002
42	2.165e+001	1.257e-002	1.690e-003	-1.088e-002
43	2.214e+001	1.419e-002	1.263e-003	-1.293e-002
44	2.262e+001	1.452e-002	9.376e-004	-1.358e-002
45	2.311e+001	1.410e-002	6.914e-004	-1.341e-002
46	2.360e+001	1.214e-002	5.068e-004	-1.163e-002
47	2.408e+001	1.121e-002	3.689e-004	-1.085e-002
48	2.457e+001	1.043e-002	2.670e-004	-1.017e-002
49	2.506e+001	1.246e-002	1.918e-004	-1.227e-002
50	2.554e+001	1.181e-002	1.370e-004	-1.167e-002
51	2.603e+001	9.977e-003	9.719e-005	-9.880e-003
52	2.651e+001	1.074e-002	6.854e-005	-1.067e-002
53	2.700e+001	1.043e-002	4.799e-005	-1.039e-002

54	2.749e+001	9.947e-003	3.340e-005	-9.914e-003
55	2.798e+001	9.769e-003	2.309e-005	-9.746e-003
56	2.846e+001	9.378e-003	1.586e-005	-9.362e-003
57	2.895e+001	1.035e-002	1.082e-005	-1.034e-002
58	2.943e+001	9.245e-003	7.341e-006	-9.238e-003
59	2.992e+001	1.053e-002	4.944e-006	-1.052e-002
60	3.041e+001	9.422e-003	3.310e-006	-9.419e-003
61	3.089e+001	8.112e-003	2.201e-006	-8.109e-003
62	3.138e+001	8.797e-003	1.455e-006	-8.795e-003
63	3.187e+001	8.404e-003	9.545e-007	-8.403e-003
64	3.235e+001	7.396e-003	6.223e-007	-7.396e-003

==========

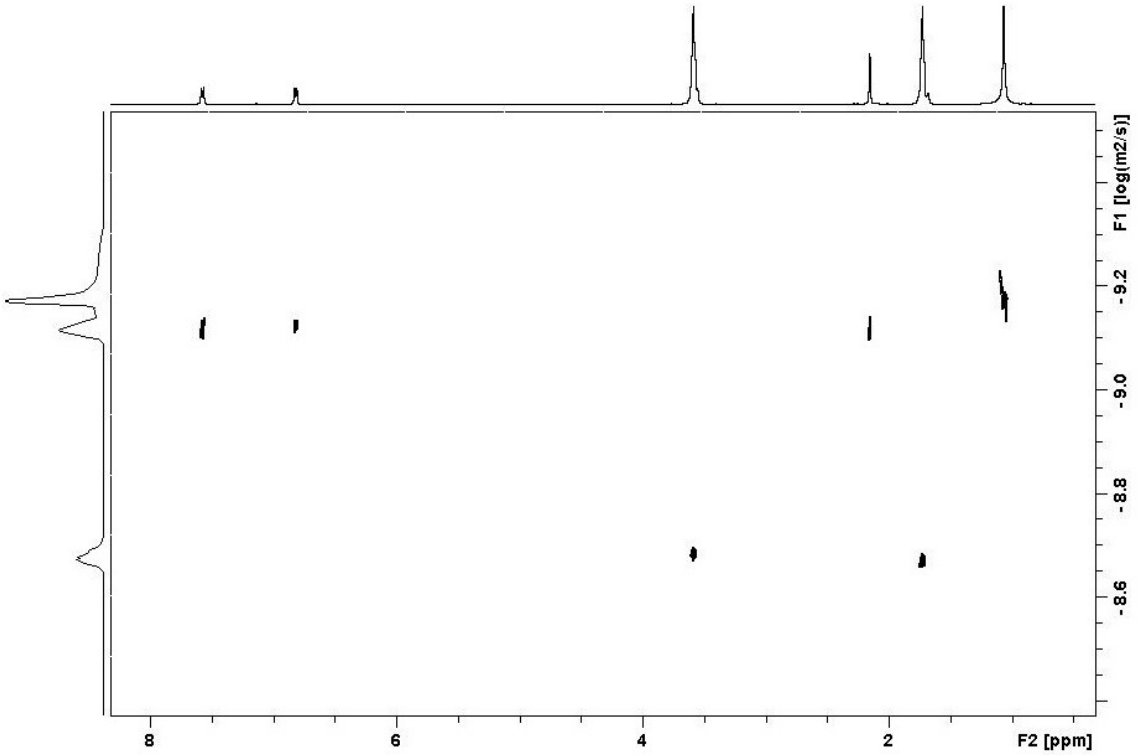

Figure S14. ^{1}H DOSY NMR spectrum of Zn(OPiv)$_2$·2LiCl and Me(*p*-C$_6$H$_4$)MgCl in [D$_8$]THF at 25°C

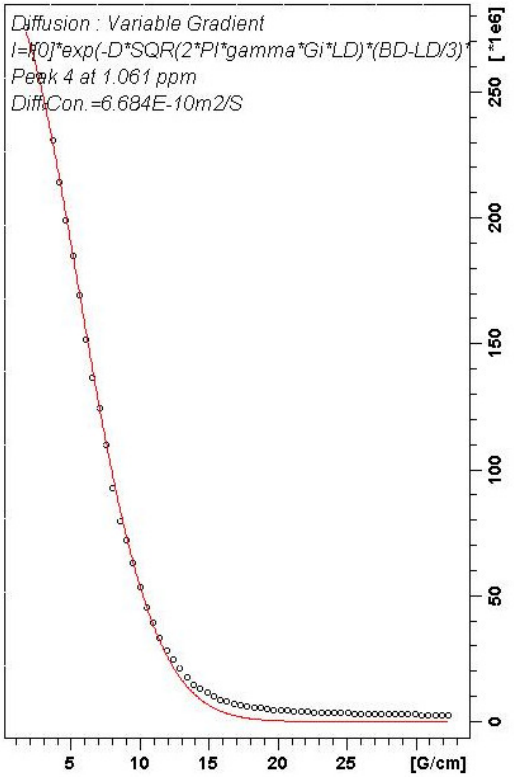

Figure S14.1. Stejskal-Tanner plot for the ^{1}H resonance at 1.061 ppm

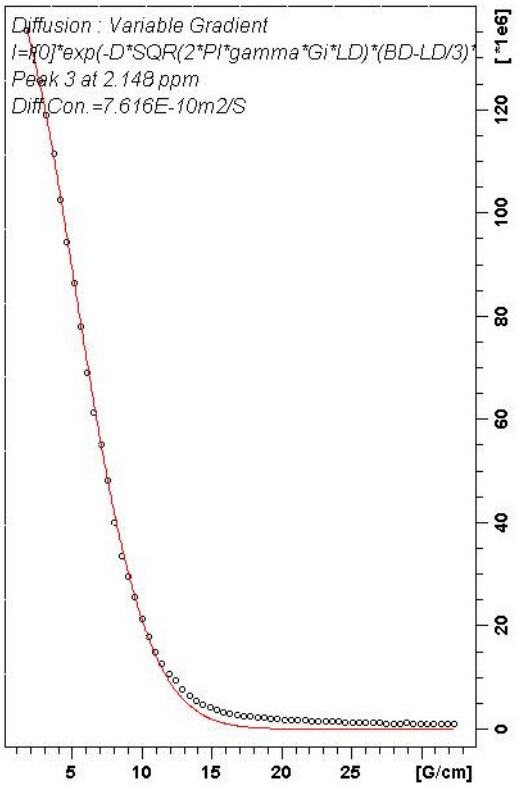

Figure S14.2. Stejskal-Tanner plot for the ^{1}H resonance at 2.148 ppm

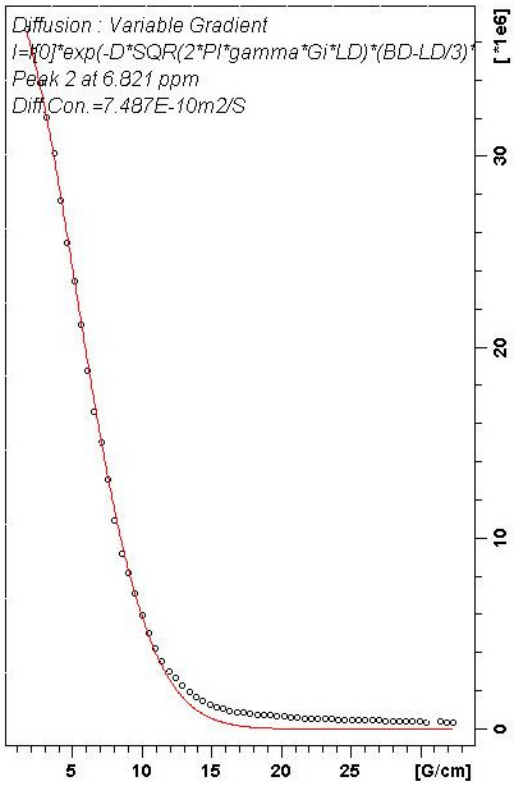

Figure S14.3. Stejskal-Tanner plot for the ^{1}H resonance at 6.821 ppm

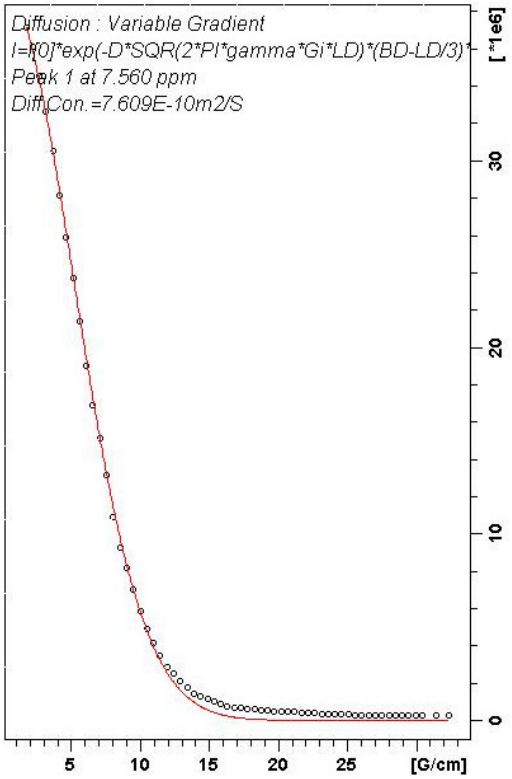

Figure S14.4. Stejskal-Tanner plot for the ^{1}H resonance at 7.56 ppm

Simfit results

Dataset : C:\NMRdata/data/REM/nmr/B23618/5/pdata/1/ct1t2.txt

INTENSITY fit : Diffusion : Variable Gradient :

I=I[0]*exp(-D*SQR(2*PI*gamma*Gi*LD)*(BD-LD/3)*1e4)

62 points for Peak 1, Peak Point = 7.560 ppm

Converged after 52 iterations!

Results Comp. 1

I[0] = 1.427e-001
Diff Con. = 7.609e-010 m2/s
Gamma = 4.258e+003 Hz/G
Little Delta = 6.000m
Big Delta = 99.900m

RSS = 1.076e-004
SD = 1.317e-003

Point	Gradient	Expt	Calc	Difference
1	1.703e+000	1.349e-001	1.349e-001	4.399e-005
2	2.189e+000	1.311e-001	1.301e-001	-9.231e-004
3	2.676e+000	1.254e-001	1.243e-001	-1.081e-003
4	3.162e+000	1.185e-001	1.178e-001	-7.471e-004
5	3.649e+000	1.108e-001	1.105e-001	-3.194e-004
6	4.135e+000	1.023e-001	1.028e-001	4.583e-004
7	4.622e+000	9.396e-002	9.468e-002	7.237e-004

8	5.108e+000	8.601e-002	8.647e-002	4.527e-004
9	5.595e+000	7.771e-002	7.823e-002	5.259e-004
10	6.081e+000	6.910e-002	7.016e-002	1.059e-003
11	6.568e+000	6.144e-002	6.234e-002	8.955e-004
12	7.055e+000	5.489e-002	5.489e-002	-6.857e-006
13	7.541e+000	4.780e-002	4.790e-002	1.030e-004
14	8.028e+000	3.970e-002	4.141e-002	1.709e-003
15	8.514e+000	3.377e-002	3.549e-002	1.718e-003
16	9.001e+000	2.966e-002	3.013e-002	4.726e-004
17	9.487e+000	2.552e-002	2.536e-002	-1.568e-004
18	9.974e+000	2.128e-002	2.114e-002	-1.349e-004
19	1.046e+001	1.781e-002	1.747e-002	-3.359e-004
20	1.095e+001	1.508e-002	1.430e-002	-7.781e-004
21	1.143e+001	1.263e-002	1.161e-002	-1.019e-003
22	1.192e+001	1.050e-002	9.333e-003	-1.166e-003
23	1.241e+001	9.177e-003	7.439e-003	-1.738e-003
24	1.289e+001	7.649e-003	5.872e-003	-1.777e-003
25	1.338e+001	6.338e-003	4.596e-003	-1.742e-003
26	1.387e+001	5.276e-003	3.563e-003	-1.714e-003
27	1.435e+001	4.681e-003	2.738e-003	-1.942e-003
28	1.484e+001	4.192e-003	2.084e-003	-2.107e-003
29	1.532e+001	3.644e-003	1.573e-003	-2.071e-003
30	1.581e+001	3.234e-003	1.176e-003	-2.058e-003
31	1.630e+001	2.833e-003	8.716e-004	-1.961e-003
32	1.678e+001	2.570e-003	6.398e-004	-1.931e-003
33	1.727e+001	2.406e-003	4.657e-004	-1.940e-003
34	1.776e+001	2.188e-003	3.357e-004	-1.853e-003
35	1.824e+001	2.125e-003	2.399e-004	-1.885e-003
36	1.873e+001	2.025e-003	1.698e-004	-1.855e-003
37	1.922e+001	1.912e-003	1.192e-004	-1.792e-003
38	1.970e+001	1.816e-003	8.285e-005	-1.733e-003
39	2.019e+001	1.754e-003	5.706e-005	-1.697e-003
40	2.068e+001	1.741e-003	3.898e-005	-1.702e-003
41	2.116e+001	1.610e-003	2.636e-005	-1.584e-003
42	2.165e+001	1.494e-003	1.768e-005	-1.476e-003
43	2.214e+001	1.528e-003	1.174e-005	-1.517e-003
44	2.262e+001	1.369e-003	7.735e-006	-1.361e-003
45	2.311e+001	1.262e-003	5.045e-006	-1.257e-003
46	2.360e+001	1.309e-003	3.263e-006	-1.306e-003
47	2.408e+001	1.290e-003	2.090e-006	-1.288e-003
48	2.457e+001	1.265e-003	1.327e-006	-1.263e-003
49	2.506e+001	1.130e-003	8.348e-007	-1.129e-003
50	2.554e+001	1.105e-003	5.207e-007	-1.105e-003
51	2.603e+001	1.088e-003	3.216e-007	-1.088e-003
52	2.651e+001	1.062e-003	1.970e-007	-1.062e-003
53	2.700e+001	1.099e-003	1.195e-007	-1.099e-003
54	2.749e+001	9.780e-004	7.186e-008	-9.779e-004
55	2.798e+001	9.173e-004	4.279e-008	-9.172e-004
56	2.846e+001	1.028e-003	2.528e-008	-1.028e-003
57	2.895e+001	9.769e-004	1.478e-008	-9.768e-004
58	2.943e+001	1.046e-003	8.575e-009	-1.046e-003
59	2.992e+001	9.558e-004	4.924e-009	-9.558e-004
60	3.041e+001	9.947e-004	2.805e-009	-9.947e-004
61	3.138e+001	9.321e-004	8.848e-010	-9.321e-004
62	3.235e+001	8.960e-004	2.688e-010	-8.960e-004

==========

63 points for Peak 2, Peak Point = 6.821 ppm

Converged after 49 iterations!

Results Comp. 1

I[0] = 1.398e-001
Diff Con. = 7.487e-010 m2/s
Gamma = 4.258e+003 Hz/G
Little Delta = 6.000m
Big Delta = 99.900m

RSS = 1.924e-004
SD = 1.748e-003

Point	Gradient	Expt	Calc	Difference
1	1.703e+000	1.331e-001	1.324e-001	-6.913e-004
2	2.189e+000	1.290e-001	1.277e-001	-1.254e-003
3	2.676e+000	1.229e-001	1.221e-001	-7.569e-004
4	3.162e+000	1.163e-001	1.158e-001	-4.960e-004
5	3.649e+000	1.094e-001	1.087e-001	-6.881e-004
6	4.135e+000	1.005e-001	1.012e-001	7.707e-004
7	4.622e+000	9.245e-002	9.341e-002	9.626e-004
8	5.108e+000	8.517e-002	8.543e-002	2.659e-004
9	5.595e+000	7.690e-002	7.742e-002	5.274e-004
10	6.081e+000	6.809e-002	6.956e-002	1.470e-003
11	6.568e+000	6.042e-002	6.192e-002	1.496e-003
12	7.055e+000	5.445e-002	5.463e-002	1.761e-004
13	7.541e+000	4.756e-002	4.778e-002	2.151e-004
14	8.028e+000	3.964e-002	4.140e-002	1.764e-003
15	8.514e+000	3.332e-002	3.557e-002	2.252e-003
16	9.001e+000	2.975e-002	3.028e-002	5.326e-004
17	9.487e+000	2.570e-002	2.555e-002	-1.508e-004
18	9.974e+000	2.167e-002	2.137e-002	-3.000e-004
19	1.046e+001	1.821e-002	1.771e-002	-5.008e-004
20	1.095e+001	1.539e-002	1.455e-002	-8.468e-004
21	1.143e+001	1.296e-002	1.185e-002	-1.115e-003
22	1.192e+001	1.107e-002	9.557e-003	-1.511e-003
23	1.241e+001	9.699e-003	7.644e-003	-2.054e-003
24	1.289e+001	8.358e-003	6.058e-003	-2.300e-003
25	1.338e+001	7.019e-003	4.760e-003	-2.260e-003
26	1.387e+001	6.027e-003	3.705e-003	-2.322e-003
27	1.435e+001	5.297e-003	2.859e-003	-2.437e-003
28	1.484e+001	4.741e-003	2.186e-003	-2.555e-003
29	1.532e+001	4.189e-003	1.658e-003	-2.531e-003
30	1.581e+001	3.858e-003	1.245e-003	-2.613e-003
31	1.630e+001	3.359e-003	9.271e-004	-2.432e-003
32	1.678e+001	3.086e-003	6.839e-004	-2.402e-003
33	1.727e+001	3.105e-003	5.003e-004	-2.605e-003
34	1.776e+001	2.933e-003	3.625e-004	-2.571e-003
35	1.824e+001	2.772e-003	2.605e-004	-2.512e-003
36	1.873e+001	2.671e-003	1.854e-004	-2.486e-003
37	1.922e+001	2.683e-003	1.309e-004	-2.552e-003
38	1.970e+001	2.499e-003	9.150e-005	-2.407e-003
39	2.019e+001	2.406e-003	6.340e-005	-2.342e-003
40	2.068e+001	2.174e-003	4.357e-005	-2.131e-003
41	2.116e+001	2.083e-003	2.965e-005	-2.053e-003
42	2.165e+001	2.058e-003	2.002e-005	-2.038e-003
43	2.214e+001	1.991e-003	1.338e-005	-1.978e-003
44	2.262e+001	2.051e-003	8.874e-006	-2.042e-003

45	2.311e+001	1.942e-003	5.827e-006	-1.936e-003
46	2.360e+001	1.925e-003	3.796e-006	-1.921e-003
47	2.408e+001	1.813e-003	2.448e-006	-1.810e-003
48	2.457e+001	1.709e-003	1.567e-006	-1.707e-003
49	2.506e+001	1.624e-003	9.925e-007	-1.623e-003
50	2.554e+001	1.642e-003	6.238e-007	-1.641e-003
51	2.603e+001	1.690e-003	3.882e-007	-1.690e-003
52	2.651e+001	1.680e-003	2.397e-007	-1.680e-003
53	2.700e+001	1.585e-003	1.465e-007	-1.585e-003
54	2.749e+001	1.520e-003	8.886e-008	-1.520e-003
55	2.798e+001	1.469e-003	5.335e-008	-1.469e-003
56	2.846e+001	1.442e-003	3.178e-008	-1.442e-003
57	2.895e+001	1.544e-003	1.875e-008	-1.544e-003
58	2.943e+001	1.466e-003	1.097e-008	-1.466e-003
59	2.992e+001	1.474e-003	6.355e-009	-1.474e-003
60	3.041e+001	1.310e-003	3.653e-009	-1.310e-003
61	3.138e+001	1.457e-003	1.174e-009	-1.457e-003
62	3.187e+001	1.273e-003	6.562e-010	-1.273e-003
63	3.235e+001	1.316e-003	3.635e-010	-1.316e-003

==========

64 points for Peak 3, Peak Point = 2.148 ppm

Converged after 42 iterations!

Results Comp. 1

I[0] = 5.199e-001
Diff Con. = 7.616e-010 m2/s
Gamma = 4.258e+003 Hz/G
Little Delta = 6.000m
Big Delta = 99.900m

RSS = 1.632e-003
SD = 5.049e-003

Point	Gradient	Expt	Calc	Difference
1	1.703e+000	4.917e-001	4.917e-001	2.339e-005
2	2.189e+000	4.781e-001	4.742e-001	-3.938e-003
3	2.676e+000	4.558e-001	4.531e-001	-2.748e-003
4	3.162e+000	4.315e-001	4.291e-001	-2.414e-003
5	3.649e+000	4.049e-001	4.026e-001	-2.299e-003
6	4.135e+000	3.727e-001	3.744e-001	1.634e-003
7	4.622e+000	3.422e-001	3.449e-001	2.753e-003
8	5.108e+000	3.136e-001	3.150e-001	1.361e-003
9	5.595e+000	2.833e-001	2.850e-001	1.620e-003
10	6.081e+000	2.509e-001	2.555e-001	4.679e-003
11	6.568e+000	2.228e-001	2.270e-001	4.194e-003
12	7.055e+000	2.003e-001	1.999e-001	-4.779e-004
13	7.541e+000	1.746e-001	1.744e-001	-2.385e-004
14	8.028e+000	1.450e-001	1.508e-001	5.788e-003
15	8.514e+000	1.221e-001	1.292e-001	7.085e-003
16	9.001e+000	1.077e-001	1.097e-001	1.965e-003
17	9.487e+000	9.287e-002	9.228e-002	-5.930e-004
18	9.974e+000	7.770e-002	7.692e-002	-7.814e-004
19	1.046e+001	6.448e-002	6.356e-002	-9.141e-004
20	1.095e+001	5.446e-002	5.203e-002	-2.436e-003

21	1.143e+001	4.559e-002	4.222e-002	-3.372e-003
22	1.192e+001	3.835e-002	3.393e-002	-4.416e-003
23	1.241e+001	3.383e-002	2.704e-002	-6.787e-003
24	1.289e+001	2.838e-002	2.134e-002	-7.036e-003
25	1.338e+001	2.330e-002	1.670e-002	-6.604e-003
26	1.387e+001	1.966e-002	1.294e-002	-6.717e-003
27	1.435e+001	1.733e-002	9.946e-003	-7.388e-003
28	1.484e+001	1.552e-002	7.569e-003	-7.955e-003
29	1.532e+001	1.338e-002	5.711e-003	-7.664e-003
30	1.581e+001	1.207e-002	4.268e-003	-7.806e-003
31	1.630e+001	1.081e-002	3.163e-003	-7.652e-003
32	1.678e+001	9.690e-003	2.321e-003	-7.369e-003
33	1.727e+001	8.893e-003	1.689e-003	-7.204e-003
34	1.776e+001	8.577e-003	1.217e-003	-7.360e-003
35	1.824e+001	8.125e-003	8.696e-004	-7.255e-003
36	1.873e+001	7.977e-003	6.153e-004	-7.362e-003
37	1.922e+001	7.400e-003	4.318e-004	-6.968e-003
38	1.970e+001	7.010e-003	3.000e-004	-6.710e-003
39	2.019e+001	6.713e-003	2.066e-004	-6.507e-003
40	2.068e+001	6.495e-003	1.411e-004	-6.354e-003
41	2.116e+001	6.250e-003	9.537e-005	-6.155e-003
42	2.165e+001	6.086e-003	6.395e-005	-6.022e-003
43	2.214e+001	5.686e-003	4.245e-005	-5.644e-003
44	2.262e+001	5.296e-003	2.796e-005	-5.268e-003
45	2.311e+001	5.273e-003	1.822e-005	-5.255e-003
46	2.360e+001	4.998e-003	1.178e-005	-4.986e-003
47	2.408e+001	4.985e-003	7.544e-006	-4.977e-003
48	2.457e+001	4.910e-003	4.790e-006	-4.905e-003
49	2.506e+001	4.526e-003	3.011e-006	-4.523e-003
50	2.554e+001	4.362e-003	1.878e-006	-4.360e-003
51	2.603e+001	4.307e-003	1.159e-006	-4.306e-003
52	2.651e+001	4.364e-003	7.097e-007	-4.364e-003
53	2.700e+001	4.331e-003	4.302e-007	-4.331e-003
54	2.749e+001	4.027e-003	2.587e-007	-4.026e-003
55	2.798e+001	4.015e-003	1.540e-007	-4.014e-003
56	2.846e+001	3.991e-003	9.091e-008	-3.991e-003
57	2.895e+001	4.119e-003	5.314e-008	-4.119e-003
58	2.943e+001	3.991e-003	3.081e-008	-3.991e-003
59	2.992e+001	3.826e-003	1.768e-008	-3.825e-003
60	3.041e+001	3.631e-003	1.007e-008	-3.631e-003
61	3.089e+001	3.746e-003	5.675e-009	-3.746e-003
62	3.138e+001	3.641e-003	3.173e-009	-3.641e-003
63	3.187e+001	3.664e-003	1.756e-009	-3.664e-003
64	3.235e+001	3.531e-003	9.630e-010	-3.531e-003

==========

64 points for Peak 4, Peak Point = 1.061 ppm

Converged after 36 iterations!

Results Comp. 1

I[0] = 1.044e+000
Diff Con. = 6.684e-010 m2/s
Gamma = 4.258e+003 Hz/G
Little Delta = 6.000m
Big Delta = 99.900m

RSS = 8.620e-003
SD = 1.161e-002

Point	Gradient	Expt	Calc	Difference
1	1.703e+000	1.000e+000	9.941e-001	-5.878e-003
2	2.189e+000	9.710e-001	9.629e-001	-8.026e-003
3	2.676e+000	9.309e-001	9.252e-001	-5.699e-003
4	3.162e+000	8.864e-001	8.820e-001	-4.395e-003
5	3.649e+000	8.374e-001	8.340e-001	-3.309e-003
6	4.135e+000	7.776e-001	7.825e-001	4.873e-003
7	4.622e+000	7.223e-001	7.282e-001	5.918e-003
8	5.108e+000	6.717e-001	6.724e-001	7.327e-004
9	5.595e+000	6.140e-001	6.159e-001	1.904e-003
10	6.081e+000	5.498e-001	5.597e-001	9.927e-003
11	6.568e+000	4.952e-001	5.045e-001	9.318e-003
12	7.055e+000	4.515e-001	4.511e-001	-3.546e-004
13	7.541e+000	3.990e-001	4.003e-001	1.233e-003
14	8.028e+000	3.375e-001	3.522e-001	1.474e-002
15	8.514e+000	2.893e-001	3.076e-001	1.834e-002
16	9.001e+000	2.614e-001	2.664e-001	5.032e-003
17	9.487e+000	2.286e-001	2.290e-001	3.752e-004
18	9.974e+000	1.945e-001	1.952e-001	6.564e-004
19	1.046e+001	1.654e-001	1.651e-001	-3.740e-004
20	1.095e+001	1.426e-001	1.385e-001	-4.183e-003
21	1.143e+001	1.214e-001	1.153e-001	-6.162e-003
22	1.192e+001	1.027e-001	9.516e-002	-7.549e-003
23	1.241e+001	9.047e-002	7.797e-002	-1.251e-002
24	1.289e+001	7.648e-002	6.334e-002	-1.313e-002
25	1.338e+001	6.350e-002	5.108e-002	-1.242e-002
26	1.387e+001	5.361e-002	4.084e-002	-1.277e-002
27	1.435e+001	4.714e-002	3.241e-002	-1.473e-002
28	1.484e+001	4.190e-002	2.550e-002	-1.640e-002
29	1.532e+001	3.582e-002	1.992e-002	-1.590e-002
30	1.581e+001	3.201e-002	1.543e-002	-1.658e-002
31	1.630e+001	2.864e-002	1.186e-002	-1.678e-002
32	1.678e+001	2.570e-002	9.038e-003	-1.666e-002
33	1.727e+001	2.355e-002	6.838e-003	-1.671e-002
34	1.776e+001	2.188e-002	5.129e-003	-1.675e-002
35	1.824e+001	2.073e-002	3.819e-003	-1.691e-002
36	1.873e+001	1.952e-002	2.819e-003	-1.670e-002
37	1.922e+001	1.807e-002	2.066e-003	-1.600e-002
38	1.970e+001	1.703e-002	1.501e-003	-1.553e-002
39	2.019e+001	1.646e-002	1.082e-003	-1.538e-002
40	2.068e+001	1.603e-002	7.738e-004	-1.526e-002
41	2.116e+001	1.521e-002	5.489e-004	-1.466e-002
42	2.165e+001	1.464e-002	3.865e-004	-1.425e-002
43	2.214e+001	1.422e-002	2.698e-004	-1.395e-002
44	2.262e+001	1.362e-002	1.870e-004	-1.343e-002
45	2.311e+001	1.296e-002	1.284e-004	-1.283e-002
46	2.360e+001	1.278e-002	8.761e-005	-1.269e-002
47	2.408e+001	1.259e-002	5.923e-005	-1.253e-002
48	2.457e+001	1.219e-002	3.976e-005	-1.215e-002
49	2.506e+001	1.202e-002	2.645e-005	-1.199e-002
50	2.554e+001	1.155e-002	1.748e-005	-1.154e-002
51	2.603e+001	1.139e-002	1.144e-005	-1.137e-002
52	2.651e+001	1.138e-002	7.441e-006	-1.137e-002
53	2.700e+001	1.101e-002	4.796e-006	-1.101e-002
54	2.749e+001	1.084e-002	3.069e-006	-1.083e-002
55	2.798e+001	1.054e-002	1.946e-006	-1.054e-002

56	2.846e+001	1.031e-002	1.226e-006	-1.031e-002
57	2.895e+001	1.031e-002	7.651e-007	-1.031e-002
58	2.943e+001	1.045e-002	4.743e-007	-1.045e-002
59	2.992e+001	1.013e-002	2.913e-007	-1.013e-002
60	3.041e+001	9.901e-003	1.777e-007	-9.901e-003
61	3.089e+001	9.688e-003	1.074e-007	-9.688e-003
62	3.138e+001	1.002e-002	6.451e-008	-1.002e-002
63	3.187e+001	9.692e-003	3.838e-008	-9.692e-003
64	3.235e+001	9.325e-003	2.265e-008	-9.325e-003

==========

Table S4. NMR data in [D_8]THF at 25°C

	^{1}H/δ(ppm)	^{13}C/δ(ppm)
$MgBu_2$	1.51 – 1.44 (m 4 H, CH_2, Bu), 1.24 – 1.13 (m, 4 H, CH_2, Bu) 0.79 (t, 6 H, J = 7.2 Hz, CH_3, Bu), -0.69 (t, 4 H, J = 8.2 Hz, MgCH_2, Bu)	33.8, 32.2 (*C*H_2, Bu), 14.4 (*C*H_3, Bu), 7.9 (Mg*C*H_2, Bu)
$ZnBu_2$·2LiCl	1.50 – 1.44 (m 4 H, CH_2, Bu), 1.27 – 1.18 (m, 4 H, CH_2, Bu) 0.79 (t, 6 H, J = 7.2 Hz, CH_3, Bu), 0.02 (t, 4 H, J = 7.7 Hz, ZnCH_2, Bu)	31.8, 30.1 (*C*H_2, Bu), 14.5 (*C*H_3, Bu), 12.2 (Zn*C*H_2, Bu)
$MgBu_2$ + Zn(OPiv)$_2$·LiCl	1.50 – 1.43 (m 4 H, CH_2, Bu), 1.23 – 1.18 (m, 4 H, CH_2, Bu) 1.06 (s, 18 H, CO_2CCH_3), 0.81 (t, 6 H, J = 7.2 Hz, CH_3, Bu), 0.07 (t, 4 H, J = 7.8 Hz, ZnCH_2, Bu)	187.5 (*C*O_2CCH_3), 39.8 (CO_2*C*CH_3), 31.4, 30.3 (*C*H_2, Bu), 28.4 (CO_2CCH_3), 14.4 (*C*H_3, Bu), 12.3 (Zn*C*H_2, Bu)
$MgBu_2$ + Zn(OPiv)$_2$·2LiCl	1.48 – 1.44 (m 4 H, CH_2, Bu), 1.25 – 1.19 (m, 4 H, CH_2, Bu) 1.06 (s, 18 H, CO_2CCH_3), 0.80 (t, 6 H, J = 7.2 Hz, CH_3, Bu), 0.06 (t, 4 H, J = 7 Hz, ZnCH_2, Bu),	186.5 (*C*O_2CCH_3), 39.9 (CO_2*C*CH_3), 31.7, 30.2 (*C*H_2, Bu), 28.8 (CO_2CCH_3), 14.5 (*C*H_3, Bu), 12.9 (Zn*C*H_2, Bu)

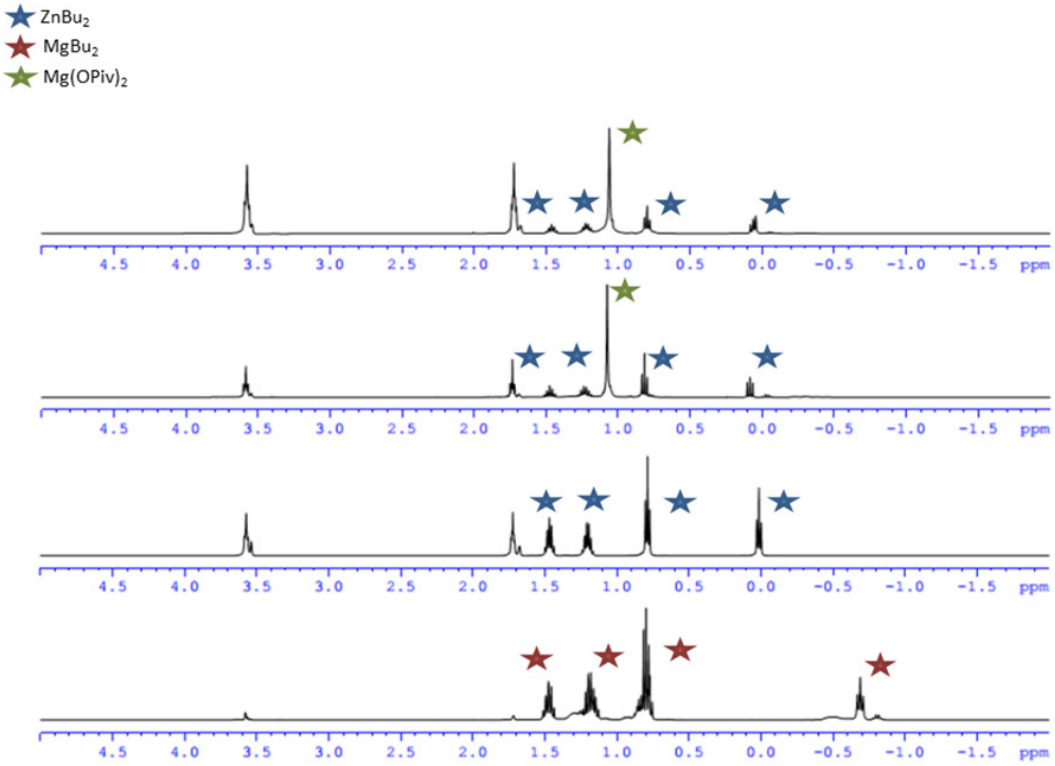

Figure S15. ^{1}H NMR spectrum of a) $MgBu_2$; b) $ZnBu_2$·2LiCl; c) Zn(OPiv)$_2$·LiCl and $MgBu_2$; d) Zn(OPiv)$_2$·2LiCl and $MgBu_2$ in [D_8]THF at 25°C.

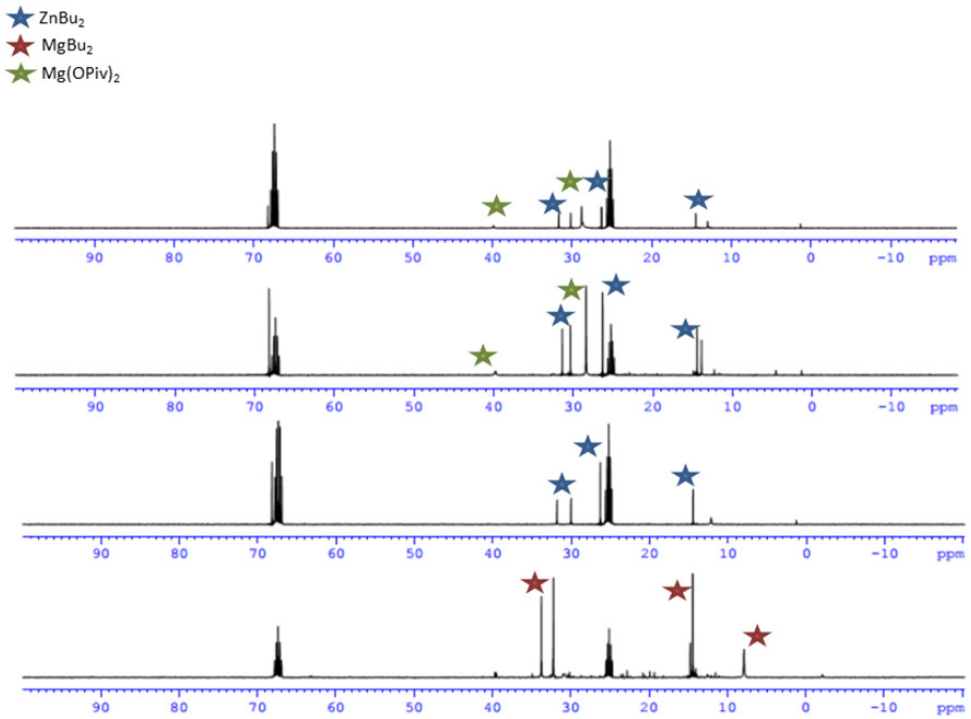

Figure S16. ^{1}H NMR spectrum of a) $MgBu_2$; b) $ZnBu_2 \cdot 2LiCl$; c) $Zn(OPiv)_2 \cdot LiCl$ and $MgBu_2$; d) $Zn(OPiv)_2 \cdot 2LiCl$ and $MgBu_2$ in [D_8]THF at 25°C.

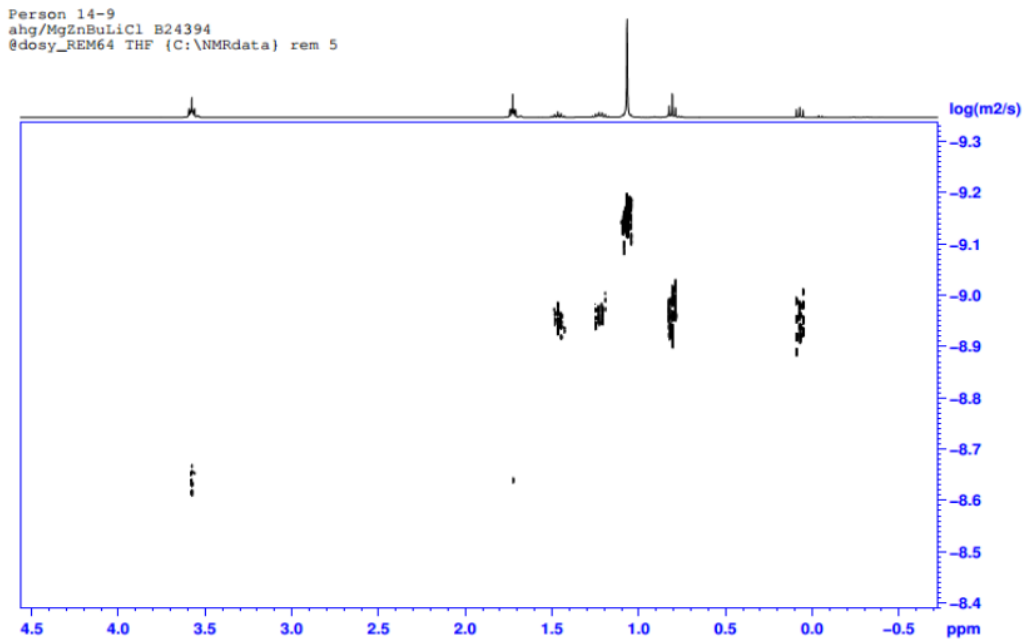

Figure S17. ^{1}H DOSY NMR spectrum of Zn(OPiv)$_2$·LiCl and MgBu in [D$_8$]THF at 25°C

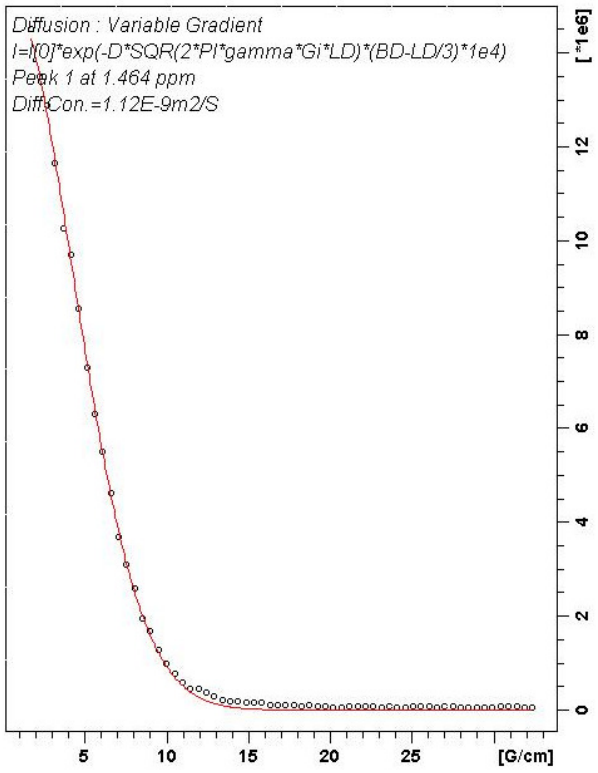

Figure S17.1. Stejskal-Tanner plot for the ^{1}H resonance at 1.464 ppm

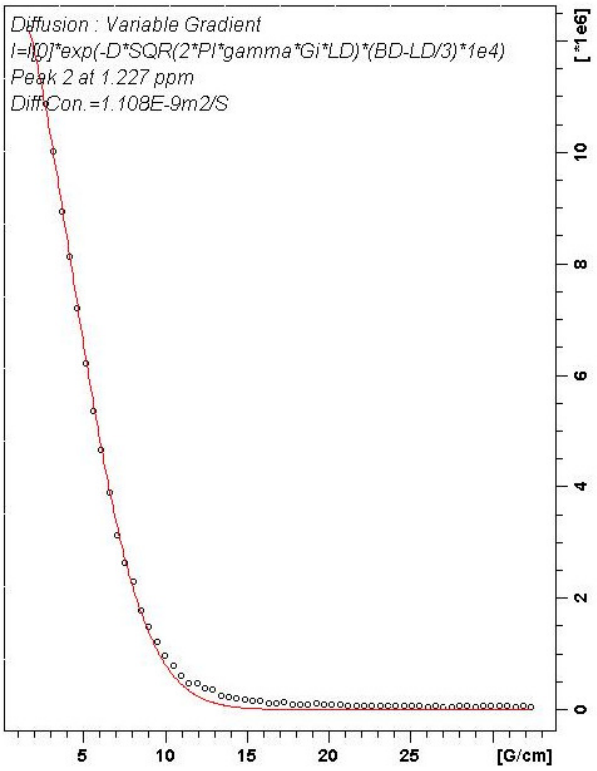

Figure S17.2. Stejskal-Tanner plot for the ^{1}H resonance at 1.227 ppm

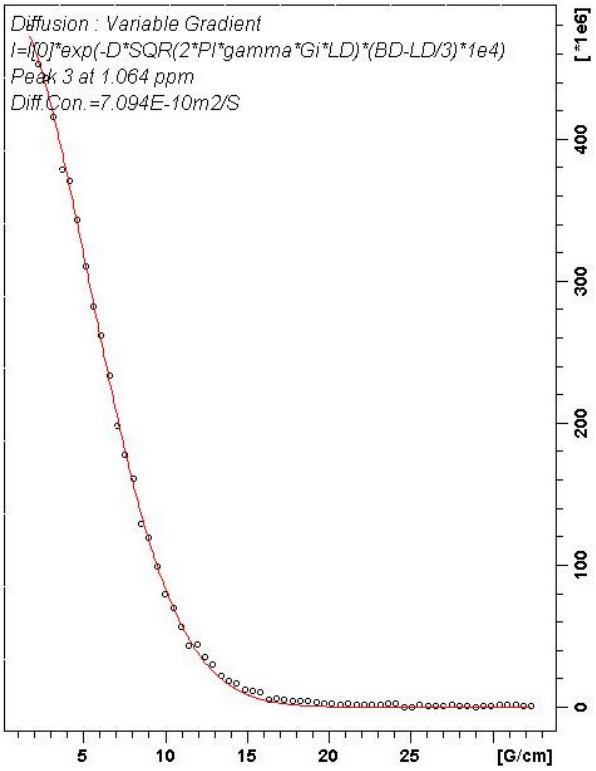

Figure S17.3. Stejskal-Tanner plot for the ^{1}H resonance at 1.064 ppm

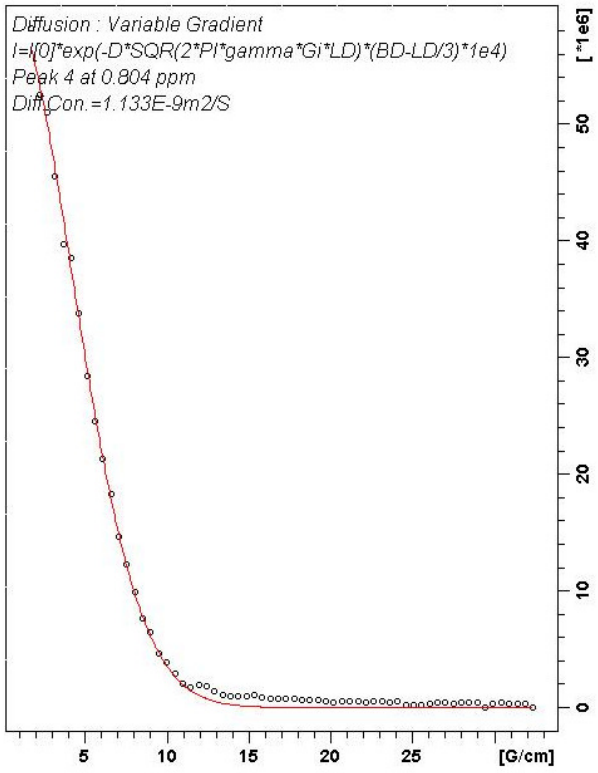

Figure S17.4. Stejskal-Tanner plot for the ^{1}H resonance at 0.804 ppm

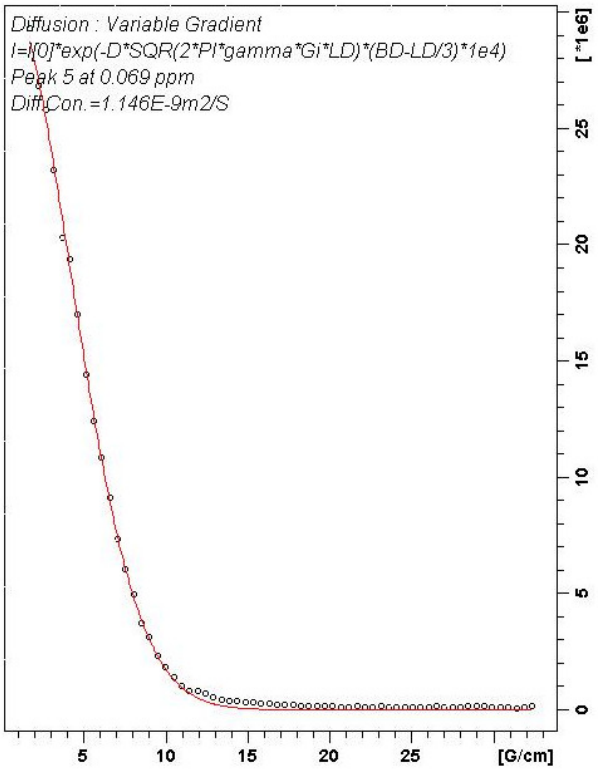

Figure S17.5. Stejskal-Tanner plot for the ^{1}H resonance at 0.069 ppm

Simfit Results

Dataset : C:\NMRdata/data/REM/nmr/B24394/4/pdata/1/ct1t2.txt

INTENSITY fit : Diffusion : Variable Gradient :

I=I[0]*exp(-D*SQR(2*PI*gamma*Gi*LD)*(BD-LD/3)*1e4)

64 points for Peak 1, Peak Point = 1.464 ppm

Converged after 53 iterations!

Results Comp. 1

I[0] = 3.245e-002
Diff Con. = 1.120e-009 m2/s
Gamma = 4.258e+003 Hz/G
Little Delta = 6.000m
Big Delta = 99.900m

RSS = 3.053e-006
SD = 2.184e-004

Point	Gradient	Expt	Calc	Difference
1	1.703e+000	3.032e-002	2.990e-002	-4.240e-004
2	2.189e+000	2.820e-002	2.834e-002	1.395e-004
3	2.676e+000	2.690e-002	2.651e-002	-3.854e-004
4	3.162e+000	2.433e-002	2.447e-002	1.379e-004
5	3.649e+000	2.147e-002	2.228e-002	8.134e-004
6	4.135e+000	2.028e-002	2.002e-002	-2.552e-004
7	4.622e+000	1.788e-002	1.775e-002	-1.289e-004
8	5.108e+000	1.524e-002	1.553e-002	2.915e-004
9	5.595e+000	1.320e-002	1.341e-002	2.039e-004
10	6.081e+000	1.151e-002	1.142e-002	-8.558e-005
11	6.568e+000	9.678e-003	9.597e-003	-8.084e-005
12	7.055e+000	7.727e-003	7.957e-003	2.303e-004
13	7.541e+000	6.503e-003	6.513e-003	9.958e-006
14	8.028e+000	5.390e-003	5.257e-003	-1.322e-004
15	8.514e+000	4.085e-003	4.190e-003	1.044e-004
16	9.001e+000	3.508e-003	3.293e-003	-2.151e-004
17	9.487e+000	2.666e-003	2.555e-003	-1.113e-004
18	9.974e+000	2.048e-003	1.955e-003	-9.289e-005
19	1.046e+001	1.645e-003	1.477e-003	-1.687e-004
20	1.095e+001	1.243e-003	1.100e-003	-1.426e-004
21	1.143e+001	9.584e-004	8.092e-004	-1.492e-004
22	1.192e+001	9.352e-004	5.869e-004	-3.483e-004
23	1.241e+001	7.570e-004	4.203e-004	-3.367e-004
24	1.289e+001	6.163e-004	2.968e-004	-3.195e-004
25	1.338e+001	4.720e-004	2.069e-004	-2.650e-004
26	1.387e+001	4.097e-004	1.423e-004	-2.674e-004
27	1.435e+001	3.805e-004	9.658e-005	-2.839e-004
28	1.484e+001	3.491e-004	6.465e-005	-2.845e-004
29	1.532e+001	3.336e-004	4.273e-005	-2.908e-004
30	1.581e+001	3.077e-004	2.785e-005	-2.799e-004
31	1.630e+001	2.066e-004	1.792e-005	-1.886e-004
32	1.678e+001	2.377e-004	1.137e-005	-2.263e-004
33	1.727e+001	2.143e-004	7.125e-006	-2.072e-004
34	1.776e+001	2.341e-004	4.401e-006	-2.297e-004
35	1.824e+001	1.685e-004	2.685e-006	-1.658e-004

36	1.873e+001	1.998e-004	1.615e-006	-1.982e-004
37	1.922e+001	1.476e-004	9.591e-007	-1.466e-004
38	1.970e+001	1.419e-004	5.616e-007	-1.413e-004
39	2.019e+001	1.293e-004	3.244e-007	-1.290e-004
40	2.068e+001	1.072e-004	1.851e-007	-1.071e-004
41	2.116e+001	1.881e-004	1.041e-007	-1.880e-004
42	2.165e+001	1.423e-004	5.786e-008	-1.422e-004
43	2.214e+001	1.819e-004	3.168e-008	-1.819e-004
44	2.262e+001	1.444e-004	1.714e-008	-1.444e-004
45	2.311e+001	1.302e-004	9.138e-009	-1.302e-004
46	2.360e+001	1.515e-004	4.814e-009	-1.515e-004
47	2.408e+001	1.350e-004	2.498e-009	-1.350e-004
48	2.457e+001	1.091e-004	1.281e-009	-1.091e-004
49	2.506e+001	1.444e-004	6.475e-010	-1.444e-004
50	2.554e+001	1.503e-004	3.233e-010	-1.503e-004
51	2.603e+001	1.571e-004	1.591e-010	-1.571e-004
52	2.651e+001	1.236e-004	7.734e-011	-1.236e-004
53	2.700e+001	1.550e-004	3.705e-011	-1.550e-004
54	2.749e+001	1.750e-004	1.754e-011	-1.750e-004
55	2.798e+001	1.052e-004	8.179e-012	-1.052e-004
56	2.846e+001	1.272e-004	3.769e-012	-1.272e-004
57	2.895e+001	8.379e-005	1.711e-012	-8.379e-005
58	2.943e+001	9.968e-005	7.680e-013	-9.968e-005
59	2.992e+001	1.039e-004	3.395e-013	-1.039e-004
60	3.041e+001	1.465e-004	1.483e-013	-1.465e-004
61	3.089e+001	1.438e-004	6.384e-014	-1.438e-004
62	3.138e+001	1.460e-004	2.716e-014	-1.460e-004
63	3.187e+001	1.184e-004	1.138e-014	-1.184e-004
64	3.235e+001	1.048e-004	4.704e-015	-1.048e-004

==========

64 points for Peak 2, Peak Point = 1.227 ppm

Converged after 63 iterations!

Results Comp. 1

I[0] = 2.756e-002
Diff Con. = 1.108e-009 m2/s
Gamma = 4.258e+003 Hz/G
Little Delta = 6.000m
Big Delta = 99.900m

RSS = 3.283e-006
SD = 2.265e-004

Point	Gradient	Expt	Calc	Difference
1	1.703e+000	2.556e-002	2.541e-002	-1.463e-004
2	2.189e+000	2.444e-002	2.410e-002	-3.344e-004
3	2.676e+000	2.271e-002	2.256e-002	-1.470e-004
4	3.162e+000	2.091e-002	2.084e-002	-7.166e-005
5	3.649e+000	1.870e-002	1.900e-002	3.011e-004
6	4.135e+000	1.697e-002	1.709e-002	1.250e-004
7	4.622e+000	1.505e-002	1.517e-002	1.204e-004
8	5.108e+000	1.300e-002	1.330e-002	2.953e-004
9	5.595e+000	1.119e-002	1.149e-002	3.004e-004
10	6.081e+000	9.747e-003	9.809e-003	6.232e-005

11	6.568e+000	8.149e-003	8.258e-003	1.094e-004
12	7.055e+000	6.549e-003	6.861e-003	3.121e-004
13	7.541e+000	5.487e-003	5.628e-003	1.412e-004
14	8.028e+000	4.800e-003	4.554e-003	-2.458e-004
15	8.514e+000	3.719e-003	3.638e-003	-8.167e-005
16	9.001e+000	3.121e-003	2.867e-003	-2.542e-004
17	9.487e+000	2.531e-003	2.230e-003	-3.009e-004
18	9.974e+000	2.008e-003	1.711e-003	-2.968e-004
19	1.046e+001	1.627e-003	1.297e-003	-3.299e-004
20	1.095e+001	1.275e-003	9.692e-004	-3.062e-004
21	1.143e+001	9.849e-004	7.153e-004	-2.696e-004
22	1.192e+001	9.779e-004	5.206e-004	-4.573e-004
23	1.241e+001	7.957e-004	3.742e-004	-4.215e-004
24	1.289e+001	7.373e-004	2.652e-004	-4.721e-004
25	1.338e+001	5.284e-004	1.857e-004	-3.428e-004
26	1.387e+001	4.830e-004	1.282e-004	-3.548e-004
27	1.435e+001	4.225e-004	8.737e-005	-3.352e-004
28	1.484e+001	3.868e-004	5.874e-005	-3.280e-004
29	1.532e+001	3.327e-004	3.900e-005	-2.937e-004
30	1.581e+001	3.194e-004	2.553e-005	-2.939e-004
31	1.630e+001	2.569e-004	1.651e-005	-2.404e-004
32	1.678e+001	2.573e-004	1.053e-005	-2.468e-004
33	1.727e+001	2.820e-004	6.630e-006	-2.754e-004
34	1.776e+001	2.080e-004	4.117e-006	-2.039e-004
35	1.824e+001	2.110e-004	2.525e-006	-2.085e-004
36	1.873e+001	1.858e-004	1.527e-006	-1.843e-004
37	1.922e+001	2.203e-004	9.122e-007	-2.194e-004
38	1.970e+001	1.883e-004	5.372e-007	-1.877e-004
39	2.019e+001	1.739e-004	3.122e-007	-1.736e-004
40	2.068e+001	1.697e-004	1.793e-007	-1.695e-004
41	2.116e+001	1.517e-004	1.015e-007	-1.516e-004
42	2.165e+001	1.418e-004	5.674e-008	-1.417e-004
43	2.214e+001	1.598e-004	3.127e-008	-1.598e-004
44	2.262e+001	1.394e-004	1.703e-008	-1.394e-004
45	2.311e+001	1.598e-004	9.143e-009	-1.598e-004
46	2.360e+001	1.251e-004	4.850e-009	-1.251e-004
47	2.408e+001	1.519e-004	2.535e-009	-1.519e-004
48	2.457e+001	1.475e-004	1.310e-009	-1.475e-004
49	2.506e+001	1.283e-004	6.668e-010	-1.283e-004
50	2.554e+001	1.279e-004	3.355e-010	-1.279e-004
51	2.603e+001	8.271e-005	1.663e-010	-8.271e-005
52	2.651e+001	1.251e-004	8.150e-011	-1.251e-004
53	2.700e+001	1.103e-004	3.935e-011	-1.103e-004
54	2.749e+001	1.145e-004	1.878e-011	-1.145e-004
55	2.798e+001	1.273e-004	8.831e-012	-1.273e-004
56	2.846e+001	1.286e-004	4.105e-012	-1.286e-004
57	2.895e+001	1.146e-004	1.880e-012	-1.146e-004
58	2.943e+001	1.384e-004	8.509e-013	-1.384e-004
59	2.992e+001	1.253e-004	3.795e-013	-1.253e-004
60	3.041e+001	1.329e-004	1.673e-013	-1.329e-004
61	3.089e+001	1.311e-004	7.267e-014	-1.311e-004
62	3.138e+001	8.156e-005	3.120e-014	-8.156e-005
63	3.187e+001	1.205e-004	1.320e-014	-1.205e-004
64	3.235e+001	1.169e-004	5.509e-015	-1.169e-004

==========

64 points for Peak 3, Peak Point = 1.064 ppm

Converged after 31 iterations!

Results Comp. 1

I[0] = 1.040e+000
Diff Con. = 7.094e-010 m2/s
Gamma = 4.258e+003 Hz/G
Little Delta = 6.000m
Big Delta = 99.900m

RSS = 3.233e-003
SD = 7.108e-003

Point	Gradient	Expt	Calc	Difference
1	1.703e+000	1.000e+000	9.872e-001	-1.279e-002
2	2.189e+000	9.468e-001	9.544e-001	7.517e-003
3	2.676e+000	9.256e-001	9.147e-001	-1.087e-002
4	3.162e+000	8.680e-001	8.695e-001	1.457e-003
5	3.649e+000	7.915e-001	8.194e-001	2.788e-002
6	4.135e+000	7.744e-001	7.657e-001	-8.605e-003
7	4.622e+000	7.178e-001	7.095e-001	-8.354e-003
8	5.108e+000	6.478e-001	6.519e-001	4.125e-003
9	5.595e+000	5.897e-001	5.939e-001	4.150e-003
10	6.081e+000	5.464e-001	5.365e-001	-9.860e-003
11	6.568e+000	4.873e-001	4.806e-001	-6.738e-003
12	7.055e+000	4.142e-001	4.268e-001	1.255e-002
13	7.541e+000	3.710e-001	3.759e-001	4.902e-003
14	8.028e+000	3.358e-001	3.282e-001	-7.632e-003
15	8.514e+000	2.704e-001	2.842e-001	1.381e-002
16	9.001e+000	2.504e-001	2.440e-001	-6.395e-003
17	9.487e+000	2.078e-001	2.078e-001	-4.166e-005
18	9.974e+000	1.657e-001	1.754e-001	9.682e-003
19	1.046e+001	1.463e-001	1.468e-001	5.202e-004
20	1.095e+001	1.189e-001	1.218e-001	2.892e-003
21	1.143e+001	9.019e-002	1.003e-001	1.010e-002
22	1.192e+001	9.182e-002	8.183e-002	-9.990e-003
23	1.241e+001	7.483e-002	6.623e-002	-8.600e-003
24	1.289e+001	6.211e-002	5.312e-002	-8.984e-003
25	1.338e+001	4.590e-002	4.227e-002	-3.624e-003
26	1.387e+001	3.965e-002	3.334e-002	-6.304e-003
27	1.435e+001	3.430e-002	2.609e-002	-8.217e-003
28	1.484e+001	2.603e-002	2.023e-002	-5.806e-003
29	1.532e+001	2.347e-002	1.556e-002	-7.912e-003
30	1.581e+001	2.150e-002	1.186e-002	-9.635e-003
31	1.630e+001	1.156e-002	8.974e-003	-2.585e-003
32	1.678e+001	1.366e-002	6.726e-003	-6.930e-003
33	1.727e+001	1.161e-002	5.002e-003	-6.605e-003
34	1.776e+001	9.659e-003	3.687e-003	-5.972e-003
35	1.824e+001	8.511e-003	2.696e-003	-5.815e-003
36	1.873e+001	8.697e-003	1.953e-003	-6.744e-003
37	1.922e+001	7.582e-003	1.404e-003	-6.177e-003
38	1.970e+001	5.430e-003	1.000e-003	-4.430e-003
39	2.019e+001	5.677e-003	7.066e-004	-4.971e-003
40	2.068e+001	3.677e-003	4.953e-004	-3.182e-003
41	2.116e+001	5.363e-003	3.440e-004	-5.019e-003
42	2.165e+001	4.033e-003	2.371e-004	-3.796e-003
43	2.214e+001	4.068e-003	1.619e-004	-3.906e-003
44	2.262e+001	2.990e-003	1.097e-004	-2.881e-003
45	2.311e+001	4.347e-003	7.363e-005	-4.273e-003

46	2.360e+001	5.330e-003	4.905e-005	-5.281e-003
47	2.408e+001	4.728e-003	3.238e-005	-4.695e-003
48	2.457e+001	-6.160e-004	2.121e-005	6.372e-004
49	2.506e+001	-8.366e-004	1.376e-005	8.504e-004
50	2.554e+001	4.588e-003	8.865e-006	-4.579e-003
51	2.603e+001	1.028e-003	5.656e-006	-1.022e-003
52	2.651e+001	1.619e-003	3.582e-006	-1.616e-003
53	2.700e+001	2.102e-003	2.247e-006	-2.100e-003
54	2.749e+001	4.259e-003	1.399e-006	-4.258e-003
55	2.798e+001	1.957e-003	8.628e-007	-1.956e-003
56	2.846e+001	2.492e-003	5.282e-007	-2.492e-003
57	2.895e+001	-3.602e-004	3.203e-007	3.606e-004
58	2.943e+001	2.309e-003	1.928e-007	-2.309e-003
59	2.992e+001	2.286e-003	1.149e-007	-2.285e-003
60	3.041e+001	3.310e-003	6.802e-008	-3.310e-003
61	3.089e+001	3.632e-003	3.987e-008	-3.632e-003
62	3.138e+001	3.730e-003	2.320e-008	-3.730e-003
63	3.187e+001	2.526e-003	1.337e-008	-2.526e-003
64	3.235e+001	1.977e-003	7.641e-009	-1.977e-003

==========

64 points for Peak 4, Peak Point = 0.804 ppm

Converged after 50 iterations!

Results Comp. 1

I[0] = 1.283e-001
Diff Con. = 1.133e-009 m2/s
Gamma = 4.258e+003 Hz/G
Little Delta = 6.000m
Big Delta = 99.900m

RSS = 1.206e-004
SD = 1.373e-003

Point	Gradient	Expt	Calc	Difference
1	1.703e+000	1.217e-001	1.181e-001	-3.618e-003
2	2.189e+000	1.098e-001	1.119e-001	2.106e-003
3	2.676e+000	1.067e-001	1.045e-001	-2.144e-003
4	3.162e+000	9.510e-002	9.640e-002	1.294e-003
5	3.649e+000	8.296e-002	8.768e-002	4.724e-003
6	4.135e+000	8.044e-002	7.870e-002	-1.745e-003
7	4.622e+000	7.068e-002	6.967e-002	-1.014e-003
8	5.108e+000	5.942e-002	6.086e-002	1.444e-003
9	5.595e+000	5.126e-002	5.244e-002	1.184e-003
10	6.081e+000	4.464e-002	4.459e-002	-4.523e-005
11	6.568e+000	3.824e-002	3.740e-002	-8.446e-004
12	7.055e+000	3.060e-002	3.094e-002	3.393e-004
13	7.541e+000	2.553e-002	2.526e-002	-2.664e-004
14	8.028e+000	2.073e-002	2.034e-002	-3.895e-004
15	8.514e+000	1.596e-002	1.617e-002	2.027e-004
16	9.001e+000	1.344e-002	1.267e-002	-7.684e-004
17	9.487e+000	9.655e-003	9.802e-003	1.463e-004
18	9.974e+000	8.158e-003	7.476e-003	-6.812e-004
19	1.046e+001	6.008e-003	5.629e-003	-3.789e-004
20	1.095e+001	4.269e-003	4.179e-003	-9.018e-005

21	1.143e+001	3.570e-003	3.063e-003	-5.075e-004
22	1.192e+001	4.013e-003	2.213e-003	-1.800e-003
23	1.241e+001	3.748e-003	1.579e-003	-2.169e-003
24	1.289e+001	2.942e-003	1.110e-003	-1.832e-003
25	1.338e+001	2.227e-003	7.709e-004	-1.456e-003
26	1.387e+001	2.136e-003	5.276e-004	-1.609e-003
27	1.435e+001	2.057e-003	3.566e-004	-1.700e-003
28	1.484e+001	2.061e-003	2.375e-004	-1.824e-003
29	1.532e+001	2.183e-003	1.563e-004	-2.027e-003
30	1.581e+001	1.905e-003	1.013e-004	-1.803e-003
31	1.630e+001	1.566e-003	6.487e-005	-1.501e-003
32	1.678e+001	1.612e-003	4.094e-005	-1.571e-003
33	1.727e+001	1.657e-003	2.551e-005	-1.631e-003
34	1.776e+001	1.578e-003	1.567e-005	-1.562e-003
35	1.824e+001	1.370e-003	9.504e-006	-1.361e-003
36	1.873e+001	1.306e-003	5.682e-006	-1.301e-003
37	1.922e+001	1.450e-003	3.354e-006	-1.446e-003
38	1.970e+001	1.194e-003	1.952e-006	-1.192e-003
39	2.019e+001	9.768e-004	1.120e-006	-9.756e-004
40	2.068e+001	1.032e-003	6.351e-007	-1.032e-003
41	2.116e+001	1.082e-003	3.548e-007	-1.081e-003
42	2.165e+001	1.171e-003	1.958e-007	-1.171e-003
43	2.214e+001	9.987e-004	1.065e-007	-9.986e-004
44	2.262e+001	1.090e-003	5.718e-008	-1.090e-003
45	2.311e+001	1.151e-003	3.026e-008	-1.151e-003
46	2.360e+001	9.460e-004	1.582e-008	-9.460e-004
47	2.408e+001	1.029e-003	8.149e-009	-1.029e-003
48	2.457e+001	3.520e-004	4.147e-009	-3.520e-004
49	2.506e+001	3.664e-004	2.079e-009	-3.664e-004
50	2.554e+001	4.209e-004	1.030e-009	-4.209e-004
51	2.603e+001	5.977e-004	5.023e-010	-5.977e-004
52	2.651e+001	8.886e-004	2.422e-010	-8.886e-004
53	2.700e+001	8.842e-004	1.150e-010	-8.842e-004
54	2.749e+001	6.724e-004	5.396e-011	-6.724e-004
55	2.798e+001	8.685e-004	2.494e-011	-8.685e-004
56	2.846e+001	9.338e-004	1.139e-011	-9.338e-004
57	2.895e+001	9.654e-004	5.124e-012	-9.654e-004
58	2.943e+001	-9.495e-005	2.278e-012	9.495e-005
59	2.992e+001	6.673e-004	9.974e-013	-6.673e-004
60	3.041e+001	8.101e-004	4.316e-013	-8.101e-004
61	3.089e+001	6.813e-004	1.839e-013	-6.813e-004
62	3.138e+001	5.751e-004	7.745e-014	-5.751e-004
63	3.187e+001	7.594e-004	3.212e-014	-7.594e-004
64	3.235e+001	7.048e-005	1.314e-014	-7.048e-005

==========

64 points for Peak 5, Peak Point = 0.069 ppm

Converged after 61 iterations!

Results Comp. 1

I[0] = 6.522e-002
Diff Con. = 1.146e-009 m2/s
Gamma = 4.258e+003 Hz/G
Little Delta = 6.000m
Big Delta = 99.900m

RSS = 1.469e-005
SD = 4.791e-004

Point	Gradient	Expt	Calc	Difference
1	1.703e+000	6.121e-002	5.998e-002	-1.232e-003
2	2.189e+000	5.610e-002	5.679e-002	6.875e-004
3	2.676e+000	5.388e-002	5.303e-002	-8.489e-004
4	3.162e+000	4.846e-002	4.886e-002	3.969e-004
5	3.649e+000	4.238e-002	4.439e-002	2.012e-003
6	4.135e+000	4.050e-002	3.979e-002	-7.100e-004
7	4.622e+000	3.558e-002	3.518e-002	-3.997e-004
8	5.108e+000	3.012e-002	3.069e-002	5.639e-004
9	5.595e+000	2.594e-002	2.639e-002	4.503e-004
10	6.081e+000	2.264e-002	2.240e-002	-2.416e-004
11	6.568e+000	1.906e-002	1.875e-002	-3.153e-004
12	7.055e+000	1.534e-002	1.548e-002	1.384e-004
13	7.541e+000	1.258e-002	1.261e-002	3.074e-005
14	8.028e+000	1.041e-002	1.013e-002	-2.812e-004
15	8.514e+000	7.772e-003	8.028e-003	2.562e-004
16	9.001e+000	6.592e-003	6.274e-003	-3.177e-004
17	9.487e+000	4.894e-003	4.840e-003	-5.414e-005
18	9.974e+000	3.874e-003	3.680e-003	-1.938e-004
19	1.046e+001	2.937e-003	2.762e-003	-1.750e-004
20	1.095e+001	2.148e-003	2.043e-003	-1.041e-004
21	1.143e+001	1.653e-003	1.492e-003	-1.611e-004
22	1.192e+001	1.648e-003	1.074e-003	-5.733e-004
23	1.241e+001	1.484e-003	7.634e-004	-7.205e-004
24	1.289e+001	1.123e-003	5.347e-004	-5.883e-004
25	1.338e+001	8.492e-004	3.697e-004	-4.795e-004
26	1.387e+001	7.966e-004	2.520e-004	-5.447e-004
27	1.435e+001	7.390e-004	1.695e-004	-5.695e-004
28	1.484e+001	6.658e-004	1.124e-004	-5.534e-004
29	1.532e+001	6.321e-004	7.359e-005	-5.585e-004
30	1.581e+001	5.658e-004	4.748e-005	-5.183e-004
31	1.630e+001	5.277e-004	3.024e-005	-4.975e-004
32	1.678e+001	4.941e-004	1.899e-005	-4.751e-004
33	1.727e+001	5.039e-004	1.177e-005	-4.922e-004
34	1.776e+001	4.039e-004	7.188e-006	-3.967e-004
35	1.824e+001	3.734e-004	4.335e-006	-3.691e-004
36	1.873e+001	3.659e-004	2.576e-006	-3.633e-004
37	1.922e+001	3.793e-004	1.512e-006	-3.778e-004
38	1.970e+001	3.443e-004	8.743e-007	-3.434e-004
39	2.019e+001	3.032e-004	4.986e-007	-3.027e-004
40	2.068e+001	2.613e-004	2.809e-007	-2.610e-004
41	2.116e+001	2.634e-004	1.559e-007	-2.633e-004
42	2.165e+001	3.226e-004	8.543e-008	-3.225e-004
43	2.214e+001	2.473e-004	4.613e-008	-2.473e-004
44	2.262e+001	2.542e-004	2.460e-008	-2.542e-004
45	2.311e+001	2.835e-004	1.293e-008	-2.835e-004
46	2.360e+001	2.385e-004	6.707e-009	-2.385e-004
47	2.408e+001	2.346e-004	3.429e-009	-2.346e-004
48	2.457e+001	2.510e-004	1.731e-009	-2.510e-004
49	2.506e+001	2.001e-004	8.611e-010	-2.001e-004
50	2.554e+001	1.980e-004	4.231e-010	-1.980e-004
51	2.603e+001	1.738e-004	2.047e-010	-1.738e-004
52	2.651e+001	2.955e-004	9.789e-011	-2.955e-004
53	2.700e+001	2.533e-004	4.609e-011	-2.533e-004
54	2.749e+001	1.997e-004	2.144e-011	-1.997e-004
55	2.798e+001	2.594e-004	9.823e-012	-2.594e-004

56	2.846e+001	3.078e-004	4.446e-012	-3.078e-004
57	2.895e+001	2.918e-004	1.982e-012	-2.918e-004
58	2.943e+001	2.977e-004	8.730e-013	-2.977e-004
59	2.992e+001	2.709e-004	3.786e-013	-2.709e-004
60	3.041e+001	2.146e-004	1.623e-013	-2.146e-004
61	3.089e+001	2.512e-004	6.848e-014	-2.512e-004
62	3.138e+001	1.312e-004	2.856e-014	-1.312e-004
63	3.187e+001	2.504e-004	1.173e-014	-2.504e-004
64	3.235e+001	3.314e-004	4.749e-015	-3.314e-004

==========

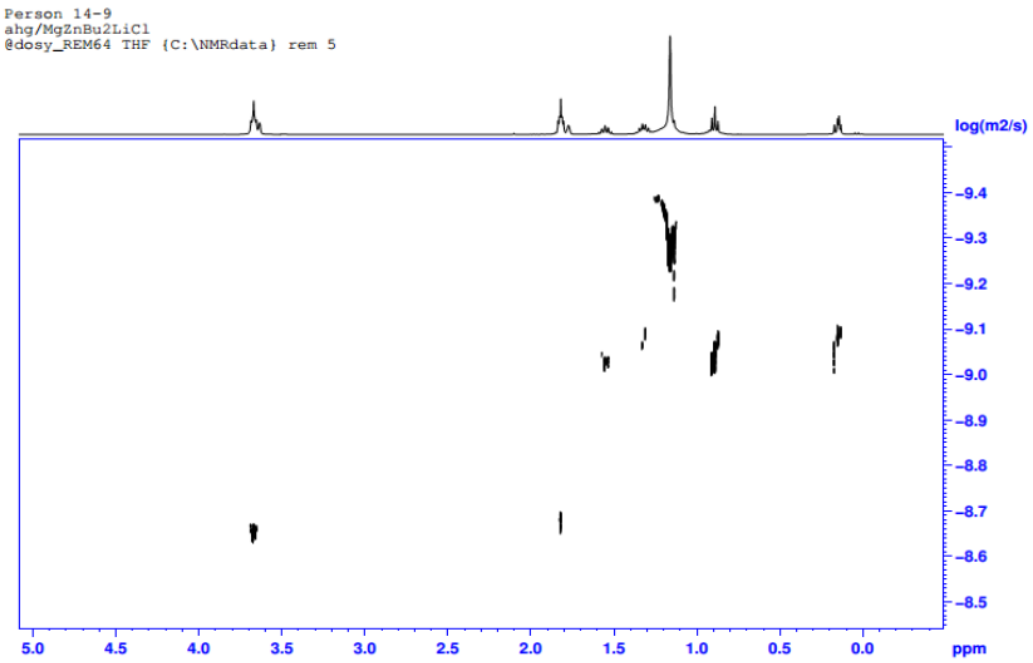

Figure S18. ^{1}H DOSY NMR spectrum of $Zn(OPiv)_2 \cdot 2LiCl$ and $MgBu_2$ in [D_8]THF at 25°C

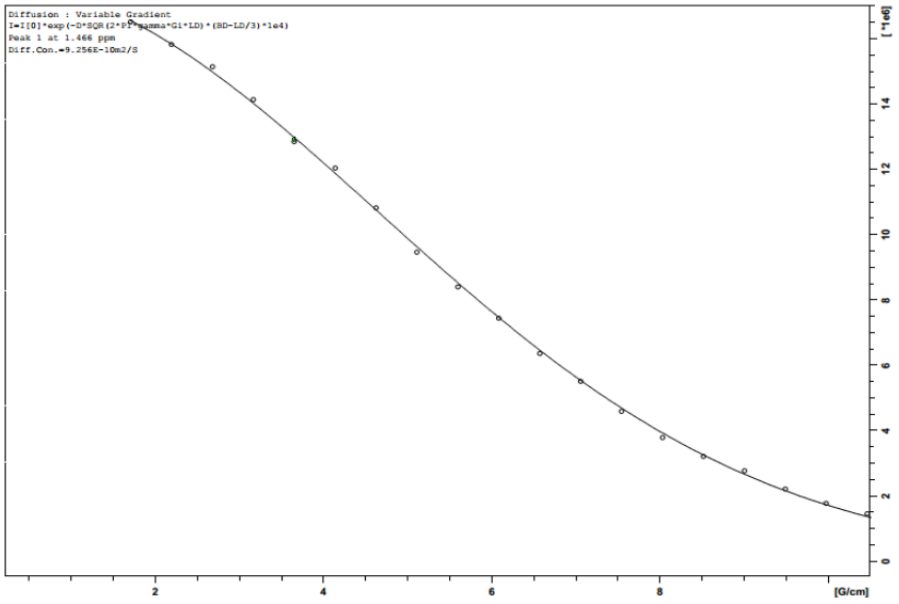

Figure S18.1. Stejskal-Tanner plot for the ^{1}H resonance at 1.466 ppm

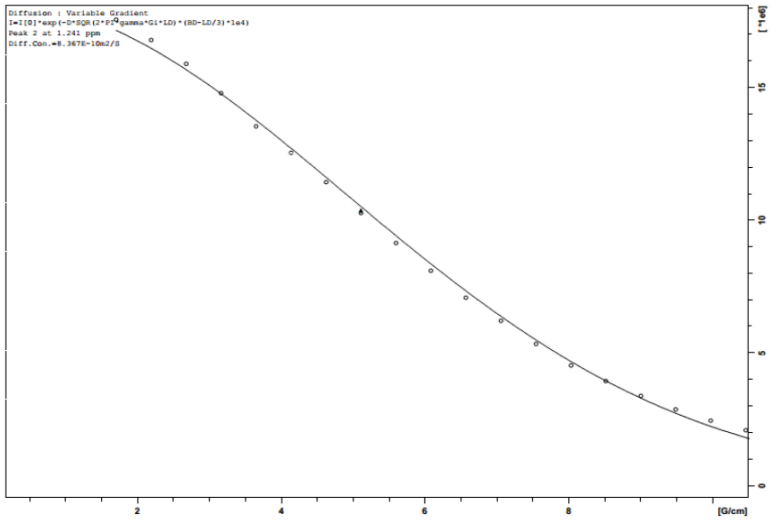

Figure S18.2. Stejskal-Tanner plot for the ^{1}H resonance at 1.241 ppm

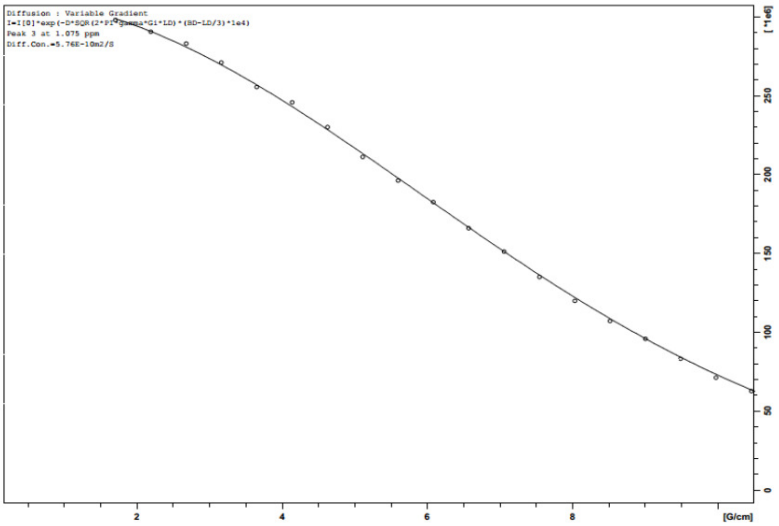

Figure S18.3. Stejskal-Tanner plot for the ^{1}H resonance at 1.075 ppm

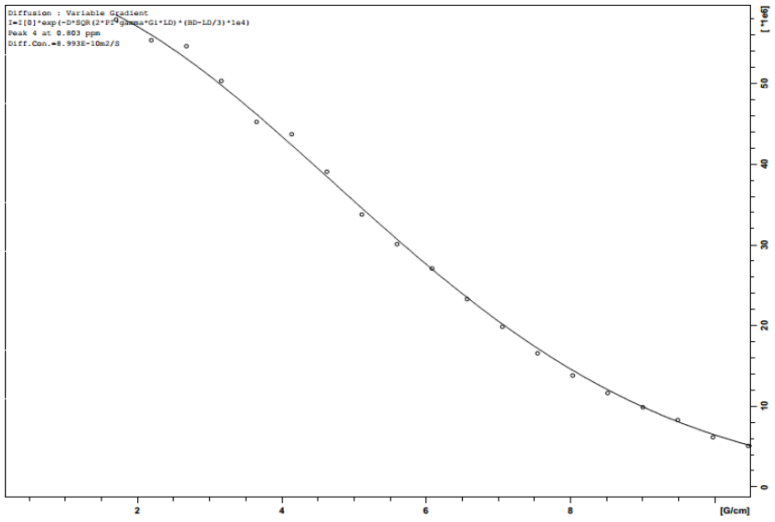

Figure S18.4. Stejskal-Tanner plot for the ^{1}H resonance at 0.803 ppm

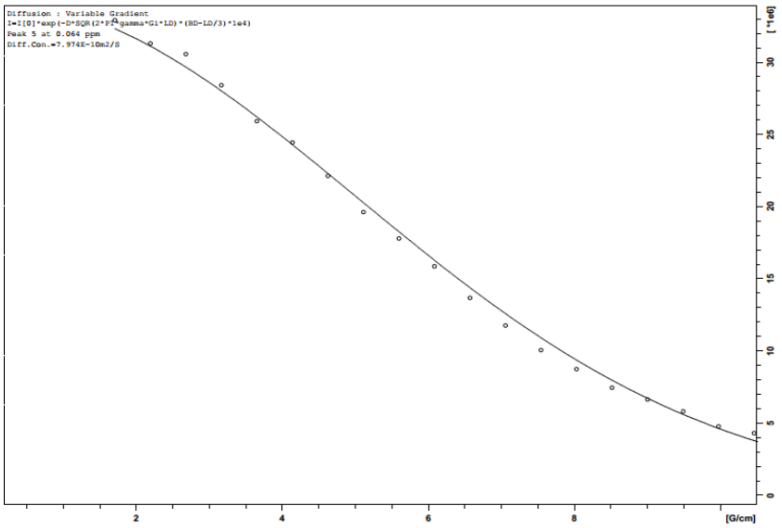

Figure S18.5. Stejskal-Tanner plot for the ^{1}H resonance at 0.064 ppm

Simfit Results

Dataset : C:/NMRdata/data/REM/nmr/B24178/4/pdata/1/ct1t2.txt

INTENSITY fit : Diffusion : Variable Gradient :

I=I[0]*exp(-D*SQR(2*PI*gamma*Gi*LD)*(BD-LD/3)*1e4)

41 points for Peak 1, Peak Point = 1.466 ppm

Converged after 64 iterations!

Results Comp. 1

I[0] = 5.942e-002
Diff Con. = 9.256e-010 m2/s
Gamma = 4.258e+003 Hz/G
Little Delta = 6.000m
Big Delta = 99.900m

RSS = 6.315e-006
SD = 3.925e-004

Point	Gradient	Expt	Calc	Difference
1	1.703e+000	5.538e-002	5.553e-002	1.498e-004
2	2.189e+000	5.308e-002	5.313e-002	4.917e-005
3	2.676e+000	5.078e-002	5.027e-002	-5.081e-004
4	3.162e+000	4.742e-002	4.705e-002	-3.640e-004
5	3.649e+000	4.312e-002	4.355e-002	4.244e-004
6	4.135e+000	4.040e-002	3.987e-002	-5.303e-004
7	4.622e+000	3.631e-002	3.609e-002	-2.170e-004
8	5.108e+000	3.176e-002	3.232e-002	5.531e-004
9	5.595e+000	2.819e-002	2.861e-002	4.269e-004
10	6.081e+000	2.496e-002	2.506e-002	1.001e-004
11	6.568e+000	2.135e-002	2.171e-002	3.583e-004
12	7.055e+000	1.850e-002	1.859e-002	9.152e-005
13	7.541e+000	1.540e-002	1.576e-002	3.533e-004
14	8.028e+000	1.271e-002	1.320e-002	4.862e-004
15	8.514e+000	1.078e-002	1.094e-002	1.594e-004
16	9.001e+000	9.321e-003	8.966e-003	-3.557e-004
17	9.487e+000	7.446e-003	7.269e-003	-1.769e-004
18	9.974e+000	5.957e-003	5.826e-003	-1.304e-004
19	1.046e+001	4.901e-003	4.621e-003	-2.807e-004
20	1.095e+001	4.032e-003	3.623e-003	-4.095e-004
21	1.143e+001	3.163e-003	2.810e-003	-3.525e-004
22	1.192e+001	2.627e-003	2.155e-003	-4.722e-004
23	1.241e+001	2.261e-003	1.635e-003	-6.258e-004
24	1.289e+001	1.898e-003	1.227e-003	-6.714e-004
25	1.338e+001	1.372e-003	9.104e-004	-4.616e-004
26	1.387e+001	1.503e-003	6.679e-004	-8.351e-004
27	1.435e+001	9.535e-004	4.849e-004	-4.685e-004
28	1.532e+001	8.734e-004	2.471e-004	-6.262e-004
29	1.678e+001	4.751e-004	8.273e-005	-3.924e-004
30	2.068e+001	3.306e-004	2.751e-006	-3.278e-004
31	2.116e+001	4.289e-004	1.710e-006	-4.272e-004
32	2.603e+001	2.343e-004	8.040e-009	-2.343e-004
33	2.651e+001	3.221e-004	4.429e-009	-3.221e-004
34	2.700e+001	3.340e-004	2.411e-009	-3.340e-004

35	2.749e+001	4.352e-004	1.299e-009	-4.352e-004
36	2.798e+001	1.690e-004	6.915e-010	-1.690e-004
37	2.846e+001	2.150e-004	3.645e-010	-2.150e-004
38	2.943e+001	2.402e-004	9.786e-011	-2.402e-004
39	3.041e+001	1.814e-004	2.514e-011	-1.814e-004
40	3.089e+001	3.226e-004	1.252e-011	-3.226e-004
41	3.138e+001	2.519e-004	6.178e-012	-2.519e-004

==========

61 points for Peak 2, Peak Point = 1.241 ppm

Converged after 60 iterations!

Results Comp. 1

I[0] = 6.117e-002
Diff Con. = 8.367e-010 m2/s
Gamma = 4.258e+003 Hz/G
Little Delta = 6.000m
Big Delta = 99.900m

RSS = 3.675e-005
SD = 7.762e-004

Point	Gradient	Expt	Calc	Difference
1	1.703e+000	5.889e-002	5.754e-002	-1.352e-003
2	2.189e+000	5.631e-002	5.529e-002	-1.022e-003
3	2.676e+000	5.331e-002	5.259e-002	-7.235e-004
4	3.162e+000	4.960e-002	4.953e-002	-6.700e-005
5	3.649e+000	4.540e-002	4.619e-002	7.827e-004
6	4.135e+000	4.205e-002	4.264e-002	5.882e-004
7	4.622e+000	3.836e-002	3.897e-002	6.175e-004
8	5.108e+000	3.445e-002	3.527e-002	8.191e-004
9	5.595e+000	3.067e-002	3.160e-002	9.299e-004
10	6.081e+000	2.716e-002	2.803e-002	8.715e-004
11	6.568e+000	2.375e-002	2.461e-002	8.644e-004
12	7.055e+000	2.083e-002	2.140e-002	5.672e-004
13	7.541e+000	1.791e-002	1.842e-002	5.138e-004
14	8.028e+000	1.518e-002	1.570e-002	5.209e-004
15	8.514e+000	1.322e-002	1.325e-002	3.403e-005
16	9.001e+000	1.133e-002	1.107e-002	-2.630e-004
17	9.487e+000	9.628e-003	9.156e-003	-4.720e-004
18	9.974e+000	8.207e-003	7.496e-003	-7.114e-004
19	1.046e+001	7.004e-003	6.079e-003	-9.255e-004
20	1.095e+001	5.870e-003	4.878e-003	-9.915e-004
21	1.143e+001	5.185e-003	3.878e-003	-1.307e-003
22	1.192e+001	4.215e-003	3.050e-003	-1.165e-003
23	1.241e+001	3.612e-003	2.377e-003	-1.235e-003
24	1.289e+001	3.267e-003	1.833e-003	-1.434e-003
25	1.338e+001	2.875e-003	1.400e-003	-1.475e-003
26	1.387e+001	2.315e-003	1.058e-003	-1.257e-003
27	1.435e+001	2.270e-003	7.922e-004	-1.478e-003
28	1.484e+001	1.931e-003	5.868e-004	-1.344e-003
29	1.532e+001	1.631e-003	4.307e-004	-1.201e-003
30	1.581e+001	1.394e-003	3.128e-004	-1.082e-003
31	1.630e+001	1.156e-003	2.250e-004	-9.314e-004
32	1.678e+001	1.113e-003	1.602e-004	-9.530e-004

33	1.727e+001	1.082e-003	1.129e-004	-9.690e-004
34	1.824e+001	8.241e-004	5.447e-005	-7.696e-004
35	1.873e+001	7.524e-004	3.725e-005	-7.152e-004
36	1.922e+001	7.281e-004	2.524e-005	-7.029e-004
37	1.970e+001	5.120e-004	1.692e-005	-4.951e-004
38	2.019e+001	6.311e-004	1.123e-005	-6.198e-004
39	2.068e+001	6.412e-004	7.384e-006	-6.339e-004
40	2.116e+001	4.404e-004	4.804e-006	-4.356e-004
41	2.165e+001	5.155e-004	3.096e-006	-5.124e-004
42	2.262e+001	5.128e-004	1.248e-006	-5.116e-004
43	2.311e+001	4.232e-004	7.798e-007	-4.224e-004
44	2.360e+001	3.996e-004	4.830e-007	-3.991e-004
45	2.457e+001	5.196e-004	1.797e-007	-5.195e-004
46	2.506e+001	2.966e-004	1.079e-007	-2.965e-004
47	2.554e+001	2.902e-004	6.421e-008	-2.902e-004
48	2.603e+001	5.298e-004	3.779e-008	-5.298e-004
49	2.651e+001	3.235e-004	2.205e-008	-3.235e-004
50	2.700e+001	3.705e-004	1.272e-008	-3.704e-004
51	2.749e+001	3.540e-004	7.275e-009	-3.540e-004
52	2.798e+001	3.947e-004	4.114e-009	-3.947e-004
53	2.846e+001	2.541e-004	2.306e-009	-2.541e-004
54	2.895e+001	3.194e-004	1.278e-009	-3.194e-004
55	2.943e+001	3.303e-004	7.025e-010	-3.303e-004
56	2.992e+001	3.801e-004	3.817e-010	-3.801e-004
57	3.041e+001	3.197e-004	2.056e-010	-3.197e-004
58	3.089e+001	2.888e-004	1.095e-010	-2.888e-004
59	3.138e+001	2.918e-004	5.782e-011	-2.918e-004
60	3.187e+001	2.442e-004	3.018e-011	-2.442e-004
61	3.235e+001	2.654e-004	1.560e-011	-2.654e-004

==========

61 points for Peak 3, Peak Point = 1.075 ppm

Converged after 38 iterations!

Results Comp. 1

I[0] = 1.046e+000
Diff Con. = 5.760e-010 m2/s
Gamma = 4.258e+003 Hz/G
Little Delta = 6.000m
Big Delta = 99.900m

RSS = 1.845e-003
SD = 5.500e-003

Point	Gradient	Expt	Calc	Difference
1	1.703e+000	1.000e+000	1.003e+000	2.720e-003
2	2.189e+000	9.750e-001	9.755e-001	5.246e-004
3	2.676e+000	9.497e-001	9.425e-001	-7.213e-003
4	3.162e+000	9.094e-001	9.045e-001	-4.905e-003
5	3.649e+000	8.571e-001	8.619e-001	4.811e-003
6	4.135e+000	8.247e-001	8.158e-001	-8.824e-003
7	4.622e+000	7.721e-001	7.668e-001	-5.309e-003
8	5.108e+000	7.086e-001	7.159e-001	7.268e-003
9	5.595e+000	6.587e-001	6.637e-001	4.992e-003
10	6.081e+000	6.126e-001	6.112e-001	-1.462e-003

11	6.568e+000	5.569e-001	5.589e-001	1.937e-003
12	7.055e+000	5.075e-001	5.075e-001	2.495e-005
13	7.541e+000	4.534e-001	4.578e-001	4.414e-003
14	8.028e+000	4.028e-001	4.101e-001	7.257e-003
15	8.514e+000	3.597e-001	3.649e-001	5.113e-003
16	9.001e+000	3.219e-001	3.223e-001	3.900e-004
17	9.487e+000	2.794e-001	2.829e-001	3.542e-003
18	9.974e+000	2.393e-001	2.465e-001	7.246e-003
19	1.046e+001	2.106e-001	2.134e-001	2.765e-003
20	1.095e+001	1.833e-001	1.834e-001	9.054e-005
21	1.143e+001	1.561e-001	1.566e-001	5.352e-004
22	1.192e+001	1.367e-001	1.327e-001	-3.929e-003
23	1.241e+001	1.174e-001	1.118e-001	-5.610e-003
24	1.289e+001	1.001e-001	9.347e-002	-6.671e-003
25	1.338e+001	8.112e-002	7.765e-002	-3.473e-003
26	1.387e+001	7.508e-002	6.403e-002	-1.105e-002
27	1.435e+001	5.663e-002	5.247e-002	-4.167e-003
28	1.484e+001	4.587e-002	4.268e-002	-3.191e-003
29	1.532e+001	4.270e-002	3.449e-002	-8.207e-003
30	1.581e+001	3.370e-002	2.767e-002	-6.027e-003
31	1.630e+001	2.549e-002	2.206e-002	-3.431e-003
32	1.678e+001	2.204e-002	1.746e-002	-4.581e-003
33	1.727e+001	1.616e-002	1.372e-002	-2.437e-003
34	1.776e+001	1.574e-002	1.071e-002	-5.028e-003
35	1.824e+001	1.649e-002	8.308e-003	-8.180e-003
36	1.873e+001	1.389e-002	6.395e-003	-7.497e-003
37	1.922e+001	1.419e-002	4.892e-003	-9.295e-003
38	1.970e+001	1.297e-002	3.715e-003	-9.252e-003
39	2.019e+001	1.106e-002	2.801e-003	-8.257e-003
40	2.068e+001	9.442e-003	2.099e-003	-7.343e-003
41	2.116e+001	1.054e-002	1.561e-003	-8.982e-003
42	2.214e+001	5.965e-003	8.465e-004	-5.118e-003
43	2.262e+001	5.135e-003	6.171e-004	-4.517e-003
44	2.311e+001	5.603e-003	4.465e-004	-5.156e-003
45	2.360e+001	6.543e-003	3.211e-004	-6.222e-003
46	2.408e+001	4.908e-003	2.292e-004	-4.678e-003
47	2.457e+001	3.842e-003	1.625e-004	-3.679e-003
48	2.506e+001	4.288e-003	1.144e-004	-4.173e-003
49	2.554e+001	4.491e-003	8.005e-005	-4.411e-003
50	2.651e+001	4.519e-003	3.835e-005	-4.481e-003
51	2.700e+001	7.867e-003	2.626e-005	-7.841e-003
52	2.749e+001	7.374e-003	1.787e-005	-7.357e-003
53	2.798e+001	2.615e-003	1.207e-005	-2.603e-003
54	2.846e+001	4.433e-003	8.105e-006	-4.425e-003
55	2.895e+001	2.349e-003	5.400e-006	-2.344e-003
56	2.943e+001	4.132e-003	3.576e-006	-4.129e-003
57	2.992e+001	3.013e-003	2.350e-006	-3.010e-003
58	3.041e+001	3.796e-003	1.535e-006	-3.795e-003
59	3.089e+001	6.679e-003	9.946e-007	-6.678e-003
60	3.138e+001	4.083e-003	6.408e-007	-4.082e-003
61	3.235e+001	2.223e-003	2.600e-007	-2.223e-003

==========

64 points for Peak 4, Peak Point = 0.803 ppm

Converged after 56 iterations!

Results Comp. 1

I[0] = 2.096e-001
Diff Con. = 8.993e-010 m2/s
Gamma = 4.258e+003 Hz/G
Little Delta = 6.000m
Big Delta = 99.900m

RSS = 4.075e-004
SD = 2.523e-003

Point	Gradient	Expt	Calc	Difference
1	1.703e+000	1.943e-001	1.963e-001	1.961e-003
2	2.189e+000	1.858e-001	1.880e-001	2.272e-003
3	2.676e+000	1.833e-001	1.782e-001	-5.132e-003
4	3.162e+000	1.688e-001	1.671e-001	-1.713e-003
5	3.649e+000	1.518e-001	1.550e-001	3.179e-003
6	4.135e+000	1.467e-001	1.422e-001	-4.482e-003
7	4.622e+000	1.311e-001	1.291e-001	-2.001e-003
8	5.108e+000	1.133e-001	1.160e-001	2.707e-003
9	5.595e+000	1.009e-001	1.031e-001	2.138e-003
10	6.081e+000	9.085e-002	9.061e-002	-2.392e-004
11	6.568e+000	7.817e-002	7.879e-002	6.241e-004
12	7.055e+000	6.664e-002	6.779e-002	1.143e-003
13	7.541e+000	5.561e-002	5.771e-002	2.098e-003
14	8.028e+000	4.637e-002	4.859e-002	2.221e-003
15	8.514e+000	3.909e-002	4.049e-002	1.401e-003
16	9.001e+000	3.321e-002	3.337e-002	1.610e-004
17	9.487e+000	2.785e-002	2.722e-002	-6.333e-004
18	9.974e+000	2.075e-002	2.195e-002	1.204e-003
19	1.046e+001	1.714e-002	1.752e-002	3.871e-004
20	1.095e+001	1.581e-002	1.383e-002	-1.976e-003
21	1.143e+001	1.292e-002	1.081e-002	-2.109e-003
22	1.192e+001	1.109e-002	8.352e-003	-2.736e-003
23	1.241e+001	9.445e-003	6.387e-003	-3.058e-003
24	1.289e+001	8.752e-003	4.830e-003	-3.922e-003
25	1.338e+001	7.172e-003	3.616e-003	-3.557e-003
26	1.387e+001	5.800e-003	2.676e-003	-3.124e-003
27	1.435e+001	5.670e-003	1.961e-003	-3.710e-003
28	1.484e+001	4.549e-003	1.420e-003	-3.129e-003
29	1.532e+001	3.990e-003	1.018e-003	-2.971e-003
30	1.581e+001	2.909e-003	7.220e-004	-2.187e-003
31	1.630e+001	2.757e-003	5.068e-004	-2.251e-003
32	1.678e+001	2.805e-003	3.517e-004	-2.453e-003
33	1.727e+001	2.516e-003	2.416e-004	-2.274e-003
34	1.776e+001	1.875e-003	1.641e-004	-1.711e-003
35	1.824e+001	2.599e-003	1.103e-004	-2.489e-003
36	1.873e+001	3.183e-003	7.333e-005	-3.110e-003
37	1.922e+001	3.375e-003	4.826e-005	-3.326e-003
38	1.970e+001	2.751e-003	3.140e-005	-2.719e-003
39	2.019e+001	3.092e-003	2.021e-005	-3.072e-003
40	2.068e+001	3.162e-003	1.288e-005	-3.149e-003
41	2.116e+001	2.667e-003	8.112e-006	-2.659e-003
42	2.165e+001	2.980e-003	5.060e-006	-2.974e-003
43	2.214e+001	2.321e-003	3.120e-006	-2.318e-003
44	2.262e+001	2.680e-003	1.905e-006	-2.678e-003
45	2.311e+001	2.374e-003	1.149e-006	-2.373e-003
46	2.360e+001	2.415e-003	6.868e-007	-2.415e-003
47	2.408e+001	2.558e-003	4.056e-007	-2.557e-003
48	2.457e+001	2.221e-003	2.372e-007	-2.221e-003

49	2.506e+001	2.443e-003	1.371e-007	-2.443e-003
50	2.554e+001	2.155e-003	7.850e-008	-2.155e-003
51	2.603e+001	2.798e-003	4.441e-008	-2.798e-003
52	2.651e+001	2.367e-003	2.488e-008	-2.367e-003
53	2.700e+001	2.553e-003	1.378e-008	-2.553e-003
54	2.749e+001	2.125e-003	7.556e-009	-2.125e-003
55	2.798e+001	3.056e-003	4.095e-009	-3.056e-003
56	2.846e+001	2.228e-003	2.198e-009	-2.228e-003
57	2.895e+001	2.123e-003	1.166e-009	-2.123e-003
58	2.943e+001	2.555e-003	6.125e-010	-2.555e-003
59	2.992e+001	1.587e-003	3.180e-010	-1.587e-003
60	3.041e+001	2.502e-003	1.635e-010	-2.502e-003
61	3.089e+001	1.885e-003	8.308e-011	-1.885e-003
62	3.138e+001	1.964e-003	4.182e-011	-1.964e-003
63	3.187e+001	1.853e-003	2.079e-011	-1.853e-003
64	3.235e+001	1.895e-003	1.023e-011	-1.895e-003

==========

60 points for Peak 5, Peak Point = 0.064 ppm

Converged after 49 iterations!

Results Comp. 1

I[0] = 1.150e-001
Diff Con. = 7.974e-010 m2/s
Gamma = 4.258e+003 Hz/G
Little Delta = 6.000m
Big Delta = 99.900m

RSS = 4.726e-004
SD = 2.806e-003

Point	Gradient	Expt	Calc	Difference
1	1.703e+000	1.104e-001	1.085e-001	-1.900e-003
2	2.189e+000	1.051e-001	1.045e-001	-5.794e-004
3	2.676e+000	1.026e-001	9.961e-002	-2.949e-003
4	3.162e+000	9.534e-002	9.409e-002	-1.253e-003
5	3.649e+000	8.697e-002	8.801e-002	1.047e-003
6	4.135e+000	8.204e-002	8.157e-002	-4.738e-004
7	4.622e+000	7.426e-002	7.486e-002	5.993e-004
8	5.108e+000	6.582e-002	6.807e-002	2.255e-003
9	5.595e+000	5.968e-002	6.130e-002	1.617e-003
10	6.081e+000	5.323e-002	5.469e-002	1.454e-003
11	6.568e+000	4.590e-002	4.831e-002	2.419e-003
12	7.055e+000	3.948e-002	4.228e-002	2.796e-003
13	7.541e+000	3.376e-002	3.666e-002	2.902e-003
14	8.028e+000	2.931e-002	3.147e-002	2.160e-003
15	8.514e+000	2.504e-002	2.677e-002	1.737e-003
16	9.001e+000	2.226e-002	2.255e-002	2.954e-004
17	9.487e+000	1.949e-002	1.883e-002	-6.682e-004
18	9.974e+000	1.603e-002	1.556e-002	-4.709e-004
19	1.046e+001	1.443e-002	1.274e-002	-1.689e-003
20	1.095e+001	1.336e-002	1.033e-002	-3.024e-003
21	1.143e+001	1.136e-002	8.302e-003	-3.062e-003
22	1.192e+001	1.008e-002	6.605e-003	-3.472e-003
23	1.241e+001	8.819e-003	5.207e-003	-3.612e-003

24	1.289e+001	8.624e-003	4.064e-003	-4.560e-003
25	1.338e+001	7.940e-003	3.144e-003	-4.796e-003
26	1.387e+001	7.037e-003	2.408e-003	-4.629e-003
27	1.435e+001	6.486e-003	1.827e-003	-4.659e-003
28	1.484e+001	6.092e-003	1.373e-003	-4.719e-003
29	1.532e+001	5.870e-003	1.022e-003	-4.848e-003
30	1.581e+001	5.158e-003	7.536e-004	-4.405e-003
31	1.630e+001	4.446e-003	5.506e-004	-3.895e-003
32	1.678e+001	4.386e-003	3.982e-004	-3.988e-003
33	1.727e+001	4.102e-003	2.855e-004	-3.817e-003
34	1.776e+001	3.654e-003	2.026e-004	-3.452e-003
35	1.824e+001	3.804e-003	1.425e-004	-3.661e-003
36	1.873e+001	3.939e-003	9.919e-005	-3.839e-003
37	1.922e+001	3.614e-003	6.845e-005	-3.545e-003
38	1.970e+001	3.469e-003	4.676e-005	-3.422e-003
39	2.019e+001	3.462e-003	3.163e-005	-3.430e-003
40	2.068e+001	3.373e-003	2.122e-005	-3.352e-003
41	2.116e+001	3.077e-003	1.408e-005	-3.063e-003
42	2.165e+001	2.732e-003	9.267e-006	-2.722e-003
43	2.214e+001	2.486e-003	6.035e-006	-2.480e-003
44	2.262e+001	2.535e-003	3.897e-006	-2.531e-003
45	2.311e+001	2.393e-003	2.490e-006	-2.391e-003
46	2.360e+001	2.428e-003	1.577e-006	-2.427e-003
47	2.554e+001	1.944e-003	2.305e-007	-1.944e-003
48	2.603e+001	2.312e-003	1.391e-007	-2.311e-003
49	2.651e+001	2.109e-003	8.324e-008	-2.109e-003
50	2.700e+001	2.283e-003	4.929e-008	-2.283e-003
51	2.749e+001	1.622e-003	2.893e-008	-1.622e-003
52	2.798e+001	1.731e-003	1.681e-008	-1.731e-003
53	2.846e+001	1.614e-003	9.682e-009	-1.614e-003
54	2.895e+001	1.622e-003	5.518e-009	-1.622e-003
55	2.943e+001	1.803e-003	3.118e-009	-1.803e-003
56	2.992e+001	1.592e-003	1.744e-009	-1.592e-003
57	3.041e+001	1.788e-003	9.669e-010	-1.788e-003
58	3.089e+001	1.365e-003	5.304e-010	-1.365e-003
59	3.138e+001	1.453e-003	2.886e-010	-1.453e-003
60	3.187e+001	1.103e-003	1.553e-010	-1.103e-003

==========

Stability study of alkylzinc compounds towards air

To evaluate the stability of organozinc derivatives towards air two different experiments were carried out:

(i) aliquots (0.1 mmol based on RZnX·LiCl) were placed at 25 °C in open NMR tubes, evacuated and dissolved in dry [D8]THF (0.5 mL). After exposure to air for 1h the NMR tube was closed and air atmosphere was replaced by argon atmosphere (avoiding evaporation of the toluene formed in the case of Me(*p*-C_6H_4)ZnCl·LiCl).

(ii) In a similar way, aliquots (0.1 mmol based on RZnX·LiCl) placed in NMR tubes were evacuated and after exposing the solid state compound to air for 1h, the air atmosphere was replaced by argon atmosphere and then the solid dissolved in [D_8]THF.

Then the content of active zinc species was determined by comparison of the integral values of the alkylzinc RZnX·LiCl to $Mg(OPiv)_2$, because of the quantity of pivalate is not influenced by the hydrolysis process.
In the case of solutions of Me(*p*-C_6H_4)ZnCl·LiCl without magnesium pivalate derivative, the content of active zinc species was determined by comparison of the integral values founded for the alkylzinc to toluene.

Table S5. Air stability of organozinc compounds after exposure to air for 1h.

	Perecentage of the remaining active alkylzinc species	
	Exposure to air in solution	Exposure to air in solid state
Me(*p*-C_6H_4)ZnCl·LiCl	90	88
Me(*p*-C_6H_4)MgCl + $Zn(OPiv)_2$·LiCl	95	83
Me(*p*-C_6H_4)MgCl + $Zn(OPiv)_2$·2LiCl	87	69
$ZnBu_2$·2LiCl	0	0[b]
$MgBu_2$ + $Zn(OPiv)_2$·LiCl	51	[a]
$MgBu_2$ + $Zn(OPiv)_2$·2LiCl	0	0
$ZnBu_2$·2LiCl + 5 $Mg(OPiv)_2$	39	
Me(*p*-C_6H_4)MgCl + $Zn(OPiv)_2$·2LiCl[c]	93	

a. Values obtained were not consistent due to the volatility/loss of $ZnBu_2$ formed
b. Note that oxygen insertion occurs to produce alkoxides
c. Exposure only to oxygen. Moisture is avoided employing by a drying tube which contains $CaCl_2$ drying agent

Negishi cross-coupling reactions

Zinc reagents **6-9** were synthesized by transmetallation between Me(*p*-C_6H_4)MgCl·LiCl (generated *via* Mg insertion from 4-chlorotoluene) or Me(*p*-C_6H_4)Li (obtained from 4-iodotoluene *via* I/Li exchange) and either $ZnCl_2$ or $Zn(OPiv)_2$ (Scheme S1).

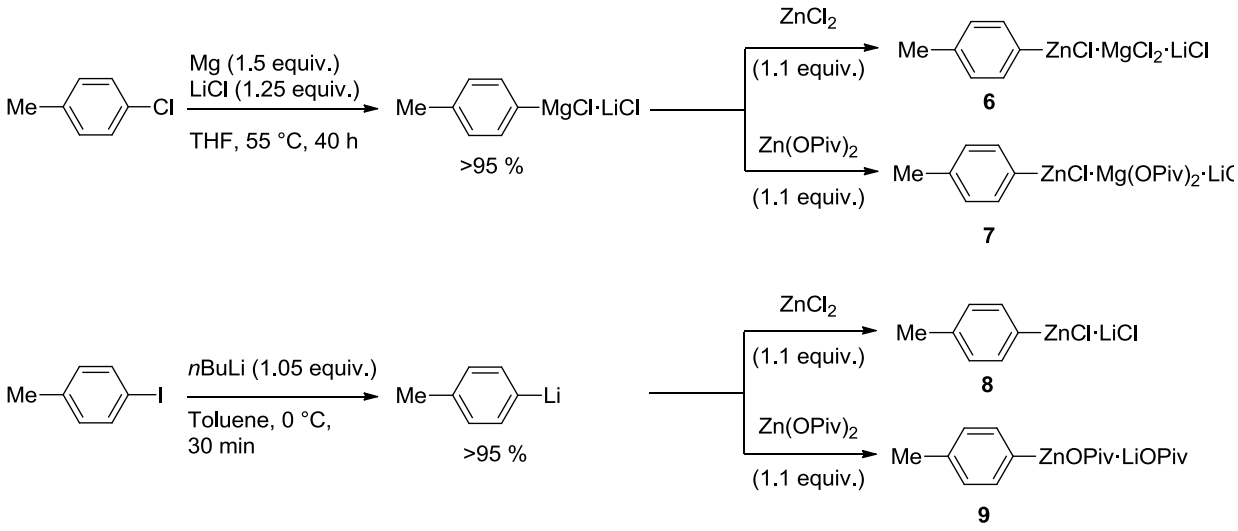

Scheme S1: Preparation of Me(*p*-C_6H_4)ZnX with X = Cl·$MgCl_2$·LiCl (**6**), Cl·$Mg(OPiv)_2$·LiCl (**7**), Cl·LiCl (**8**), OPiv·LiOPiv (**9**).

These organozinc compounds were then compared towards their reactivity in a cross-coupling reaction using ethyl 4-iodobenzoate (**10**) as electrophile and $Pd(dba)_2$ (3 mol%) and P(*o*-furyl)$_3$ (6 mol%) as catalyst system. As shown in table S6 all cross-coupling reactions proceed very fast at ambient temperature giving the biphenyl **11** in comparable yields of 89-94 %.

Table S6. Reactivity of zinc reagents **6-9** towards cross-coupling with ethyl 4-iodo benzoate (**10**).

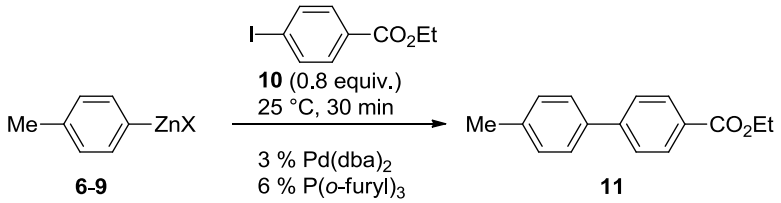

Entry	X	Isolated yield of **11**
1	Cl·$MgCl_2$·LiCl (**6**)	91 %
2	Cl·$Mg(OPiv)_2$·LiCl (**7**)	89 %
3	Cl·LiCl (**8**)	94 %
4	OPiv·LiOPiv (**9**).	93 %

We then turned to the much slower reaction with 4-bromoanisole to probe the effect of air and the more polar solvent EtOAc. To make sure the reactivity was the same, the cross-coupling with **12** (0.8 equiv.) in the presence of 3 mol% $Pd(OAc)_2$ and 6 mol% of DavePhos in THF under argon have been repeated to give the biphenyl **13** in 82 to 86 % yield (Table S7, entries 1, 5, 9 and 13; note that the homocoupled biphenyl **14** was also observed in reactions but always as the minor product in about 10% yield). Then the cross-couplings were performed on air in non-dried glassware but in dry THF. For the pivalate-free reactions the yield dropped slightly from 85 to 77 % for reagent **6** and from 86 to 81 % for

reagent **8**, respectively (entries 2 and 10). For the pivalate-containing reagents **7** and **9** however, the yield increased from 82 to 88 % for both reagents (entries 6 and 14).

Table S7. Reactivity of zinc reagents **6-9** towards cross-coupling with 4-bromoanisol (**12**).

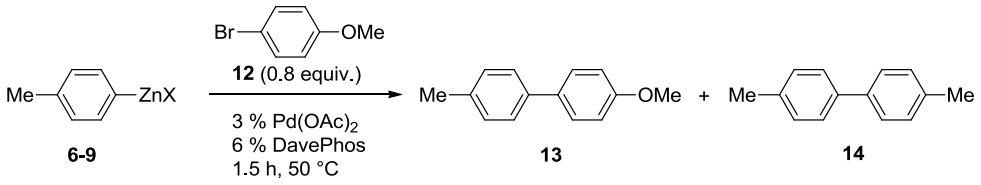

Entry	X	Solvent	Reaction Conditions	Isolated yield of **13** (%)
1	Cl·$MgCl_2$·LiCl (**6**)	THF	under Ar	85
2	Cl·$MgCl_2$·LiCl (**6**)	THF	in air	77
3	Cl·$MgCl_2$·LiCl (**6**)	EtOAc[a]	under Ar	91
4	Cl·$MgCl_2$·LiCl (**6**)	EtOAc[a]	in air	78
5	Cl·Mg$(OPiv)_2$·LiCl (**7**)	THF	under Ar	82
6	Cl·Mg$(OPiv)_2$·LiCl (**7**)	THF	in air	88
7	Cl·Mg$(OPiv)_2$·LiCl (**7**)	EtOAc[a]	under Ar	85
8	Cl·Mg$(OPiv)_2$·LiCl (**7**)	EtOAc[a]	in air	81
9	Cl·LiCl (**8**)	THF	under Ar	86
10	Cl·LiCl (**8**)	THF	in air	81
11	Cl·LiCl (**8**)	EtOAc[a]	under Ar	trace [b,c]
12	Cl·LiCl (**8**)	EtOAc[a]	in air	trace [b,c]
13	OPiv·LiOPiv (**9**)	THF	under Ar	82 %
14	OPiv·LiOPiv (**9**)	THF	in air	88 %
15	OPiv·LiOPiv (**9**)	EtOAc[a]	under Ar	trace [b,c]
16	OPiv·LiOPiv (**9**)	EtOAc[a]	in air	trace [b,c]

When the cross-couplings were carried out in EtOAc and under argon the yields for the magnesium salt containing reagents **6** and **7** increased to 91 % and to 85 %, respectively (entries 3 and 7). However the yield dropped slightly for both reagents when the reaction performed on air in non-dried glassware (entries 4 and 8). Remarkably when no magnesium salt was present, the cross-coupling did not work at all no matter if it was performed under argon or on air (entries 11, 12, 15 and 16). As GC-samples quenched with iodine showed the metal species **8** and **9** did not decompose when the reaction was performed under argon and also the amount of electrophile did not decrease significantly. A longer reaction time and a higher catalyst loading did not lead to any improvements. However, for the reactions carried out on air a slow decomposition of the metal species could be observed.

Preparation of the reagents Me(*p*-C_6H_4)ZnX 6-9

Me(*p*-C_6H_4)MgCl·LiCl and Me(*p*-C_6H_4)Li were prepared according to literature procedures.[4] The reagents Me(*p*-C_6H_4)ZnX **6-9** were generated by adding 1.1 equivalents of $ZnCl_2$ (as 1 M solution in THF) and $Zn(OPiv)_2$ (as a neat solid), respectively, to solutions of Me(*p*-C_6H_4)MgCl·LiCl and Me(*p*-C_6H_4)Li in THF at room temperature. These mixtures were stirred for further 15 min at this temperature until a clear solution formed. The concentration of the active zinc species was determined by titration against a stoichiometric amount of iodine (100 mg) in THF (2 mL). To get comparable reactivities all zinc reagents were then diluted to a concentration of ca. 0.35 mol/L.

Reaction conditions for the Negishi cross-coupling

a) Cross-coupling with ethyl 4-iodobenzoate

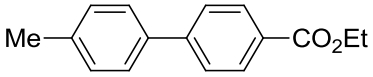

To a solution of Me(*p*-C_6H_4)ZnX (2.86 mL, 1 mmol, 0.35 M in THF) 17.3 mg $Pd(dba)_2$ (0.03 mmol), 14.0 mg P(o-furyl)$_3$ (0.06 mmol) and 221 mg ethyl 4-iodobenzoate (0.8 mmol) were added subsequently ad 25 °C. The reaction was stirred for 30 min at this temperature and then quenched with a sat. aqueous NH_4Cl solution (10 mL) followed by extraction with diethyl ether (3×10 mL). The combined organic layers were dried over Na_2SO_4 and after filtration the solvents were evaporated *in vacuo*. Purification by flash chromatography (silica gel, isohexane / Et_2O = 20:1) afforded the product **12** as a white solid.

The analytical data were in accordance with the literature data.[5]

^{1}H/δ(ppm) in $CDCl_3$: 1.43 (t, 3 H, J = 7.1 Hz, C*H*$_3$, Et) 2.28 (s, 3 H, C*H*$_3$, Me) 4.42 (q, 2 H J = 7.1 Hz, C*H*$_2$, Et) 7.17 - 7.34 (m, 4 H) 7.41 (d, 2 H, J = 8.5 Hz) 8.11 (d, 2 H, J = 8.5 Hz).

b) Cross-coupling with 4-bromoanisol

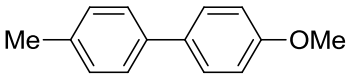

To a solution of Me(*p*-C_6H_4)ZnX (2.86 mL, 1 mmol, 0.35 M in THF) 6.74 mg $Pd(OAc)_2$ (0.03 mmol), 23.6 mg DavePhos (0.06 mmol) and 150 mg 4-bromoanisol (0.8 mmol) were added subsequently ad 25 °C. The reaction was stirred for 1.5 h at 50 °C and then quenched with a sat. aqueous NH_4Cl solution (10 mL) followed by extraction with diethyl ether (3×10 mL). The combined organic layers were dried over Na_2SO_4 and after filtration the solvents were evaporated *in vacuo*. Purification by flash chromatography (silica gel, isohexane / Et_2O = 100:1) afforded the product **13** as a white solid.

The analytical data were in accordance with the literature data.[6]

^{1}H/δ(ppm) in $CDCl_3$: 2.40 (s, 3 H, C*H*$_3$, Me) 3.86 (s, 3 H, OC*H*$_3$, OMe) 6.98 (d, 2 H, J = 8.8 Hz) 7.24 (d, 2 H, J = 7.8 Hz) 7.41 - 7.58 (m, 4 H)

---

[4] a) M. P. R. Spee, J. Boersma, M. D. Meijer, M. Q. Slagt, G. van Koten, J. W. Geus, J. Org. Chem. 2001, 66, 1647; b) A. K. Steib1, T. Thaler, K. Komeyama, P. Mayer, P. Knochel, *Angew. Chem., Int. Ed.* **2011**, 50, 3303.
[5] N. Liu, L. Wang, Z.-X. Wang, *Chem. Commun.* **2011**, 47, 1598.
[6] N. Liu, L. Wang, Z.-X. Wang, Chem. Commun. **2011**, 47, 1598.

Electrospray-Ionization Mass Spectrometric Studies

Experimental Details

For negative-ion mode measurements, sample solutions of $c \approx 25$ mM were continuously administered into the ESI source of an HCT quadrupole ion trap mass spectrometer (Bruker Daltonik) by a step motor-driven gas-tight syringe (flow rate: 0.5 mL h^{-1}). Similar to related previous experiments,[7] the ESI source was operated with N_2 as sheath and drying gas (0.7 bar backing pressure and 5 L min^{-1} flow rate, respectively) at an ESI voltage of 3000 V. To minimize decomposition reactions during the ESI process, mild conditions similar to those reported previously were applied (60 °C drying gas temperature and low potential differences along the path of the ions).[7] The helium-filled quadrupole ion trap (estimated pressure p(He) ≈ 2 mTorr) was typically operated at a trap drive of 40. This medium value ensures that all ions of the probed mass range of m/z = 50 – 1000 were detected in good signal intensity. In gas-phase fragmentation experiments, the mass-selected ions (isolation widths of 1 – 8 amu) were subjected to excitation voltages with amplitudes of V_{exc} and allowed to collide with the He gas. Only fragment ions with m/z values above the instrument's cut-off (27% of the m/z ratios of the parent ion) could be efficiently detected. Peak assignments given are based on the measured m/z values, the observed isotope patterns, and the outcome of the gas-phase fragmentation reactions.

For positive-ion mode measurements, sample solutions of $c \approx 5$ mM were continuously administered into the ESI source of a micrOTOF-Q II mass spectrometer (Bruker Daltonik) by a step motor-driven gas-tight syringe (flow rate: 0.5 mL h^{-1}). This instrument combines a quadrupole mass filter with a time-of-flight analyzer. Thanks to the latter, it achieves a much higher resolution than the quadrupole ion trap. This enhanced resolution proved essential for identifying the cations of the sampled solutions. As a drawback, the ESI source of the micrOTOF-Q II mass spectrometer is not perfectly shielded from the atmosphere and, thus, does not easily permit the detection of intact organometallic ions that are sensitive to air and/or moisture. The instrument was operated at ESI conditions analogous to those employed for the HTC ion trap. The ions produced were recorded for a mass range of m/z = 50 – 1000. In gas-phase fragmentation experiments, the mass-selected ions (isolation widths of 0.5 – 10 amu) acquired a kinetic energy of E_{LAB} by application of an acceleration voltage and collided with nitrogen gas added into the collision cell. Peak assignments given are based on the measured exact m/z ratios, the observed isotope patterns, and the outcome of the gas-phase fragmentation reactions.

Simulations of isotope patterns were performed with the CompassIsotopePattern software (Bruker Daltonik).

Anionic components of the reactive mixtures

Negative-ion mode ESI-mass spectrometric analysis of reactive mixtures of Me(p-C_6H_4)MgCl and Zn(OPiv)$_2$·nLiCl (n = 1 or 2) in THF found a multitude of organozincate ions (Figures S19 and S20), whose identities were proven by comparing the measured isotope patterns with simulated ones (Figures S21 – S27) and by analyzing their gas-phase fragmentations (Figures S28 – S32). The detected species included mono-, di-, and trinuclear complexes. Most of them exhibited a Zn:Me(p-C_6H_4) ratio of 1:1, which reflects the overall stoichiometry of the added reagents. The fact that none of the observed organozincates contained magnesium furthermore supports the notion of a complete transfer of the p-tolyl residue from magnesium to zinc. In contrast to the absence of magnesium in the anionic components of the sampled

[7] a) K. Koszinowski, *J. Am. Chem. Soc*. **2010**, *132*, 6032. b) A. Putau, K. Koszinowski, *Organometallics* **2010**, *29*, 3593; addition/correction: *Organometallics* **2010**, *29*, 6841. c) J. E. Fleckenstein, K. Koszinowski, *Organometallics* **2011**, *30*, 5018.

solutions, several of the detected organozincate complexes contained a lithium center. In the case of the reactive mixture of Me(*p*-C_6H_4)MgCl and Zn(OPiv)$_2$·LiCl, incorporation of a pivalate ligand was also seen for a few species, whereas the corresponding complexes were absent for solutions of Me(*p*-C_6H_4)MgCl/Zn(OPiv)$_2$·2LiCl. Apparently, the higher amount of chloride present in the latter resulted in a complete exchange of the pivalate ligands. Note that very similar organozincate complexes haven previously been observed in mixtures of ZnX_2/RLi and RZnX/LiX (X = halide).[7b,8]

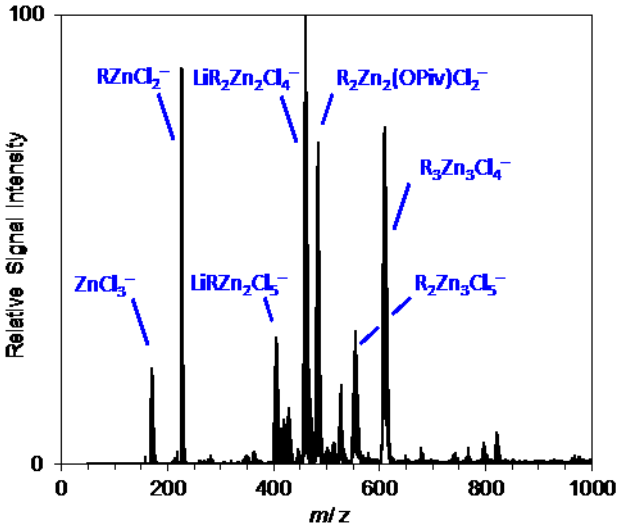

Figure S19. Negative-ion mode ESI mass spectrum of a solution of the reactive mixture Me(*p*-C_6H_4)MgCl and Zn(OPiv)$_2$·LiCl in THF ($c \approx 25$ mM). The ions centered at *m*/*z* 429 and 527 correspond to $RZn_2(OPiv)Cl_3^-$ and $LiR_2Zn_2(OPiv)Cl_3^-$, respectively. R = *p*-C_6H_4Me.

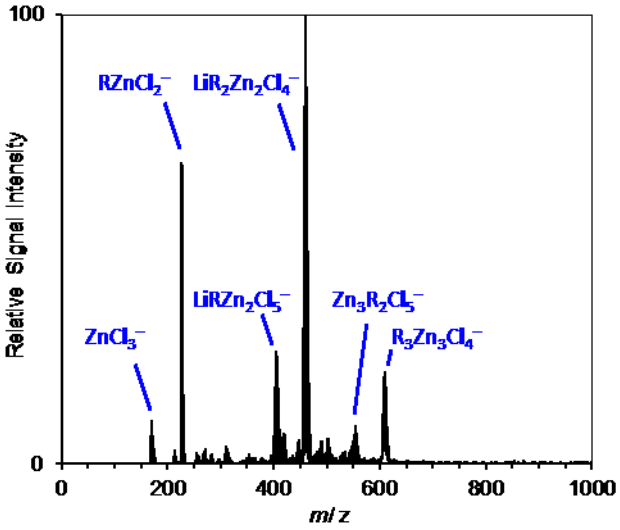

[8] a) K. Koszinowski, P. Böhrer, *Organometallics* **2009**, *28*, 100. b) K. Koszinowski, P. Böhrer, *Organometallics* **2009**, *28*, 771.

Figure S20. Negative-ion mode ESI mass spectrum of a solution of the reactive mixture Me(*p*-C_6H_4)MgCl and $Zn(OPiv)_2$·2LiCl in THF ($c \approx 25$ mM). R = *p*-C_6H_4Me.

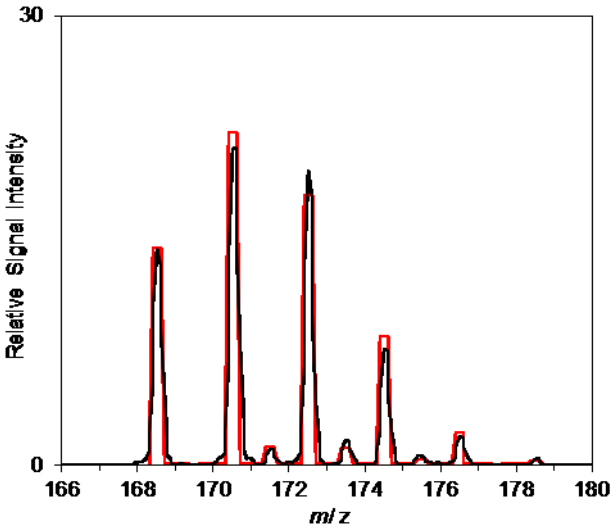

Figure S21. Measured (black) and simulated (red) isotope pattern of $ZnCl_3^-$.

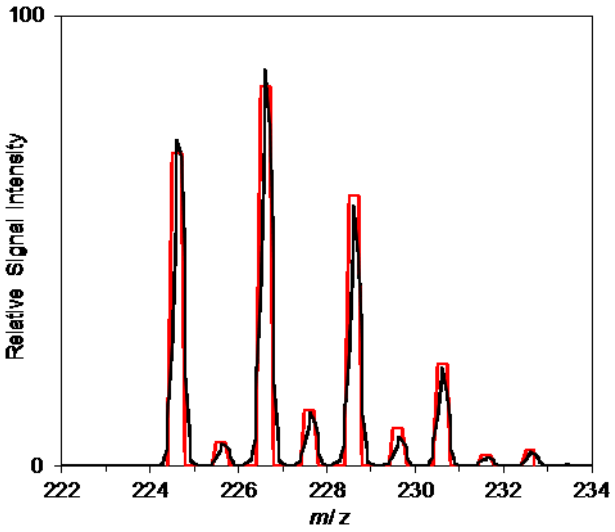

Figure S22. Measured (black) and simulated (red) isotope pattern of $RZnCl_2^-$. R = *p*-C_6H_4Me.

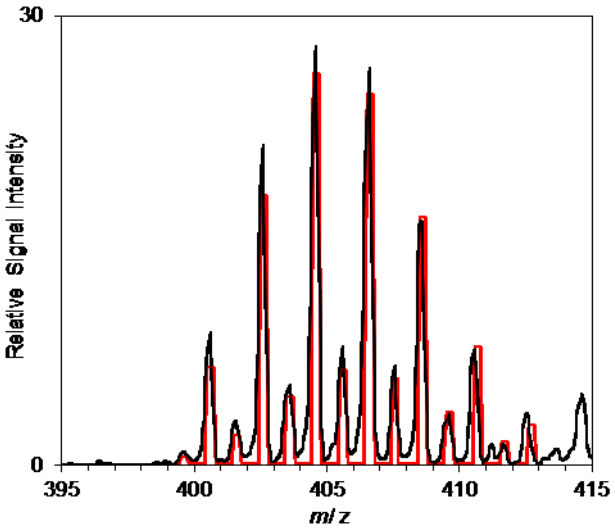

Figure S23. Measured (black) and simulated (red) isotope pattern of $LiRZn_2Cl_5^-$. R = *p*-C_6H_4Me.

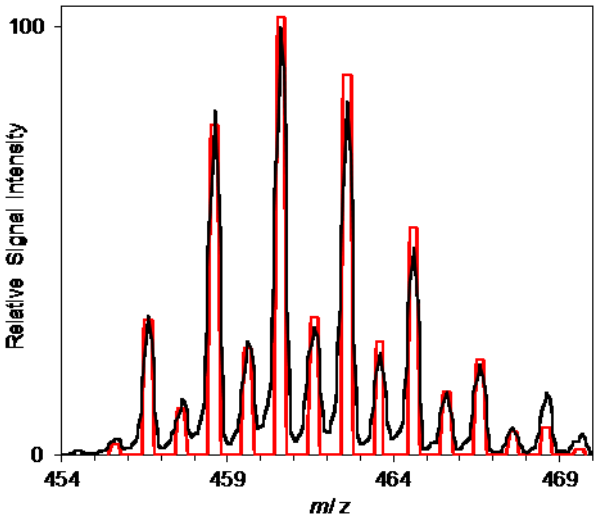

Figure S24. Measured (black) and simulated (red) isotope pattern of $LiR_2Zn_2Cl_4^-$. R = *p*-C_6H_4Me.

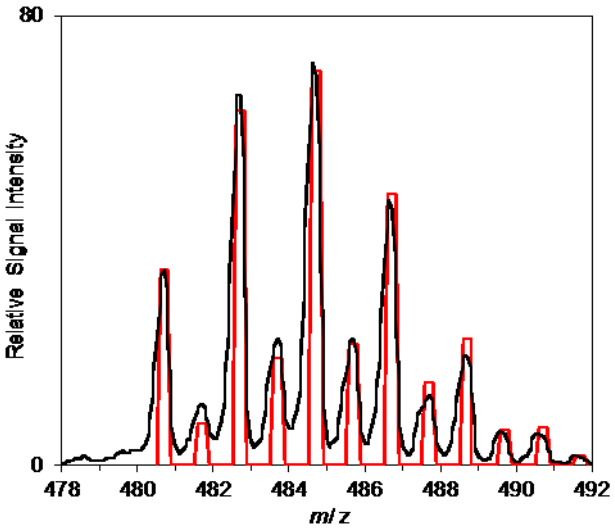

Figure S25. Measured (black) and simulated (red) isotope pattern of $R_2Zn_2(OPiv)Cl_2^-$. R = *p*-C_6H_4Me.

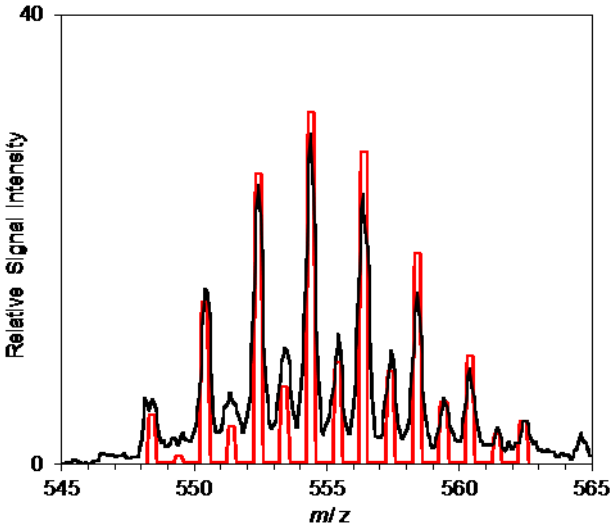

Figure S26. Measured (black) and simulated (red) isotope pattern of $R_2Zn_3Cl_5^-$. R = *p*-C_6H_4Me.

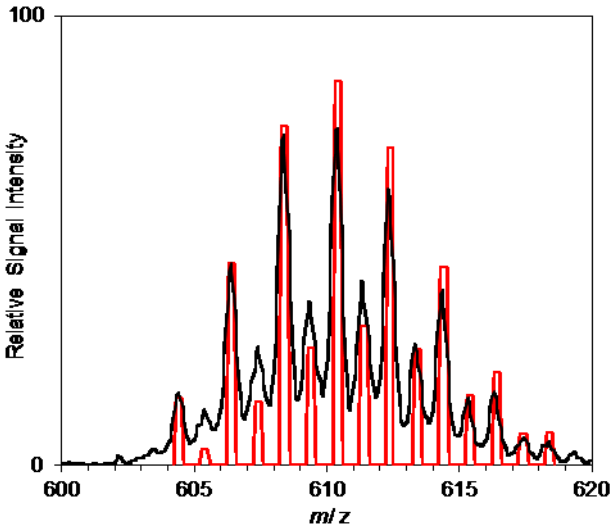

Figure S27. Measured (black) and simulated (red) isotope pattern of $R_3Zn_3Cl_4^-$. R = *p*-C_6H_4Me.

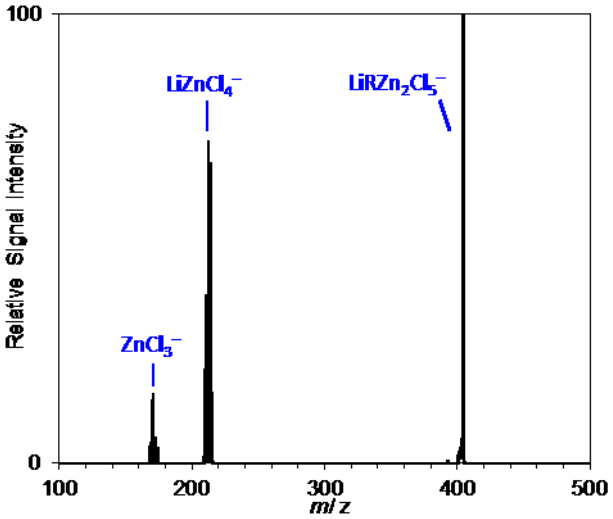

Figure S28. Mass spectrum of mass-selected $LiRZn_2Cl_5^-$ and its daughter ions resulting from fragmentation in the gas phase (V_{exc} = 0.80 V).

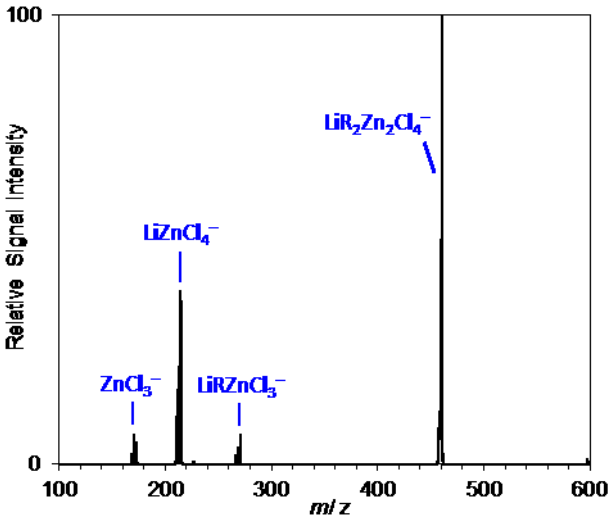

Figure S29. Mass spectrum of mass-selected $LiR_2Zn_2Cl_4^-$ and its daughter ions resulting from fragmentation in the gas phase (V_{exc} = 0.20 V).

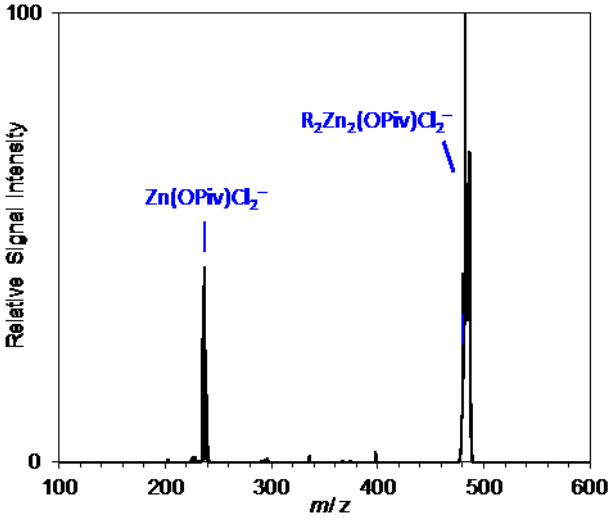

Figure S30. Mass spectrum of mass-selected $R_2Zn_2(OPiv)Cl_2^-$ and its daughter ions resulting from fragmentation in the gas phase (V_{exc} = 0.50 V).

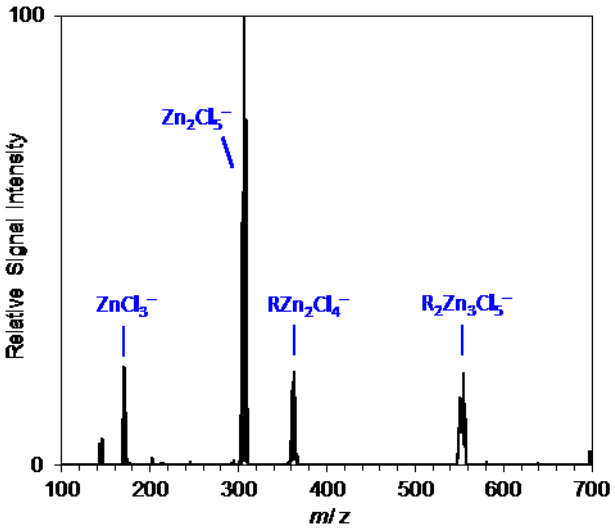

Figure S31. Mass spectrum of mass-selected $R_2Zn_3Cl_5^-$ and its daughter ions resulting from fragmentation in the gas phase (V_{exc} = 0.60 V).

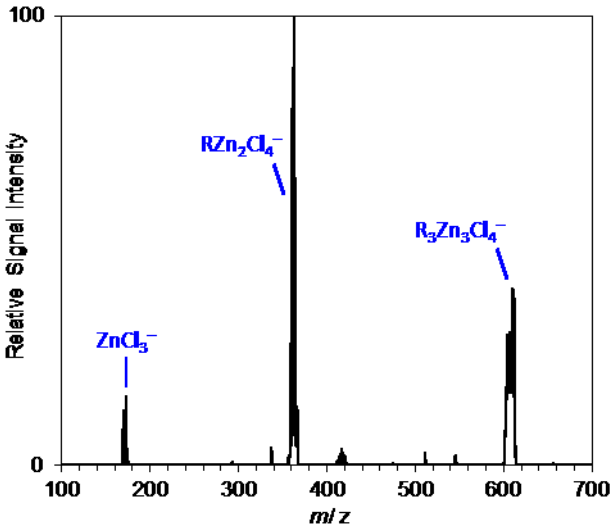

Figure S32. Mass spectrum of mass-selected $R_3Zn_3Cl_4^-$ and its daughter ions resulting from fragmentation in the gas phase (V_{exc} = 0.45 V).

Cationic components of the reactive mixtures

Positive-ion mode ESI mass spectrometry of a reactive mixture of Me(*p*-C_6H_4)MgCl and $Zn(OPiv)_2$·LiCl in THF detected several cations (Figure S30), whose compositions were derived from analyses of their exact *m*/*z* ratios (Table S8), their isotope patterns, and their gas-phase fragmentations (Figures S31 – S34). In marked contrast to the anions, the observed cations did not contain the *p*-tolyl residue, but were rich in pivalate. The two most abundant species also

featured a hydroxy group. Although the complexes contained all three metals added to the solution, magnesium clearly prevailed. The composition of the cations thus constitutes almost the exact counterpart of that of the anions. As the obtained ESI mass spectra clearly show, the transfer of the *p*-tolyl residue from magnesium to zinc is accompanied by a migration of the pivalate ligand from the latter to the former. Hence, the ESI-mass spectrometric findings fully agree with the crystallographic results.

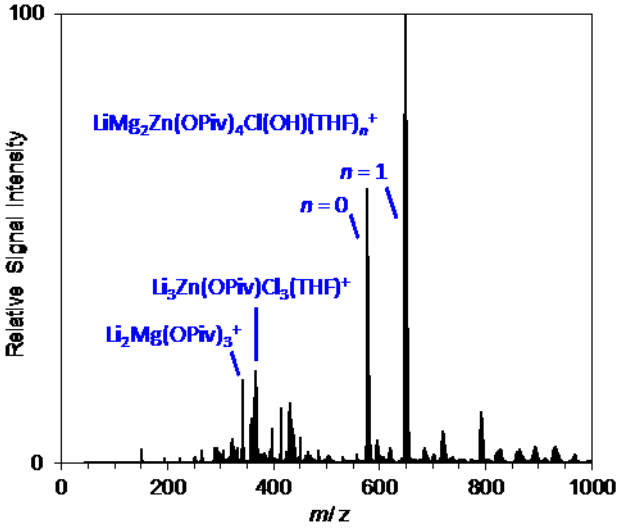

Figure S33. Positive-ion mode ESI mass spectrum of a solution of the reactive mixture Me(*p*-C_6H_4)MgCl and $Zn(OPiv)_2$·LiCl in THF ($c \approx 5$ mM).

Table S8. Measured and theoretical *m*/*z* ratios of cations observed upon ESI-mass spectrometric analysis of the reactive mixture Me(*p*-C_6H_4)MgCl and $Zn(OPiv)_2$·LiCl in THF.[a]

Cation	*m*/*z*(measured)	*m*/*z*(theoretical)
$Li_2Mg(OPiv)_3^+$	341.194	341.197
$Li_3Zn(OPiv)Cl_2(THF)^+$	364.993	364.998
$LiMg_2Zn(OPiv)_4Cl(OH)^+$	577.113	577.125
$LiMg_2Zn(OPiv)_4Cl(OH)(THF)^+$	649.181	649.183

[a] For each species, only the isotopologue of the highest abundance is listed.

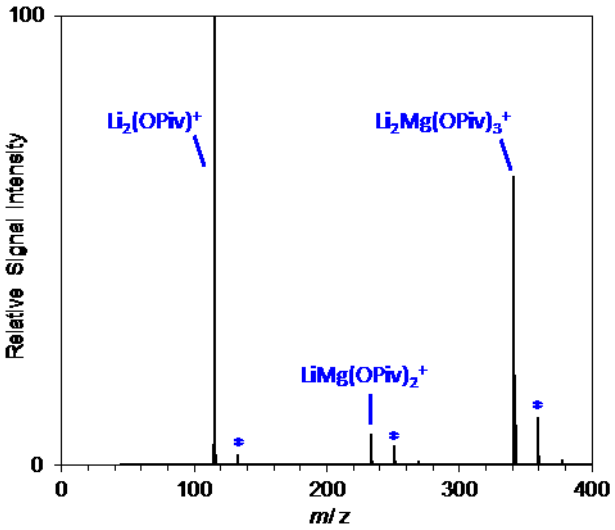

Figure S34. Mass spectrum of mass-selected $Li_2Mg(OPiv)_3^+$ and its daughter ions resulting from fragmentation in the gas phase (E_{LAB} = 20 eV). Peaks marked with an asterisk correspond to H_2O adducts resulting from reaction with background water present in the collision cell.

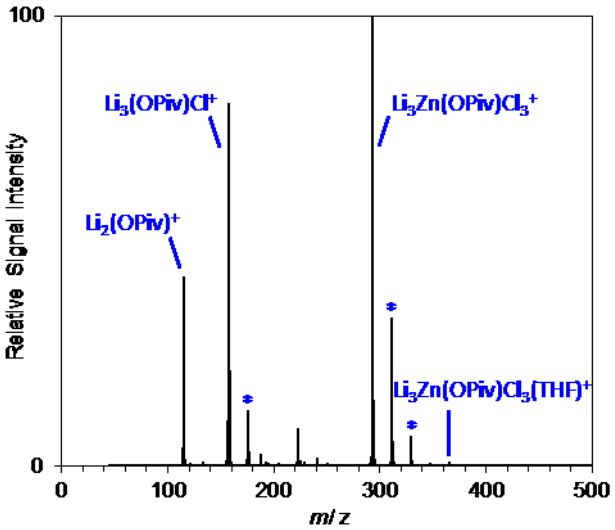

Figure S35. Mass spectrum of mass-selected $Li_3Zn(OPiv)Cl_3(THF)^+$ and its daughter ions resulting from fragmentation in the gas phase (E_{LAB} = 10 eV). Peaks marked with an asterisk correspond to H_2O adducts resulting from reaction with background water present in the collision cell.

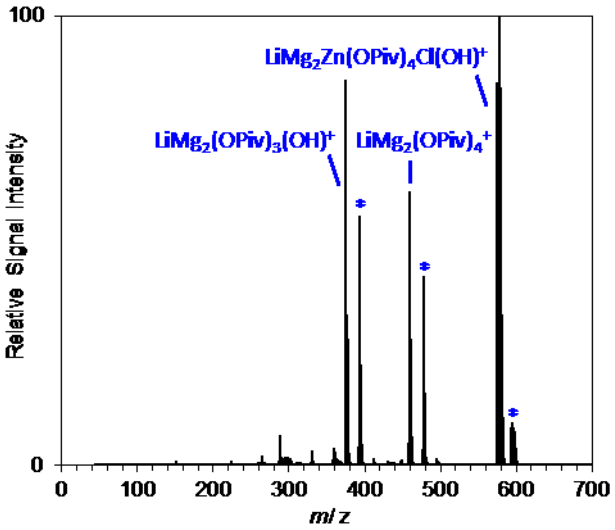

Figure S36. Mass spectrum of mass-selected $LiMg_2Zn(OPiv)_4Cl(OH)^+$ and its daughter ions resulting from fragmentation in the gas phase (E_{LAB} = 15 eV). Peaks marked with an asterisk correspond to H_2O adducts resulting from reaction with background water present in the collision cell.

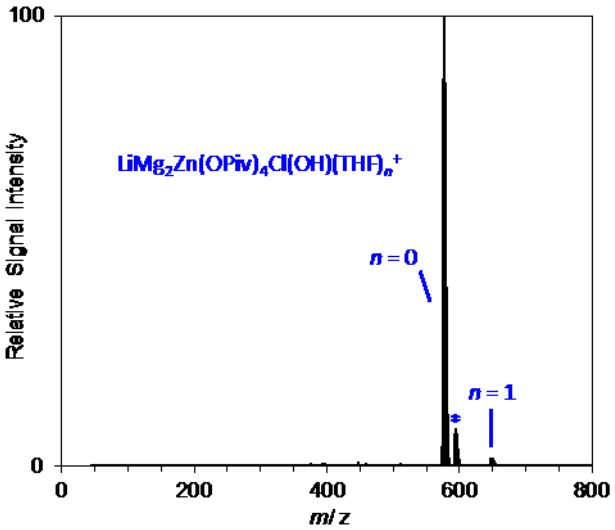

Figure S37. Mass spectrum of mass-selected $LiMg_2Zn(OPiv)_4Cl(OH)(THF)^+$ and its daughter ions resulting from fragmentation in the gas phase (E_{LAB} = 8 eV). The peak marked with an asterisk corresponds to an H_2O adduct resulting from reaction with background water present in the collision cell.